Summer 2013

A calibration free vector network analyzer

Arpit Kothari

Department:

A CALIBRATION FREE VECTOR NETWORK ANALYZER

by

ARPIT KOTHARI

A THESIS

Presented to the Faculty of the Graduate School of the

MISSOURI UNIVERSITY OF SCIENCE AND TECHNOLOGY

In Partial Fulfillment of the Requirements for the Degree

MASTER OF SCIENCE IN ELECTRICAL ENGINEERING

2013

Approved by

Dr. Reza Zoughi, Advisor
Dr. Daryl Beetner
Dr. David Pommerenke

ABSTRACT

Recently, two novel single-port, phase-shifter based vector network analyzer (VNA) systems were developed and tested at X-band (8.2 - 12.4 GHz) and Ka-band (26.4 – 40 GHz), respectively. These systems operate based on electronically moving the standing wave pattern, set up in a waveguide, over a Schottky detector and sample the standing wave voltage for several phase shift values. Once this system is fully characterized, all parameters in the system become known and hence theoretically, no other correction (or calibration) should be required to obtain the reflection coefficient, (Γ), of an unknown load. This makes this type of VNA "calibration free" which is a significant advantage over other types of VNAs. To this end, a VNA system, based on this design methodology, was developed at X-band using several design improvements (compared to the previous designs) with the aim of demonstrating this "calibration-free" feature. It was found that when a commercial VNA (HP8510C) is used as the source and the detector, the system works as expected. However, when a detector is used (Schottky diode, log detector, etc.), obtaining correct Γ still requires the customary three-load calibration. With the aim of exploring the cause, a detailed sensitivity analysis of prominent error sources was performed. Extensive measurements were done with different detection techniques including use of a spectrum analyzer as power detector. The system was tested even for electromagnetic compatibility (EMC) which may have contributed to this issue. Although desired results could not be obtained using the proposed standing-wave-power measuring devices like the Schottky diode but the principle of "calibration-free VNA" was shown to be true.

ACKNOWLEDGEMENTS

I am aware that this thesis would never have been possible without the generous help that I received from various quarters. My greatest debt of gratitude is to my supervisor, Professor Reza Zoughi for his illuminating guidance, constructive criticism and for making available to me the *amntl* lab and all the resources necessary to conduct my research.

I am deeply indebted to Dr. David Pommerenke and Dr. Daryl Beetner for their insightful suggestions and invaluable assistance during the course of my research.

My very special thanks to Dr. Mohammad Tayeb Ghasr for his motivating guidance, constant encouragement, unfailing patience and support all through my research.

I am grateful to the IEEE I&M society for the 2011 Graduate Fellowship Award which provided me with the financial assistance while doing this research.

I would like to record my appreciation of the Curtis Laws Wilson Library, which supplied me with important books, journals, and articles and to the University Librarians, who provided valuable help at the various stages of my work.

My thanks also to my lab colleagues, Mark, Mojtaba, Toby and all the others for the wonderful and enlightening discussions and episodes of Futurama.

But for the unwavering faith and steadfast support of my parents and my brother, I would not have been able to complete this work. I am indeed very thankful to them and to my family members for the moral support I always received from them.

This work
is dedicated to
my late revered grandmother
Shrimati Madan Kunwar Kothari.
(May 25, 1925 – Mar 14, 2013)

TABLE OF CONTENTS

LIST OF ILLUSTRATIONS

Page

LIST OF TABLES

Page

1. INTRODUCTION

1.1. VECTOR NETWORK ANALYZERS (VNAs)

1.1.1. Background. A vector network analyzer (VNA) is an electronic instrument used to measure frequency dependent electrical properties of a device under test (DUT). This can be accomplished over a range of frequencies starting from a few kilohertz to hundreds of gigahertz [1, 2]. The electrical properties are related to the ratios of incident, reflected and transmitted signals (waves) and hence impedance and admittance of the DUT. These ratios are usually expressed in terms of scattering or S-parameters [2] also known as reflection and transmission coefficients. The device being analyzed may range from an electrical circuit to a section of reinforced concrete whose complex reflection and transmission parameters are sought and then related to useful information about its material composition. In order to understand S-parameters, consider the system shown in Figure 1.1, where a 2-port VNA is set up to measure the S-parameters of a DUT.

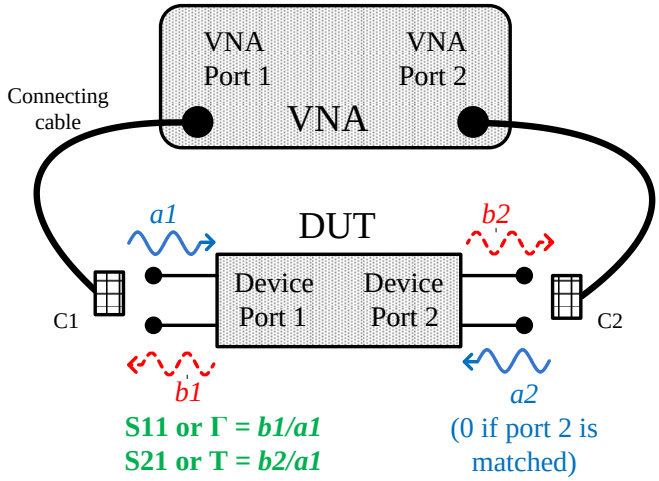

Figure 1.1. The reflection coefficient Γ and transmission coefficient T.

Prior to performing a measurement the VNA must be calibrated, i.e., all unknown and undesired internal signal reflections due to cable discontinuities within the VNA system and all the way to the ends of connectors C1 and C2 must be considered and compensated for. This process (calibration) will be further described in Section 2. For a calibrated VNA when port 1 is used as the RF source and *a1* is the voltage wave incident on the DUT, *b1* and *b2* will be the waves reflected from and transmitted through DUT respectively. Since the phase and magnitude of *a1* is known, those of *b1* and *b2* are then measured by the VNA. Reflection coefficient, Γ, or S_{11} is then the ratio of *b1* to *a1* and S_{21} - the transmission coefficient (T) is the ratio of *b2* to *a1*. Similarly, ratios at 2-port can be calculated when signal at port 2 is used as the source. Once Γ and T are known many other properties of the DUT can be inferred depending on the application. Modern day microwave and millimeter wave VNAs are used in a variety of applications such as measurement of distributed transmission line and lumped circuit impedances, high frequency circuit design, EMC [3], material characterization [4] and imaging [5], to name a few.

1.1.2. RF Detection. Signal measurement in a VNA can be coherent [1] or non-coherent [6]. In the coherent scheme, magnitude and phase of *a1, b1* and *b2* (see Figure 1.1) are measured directly as complex numbers and hence their ratios yield the S-parameters. Non-coherent VNAs commonly use standing-wave measurements to calculate Γ [6-15]. Traditionally, voltage standing-wave ratio (VSWR) measurements and owing to their broadband operating range, diode detectors have been used with waveguide-based systems for non-coherent and scalar RF measurements (in which only the magnitude of reflection coefficient |Γ| is obtained). Initially, using triodes (and later semiconductors), the commercial implementation of superheterodyne architecture-based coherent detection became possible and now it has become the prominent scheme for precision vector network measurements [2, 16, 17]. Vector network analyzers operating based on non-coherent schemes do not possess a relatively high dynamic range or a very wide bandwidth and suffer from relatively lower measurement accuracy [10] when compared to VNA designs based on tuned-receiver coherent detection scheme [1]. Yet, factors such as design simplicity and small size (i.e., portability via being hand-held), ease-of-use and the fact that they cost a fraction of that of a coherent VNA makes them

quite attractive for a number of applications involving nondestructive testing and evaluation (NDT&E) [4, 9]. Vector network analyzers can have one or multiple measurement ports but the research work described in this thesis focuses only on a one-port VNA.

1.1.3. One-Port VNAs. One port VNAs are commonly used to measure complex reflection coefficient (Γ) of a DUT. Non-coherent single port VNAs have been realized using a number of schemes: multi-probe schemes use several diode (i.e., power) detectors placed along a signal transmission path with either known distances between them [6, 7] or with known system S-parameters [11-13]. Using these detectors, the standing-wave voltage is measured at multiple points along the transmission line, in which a standing-wave is formed as a result of a reflected signal. Using at least three such measurements, as shown in Figure 1.2 using either multiple or a movable detector, a unique Γ can be estimated [6].

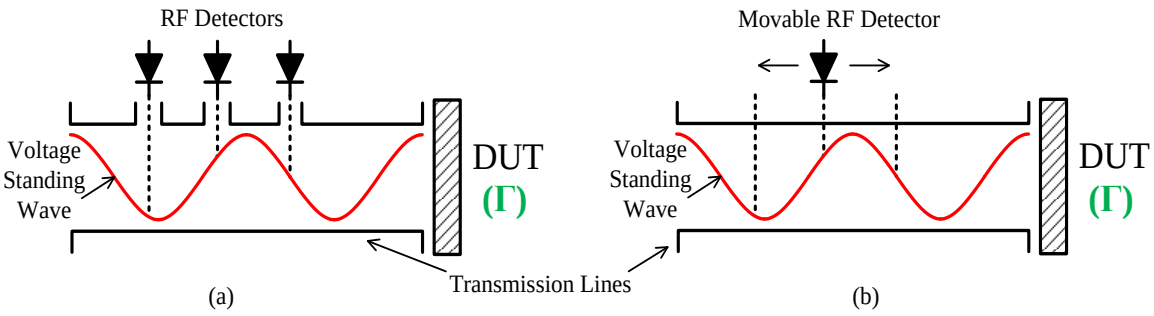

Figure 1.2. a) Multi-probe and b) movable detector based schemes for standing-wave measurement.

The problem with using multiple detectors is that each one has slightly different operating characteristics which must be taken into consideration while combining the multiple power measurements to obtain Γ. This process of "diode characterization" is explained in Section 2. Another problem associated with this method is that at relatively high frequencies it may not be possible to place several detectors adjacent to each other due to spacing requirements. In addition, mutual interaction among adjacent detectors adversely affects their voltage measurements. Alternatively, as shown in Figure 1.2 (b), a

single detector may be moved along the length of the transmission line [14] thereby removing the need for multiple detector characterization. However, the physical movement involved in this type of system is not conducive for rapid measurements and may produce measurement uncertainties.

Another approach known as the perturbation two port (PTP), uses a scalar network analyzer (SNA), a relatively expensive piece of equipment, and several two-port devices with specific and known S-parameters (or a single device with multiple such states) called PTP devices [15]. Such devices are connected between the DUT and the SNA. An SNA measures only the magnitude of reflection coefficient $|\Gamma|$. A number of these magnitude measurements in conjunction with the previously measured complex S-parameters of the PTP devices are then used to solve a set of equations to obtain five or six unknown parameters depending on the specific configuration [15, 18]. This puts very specific constraints on the insertion loss and through-phase properties of the required PTP devices. Their "magnitude-circles" need to intersect in the complex plane to arrive at a unique value for Γ and so they need to be carefully chosen. This procedure not only makes the approach complicated but the need for an SNA also makes it relatively expensive and cumbersome in addition to the fact that one of the two-port devices must have attenuation characteristics associated with it. However, since usually a commercial SNA is employed, system sensitivity may be higher than multi-probe standing-wave measuring systems.

As shown in Figure 1.3, instead of moving the detector, if the standing-wave *itself* is "moved" along the transmission line with respect to the location of a fixed detector a significant improvement over the movable-detector approach will result, and the above mentioned limitations associated with the latter approach can be overcome.

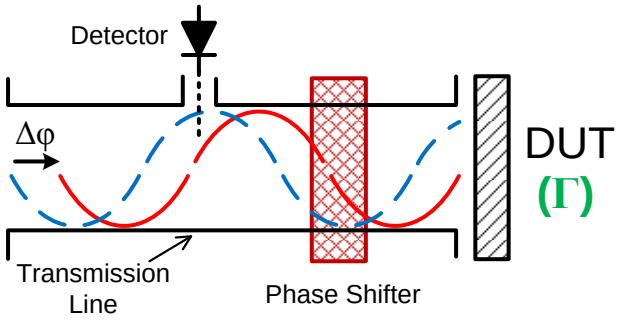

Figure 1.3. Single fixed detector with electronic phase-shifter showing change in voltage measured by detector when the standing-wave is moved by a phase of Δφ (blue to red).

Using this concept, several one-port VNA systems were developed with a single fixed detector used in conjunction with electronic phase-shifters [8-10] that "electronically" move the standing-wave over the detector location. These systems offer a number of advantages. Apart from being small, handheld and portable, they do not require physical movement of the detector. Only one detector is required for all measurements, eliminating the need for multi-step detector characterization and calibration process [12]. Also, unlike the design in [15], there is no need for several complex and physically separate PTP devices and a scalar network analyzer.

1.1.4. Previous Work. An initial version of such an electronic phase-shifter based one-port VNA was designed and successfully tested at X-band using a commercially available analog phase-shifter IC (Hittite HMC538LP4) [8]. The signal power for different, but known, phase shifts is measured using a single fixed detector. Using at least three standing-wave voltage measurements, it is possible to estimate a unique value for Γ [6, 8, 10]. To improve the accuracy, more than 3 measurements may be made and instead of the analytic approach in [6], Γ can be estimated iteratively [8-10].

At higher frequencies, such off-the-shelf phase-shifters are either difficult to obtain or do not exist altogether [9]. So, a novel electronically-controlled phase-shifter operating in Ka-band (26.5 – 40 GHz) was developed at 35.5 GHz in [9] and later improved to a wideband version in [10]. The design of these phase-shifters is based on the placement of a number of minimally-perturbing PIN diode-loaded slots along the waveguide wall with non-uniform spacing to prevent undesired resonances. These slots

are loaded with PIN diodes which act as electronic switches opening and closing the electric gap (current path) across the slot. Each diode has an ON (slot closed) and OFF (slot open) state. The Ka-band system in [10], for example, consists of 17 PIN diode-loaded slots placed on the broad dimension of a waveguide. Correspondingly, it provides for 18 different phase shift states from all PIN diodes being ON and all being OFF creating a combined phase shift of 78^{o} to 28^{o} for 26.5 to 40 GHz, respectively. The schematic of this system is shown in Figure 1.4.

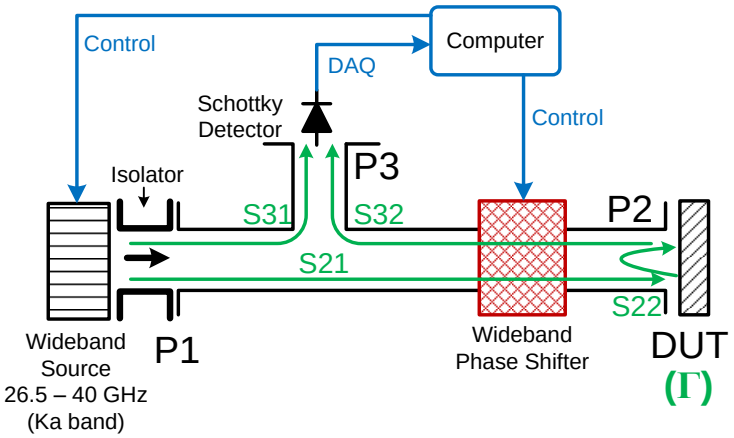

Figure 1.4. Ka-band one-port VNA based on electronic phase-shifter [10].

A personal computer is used to control the frequency sweep of the source and the phase-shifter. An isolator at P1 (port 1) ensures that no unwanted reflections enter the source. The RF travelling wave originates at P1 and together with its reflection from DUT at P2, forms a standing-wave in the transmission line. This is measured at a fixed location P3 using a Schottky diode detector, as shown. The process is repeated for the 18 states of this phase-shifter to obtain 18 distinct voltages used to form the standing-wave. By comparing this with its electromagnetic model, the unknown Γ of the DUT can be closely estimated. The VNA built using this system was developed and the (significantly improved) results were published in [10], as shown in Figure 1.5.

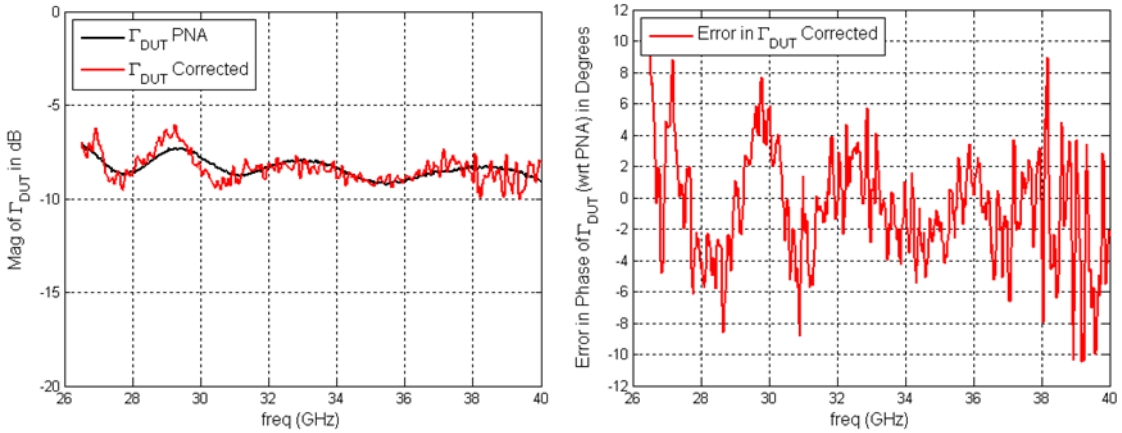

Figure 1.5. Results for the Ka-band VNA system of [10]; a shorted 3 dB attenuator is used as the DUT.

The major disadvantage of this and other one-port radiating-slot based VNAs is that they may not provide sufficient phase shift across the full operating frequency band. Periodicity and coupling between slots can cause resonances and degrade performance [9, 10]. Furthermore, to correct for unwanted reflections and losses in the system, a process of correction using three standard loads, called calibration, needs to be applied [8-10].

1.1.5. Current Work. Systems reported in [9, 10] were three-port devices with the detector port (P3) also included in the system characterization scheme using an adapter to model the signal reflections better. Some of their limitations can be overcome by using a full three-port model of the system with a fixed detector port using the same kind of adapter as P1 and P3. In this three-port system all ports are waveguides and the intermediate connectors are not moved once set. Now if reflections from ports 1 & 3 are blocked (using isolators), the source and detector mismatch will not affect the system (limited by the isolator's characteristics). Also, if no extension cables are used when connecting the DUT (at port 2), the characterization or S-parameters of this three-port device will not change (it should be mechanically stable) and all of the un-accounted errors described earlier, which were not included in the initial systems at X-band [8] and at Ka-band [9, 10] should either be removed or included in this characterization. Hence, there is no need for the three calibration standards and the usual process of calibration [19]. The only parameter which can vary is the power of RF source or if a different RF source is used. This leaves just one required correction: power scaling which can be

achieved using just one calibration-standard measurement such as a matched load or even refection due to radiation into "air", i.e., standing-wave measurement of a single DUT is sufficient to estimate its Γ. This makes the system "*calibration-free*".

Although, as stated above, an "error-free" system has been conceptualized, in practice there can still be errors due to "flange-mismatch" while connecting a load or the DUT to port-2. In waveguide measurements, these flange-mismatch errors are proportional to the electrical length of the mismatch which, in turn, is proportional to the frequency [20]. So, to achieve higher accuracy, a VNA system was developed at lower frequency or X-band (8.2 to 12.4 GHz) to demonstrate this concept and is shown in Figure 1.6.

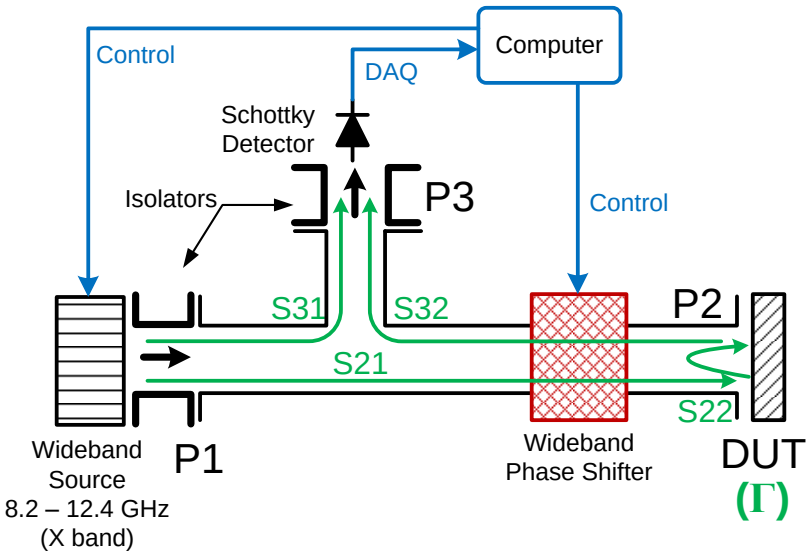

Figure 1.6. Block diagram showing the proposed calibration-free VNA.

This thesis details the modeling, simulations and measurements to realize this system, while showing that a calibration-free system of this type can be designed and built. Section 2 deals with design, characterization and testing of the discrete components which make up this X-band VNA system. Modeling of this three-port system is described in Section 3. The three-load based calibration technique is also described in this Section. Section 4 presents the sensitivity analysis of this system in which the effect of all

recognizable sources of error have been modeled based on both ideal and measured system models. Section 5 talks about the different measurements performed using this system to prove the concept of a “calibration free” system. Finally, Section 6 summarizes the work done.

2. SYSTEM DESIGN

2.1. INTRODUCTION

The proposed one-port phase-shifter based X-band VNA system comprises of four discrete components: RF Source (HP8510C VNA), a minimally perturbing coupler by which the standing-wave voltage is sampled, RF detector (Schottky diode) and a relatively low-loss electronic phase-shifter providing sufficient (>45º one way) phase shift. All of these components need to be wideband and operate throughout the X-band. A picture and the block diagram of this VNA are shown in Figure 2.1.

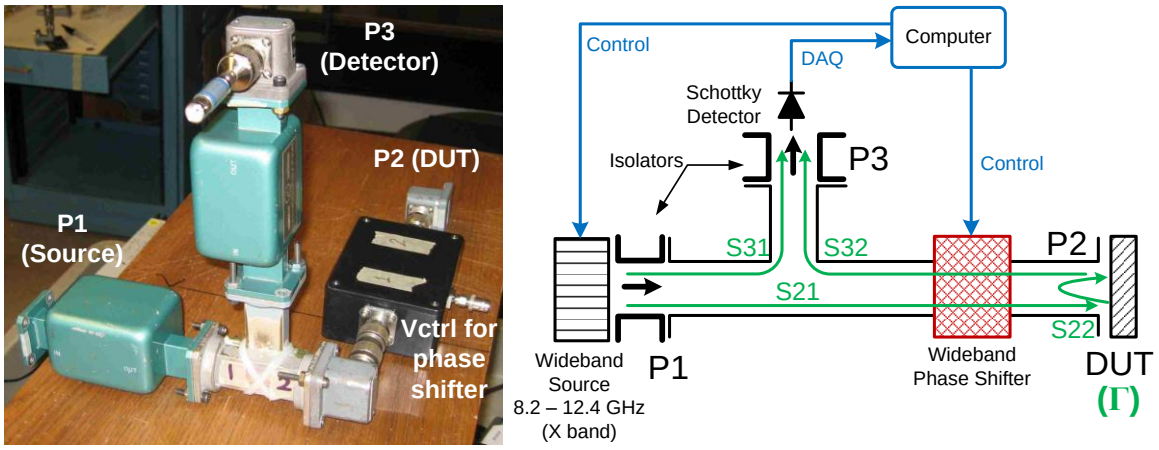

Figure 2.1. Proposed one-port VNA comprising of a three-port device.

Using a computer to control the source (HP8510C VNA) a travelling wave generated at a preset frequency from source (P1) travels through the phase-shifter and gets reflected from the DUT at P2. This reflected wave combines with incident wave to form a standing-wave in the transmission line between P1 & P2. While varying the phase shift provided by the phase-shifter (also computer controlled) through a set of predefined and known values, this standing-wave is sampled by a wideband coupler and measured using a Schottky detector set at port 3. The output of the detector is also read by the computer using a DAQ card. In this way, the whole system is automated. The design of these individual components and modeling and calibration of the complete system is described in this section.

2.2. -20 dB COUPLER

The function of the minimally perturbing RF coupler is to couple a small portion of the standing-wave into the RF detector (Schottky diode). As explained earlier, to include all possible sources of error, all internal reflections and mismatches of the VNA system including this coupler need to be fully and accurately characterized. While characterizing a multi-port device like this coupler, all ports are usually terminated with the same type of connectors. If these connectors are of different type, e.g., waveguide and SMA, a new mixed-port calibration methodology must be defined. The corresponding corrections should then be performed separately (post processing). This complicated process is beyond the scope of the present work.

The microwave coupler used in earlier version of the X-band VNA system [8], has one port terminating with an SMA connector and other two with waveguides. To avoid the mixed-port calibration, a SMA-to-waveguide adapter can be used as shown in Figure 2.2.

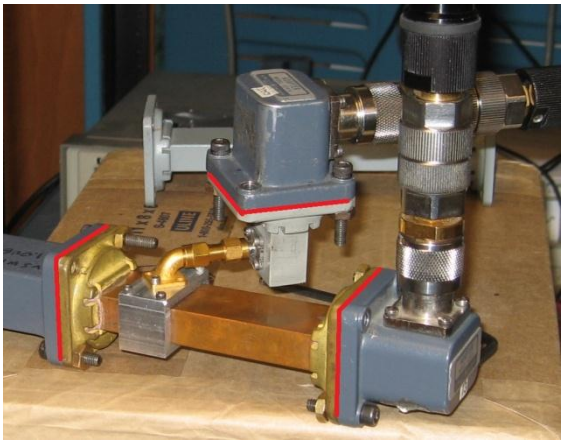

Figure 2.2. RF Coupler for the X-band VNA with the three waveguide reference planes marked in red (old design).

However, this makes the coupler mechanically unstable and any small movement can change its physical configuration. Consequently, in the present configuration, a complete three-port characterization of this device cannot be performed reliably and a new mechanically stable coupler with all three ports terminated in waveguide type

connectors was envisaged. Ideally, the signal coupled by this coupler should be small enough to minimally perturb the standing-wave, yet large enough to keep the coupled-signal power level from reaching the detector noise floor. The Schottky detector used here, operates in the square-law region till at least -30 dBm [21]. Considering possible power losses due to additional connections to this system (e.g., cables and connectors), a signal coupling of -20 dB should be optimum for this system. Since such a -20 dB coupler operating through X-band is not commercially available, one was subsequently designed and tested (as shown in Figure 2.3).

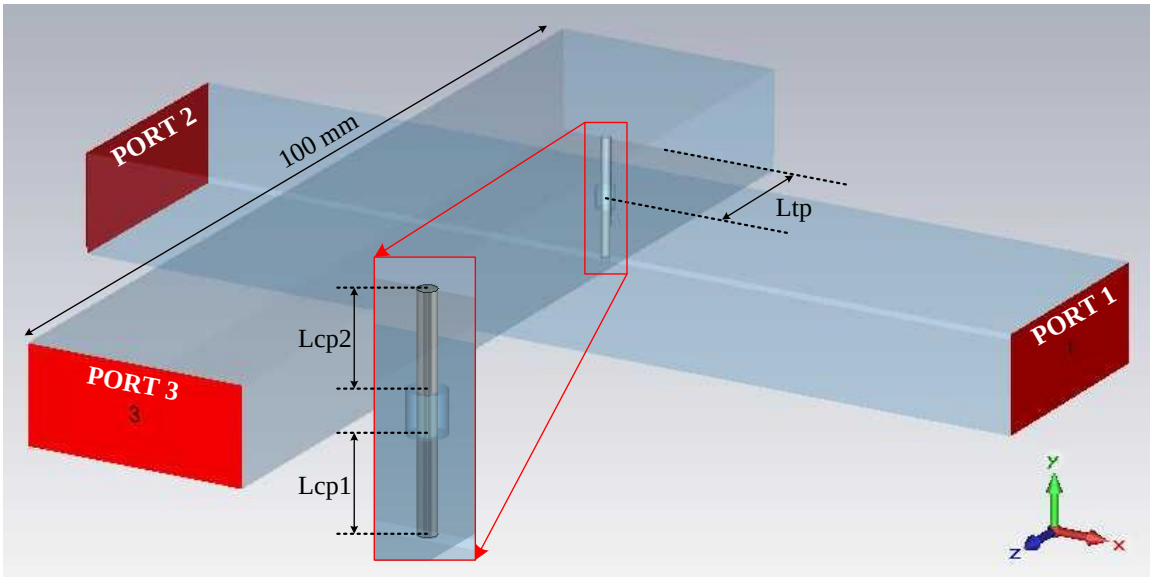

Figure 2.3. Diagram of the CST model used to simulate the RF coupler using standard X-band waveguides.

In this new design, two waveguides were used for coupling with a conductive wire in hole as the coupling mechanism. This is based on several RF design concepts but specifically, the operating principles of a magic-T and a wideband coax-to-waveguide adapter were successfully combined in this design.

Coupling-holes have traditionally been used for coupling RF signals [20]. A small coupling-hole is wideband in principle and the coupling magnitude can be controlled by varying the diameter of the hole. However, a simple hole causes resonance and changing the diameter of a hole, after device assembly, is not an easy task. So, a conductive wire

pickup pin was added to the hole. By varying the length of the pin, coupling can be fine-tuned easily even after assembling the device.

Finally, in the "coupled" waveguide, there are two ends – port 3 (detector) and a free end which is shorted at a distance of about λ/4 (at mid-band frequency) from the coupling-hole. The coupled signal is transmitted in both directions. The signal reflected from the short has a 180º phase shift and another 180º due to the extra λ/2 (2 × λ/4) path – making the net phase-shift at the coupling-hole zero. Consequently the two signals simply add up. This is the principle used in designing wideband RF adapters.

Simulations were performed in CST Microwave Studio to obtain a uniform signal coupling magnitude of -20 dB (|S31| = -20 dB) throughout the X-band by varying three parameters: length of shorted part of transmission line in the coupled waveguide (Ltp) and the length of conducting wire in both primary and coupled waveguides (Lcp1 & Lcp2). An optimum value of Ltp is first obtained for uniform broadband coupling as shown in Figure 2.4.

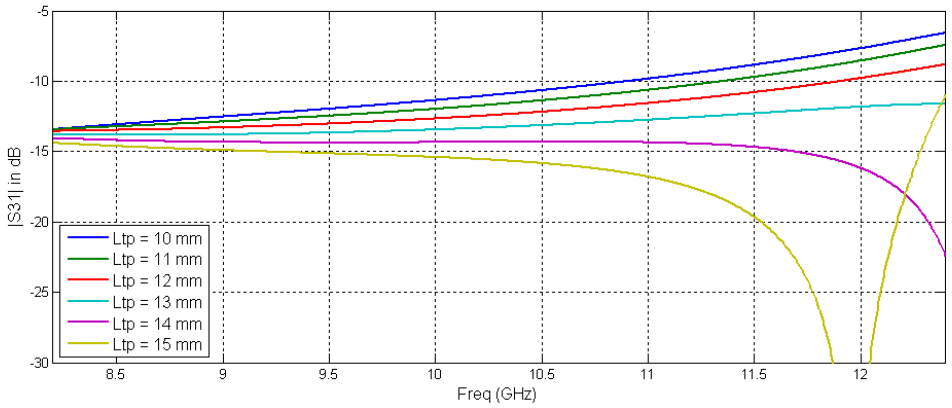

Figure 2.4. S31 for different values of length Ltp.

This optimum value of ~13 mm, as discussed earlier, corresponds to $\lambda_g/4$ at 8.7 GHz, where λ_g is the guide wavelength. Keeping Ltp as 13 mm, lengths of coupling pin Lcp1 (in primary) and Lcp2 (in secondary) are swept. As seen in Figures 2.5 and 2.6, the coupling |S31| rapidly increases with the pin-length.

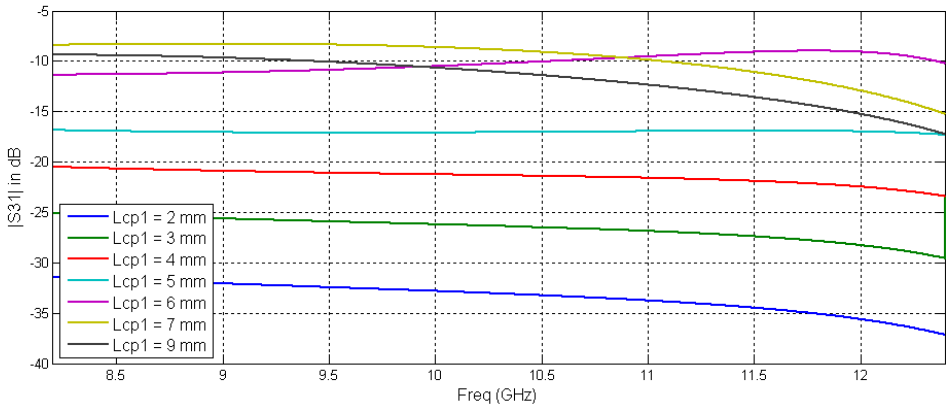

Figure 2.5. S31 for different coupling pin lengths Lcp1.

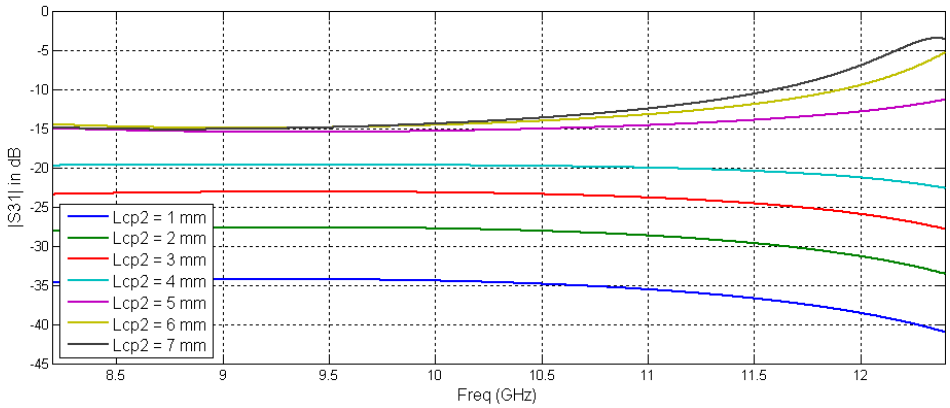

Figure 2.6. S31 for different coupling pin lengths Lcp2.

Lengths of 5 mm and 4 mm in primary and secondary waveguides respectively will provide the desired -20 dB coupling. Based on these parameters, an RF coupler was constructed. The coupler itself and a comparison of its simulation and the measurement results is shown in Figure 2.7.

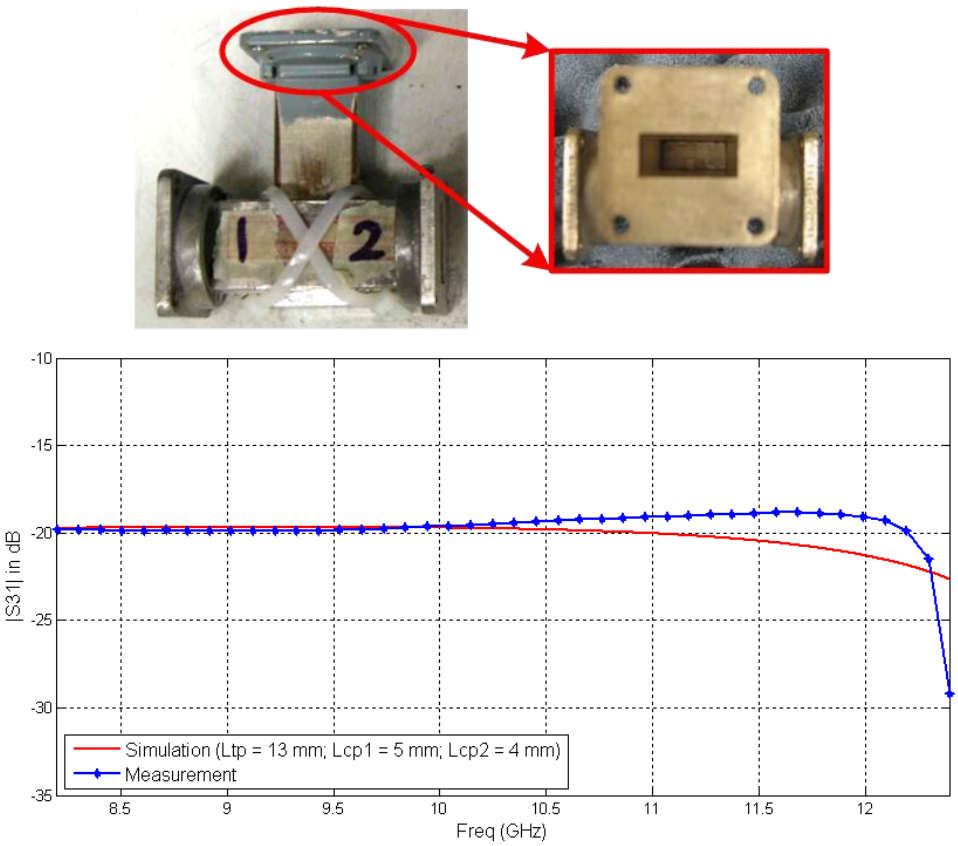

Figure 2.7. The X-band RF coupler, its top-view showing the coupling pin and the comparison of measured and simulated |S31| values.

The measurement results of coupling or |S31| in Figure 2.7 match well with the simulated value. After construction, the fine-tuning of pin-lengths described earlier, resulted in a broadband -20 dB coupling through the X-band.

2.3. PHASE-SHIFTER

2.3.1. Phase-Shifter Design. This is the most important component of this VNA system. It will be shown in Section 4 that for maximum sensitivity, a total standing-wave phase shift of $\lambda_g/4$ or 90º is the optimum value. Also, the phase-shifter should be low-loss to maintain a high SNR. So ideally, the phase-shifter should shift both the signal incident on and reflected from the DUT by 45º each so that the net phase shift seen in the

resulting standing-wave is 90º. As an improvement to the analog phase-shifter IC used in [8] (HMC538LP4), another Hittite IC, HMC935LP5E with lower insertion loss of -4 dB [22] compared to 8 dB for the previous one was used to build the phase-shifter shown in Figure 2.8.

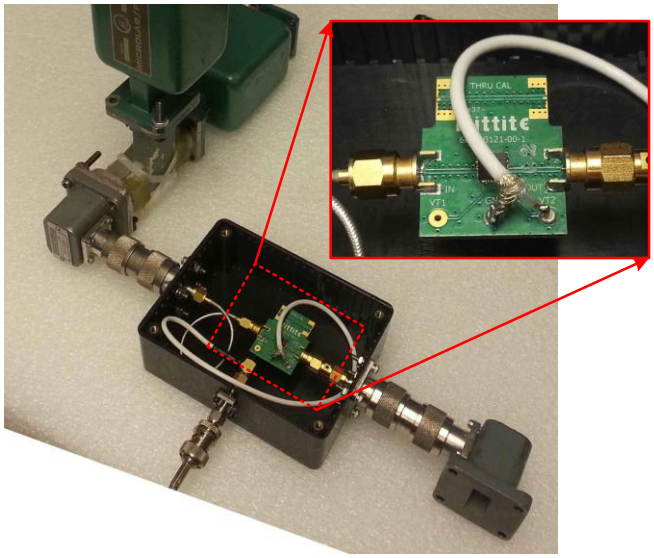

Figure 2.8. VNA system showing phase-shifter IC arrangement.

The position of phase-shifter relative to other components is very important. It is connected between the coupling system (leading to detector, P3) and the DUT port (P2) so that only the reflected signal is phase-shifted (once on the forward path and second on the return path). Thus, this resulting standing-wave changes when the phase shift is varied – which is the basic operating principle of this VNA system. Insertion loss and phase shift characteristics of the assembled VNA system are shown in Figure 2.9.

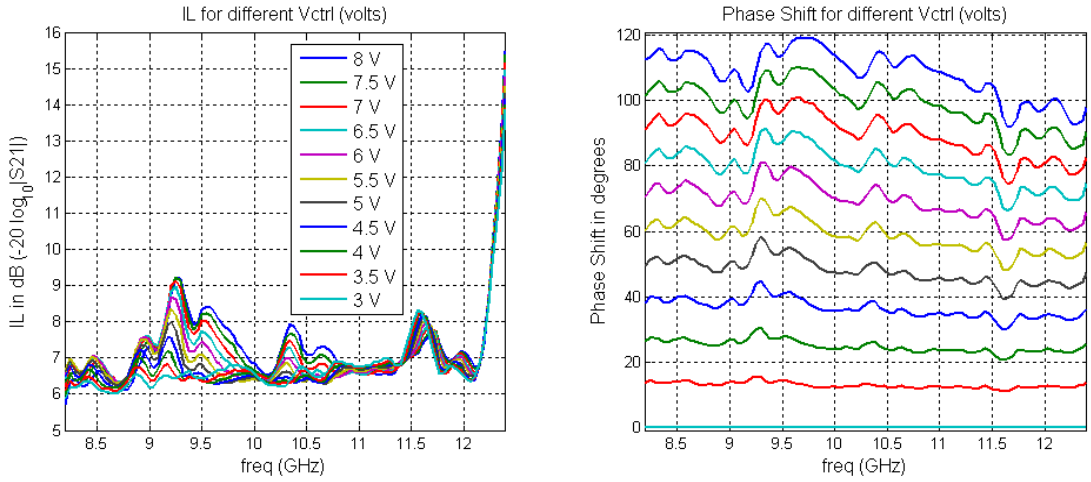

Figure 2.9. Insertion loss (one way) and 11 phase shifts in the X-band VNA system for the 11 different analog control voltages (3V to 8V).

Depending on the phase shift generated by the phase-shifter, the insertion loss (one way) varies between 6 to 9 dB. This can be attributed to 4 dB from the phase-shifter IC [22] and the rest to the reflection and transmission losses in the system. The phase shift generated by the phase-shifter is a function of DC analog voltage (Vctrl or control voltage) input to the device [22] using the analog output of DAQ card controlled using a computer. These 11 different phase shifts generated by the phase-shifter (relative to the first state) for a Vctrl of 3 to 8 volts are also shown. The total phase shift (one way) varies between 90 º and 120º and although more can be generated using this IC, this is well above the optimum value of 45º. Although insertion loss varies by a significant amount as a function of both frequency (Figure 2.9) and phase shift, the device characterization takes these into account for each state and calculations for each frequency is done independently.

2.4. DETECTOR CHARACTERIZATION

The detector used in these one-port VNAs is a reverse-biased (negative polarity) Schottky diode preceded by a matching circuit (the Krytar 202B detector of [21]). Output of this detector diode follows the square law for a wide range of input power, i.e., its output is a voltage proportional to the square of the input standing-wave voltage. This range is called the “square-law region”. Any measurements lying outside this square-law

region constitute a non-linear output, i.e., output voltage is not proportional to input power and needs to be corrected. A thorough characterization of the detector in and beyond the operating range will ensure that there is no non-linearity in the measured output. To characterize the detector, setup shown in Figure 2.10 was used.

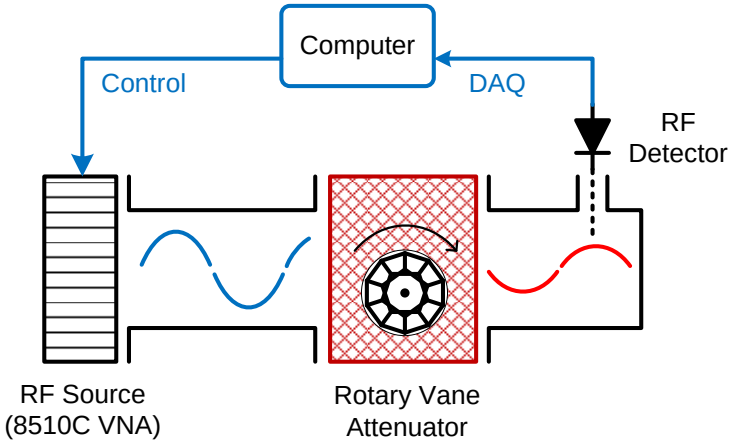

Figure 2.10. Setup for detector characterization.

A rotary vane attenuator was used to attenuate a signal from RF source (8510C VNA) by known increments. For each value of attenuation, the output of the detector was measured using a DAQ (data acquisition) system. This was repeated for 101 frequency points through X-band (8.2 to 12.4 GHz) by sweeping the source frequency. The resultant detector characterization is shown in Figure 2.11.

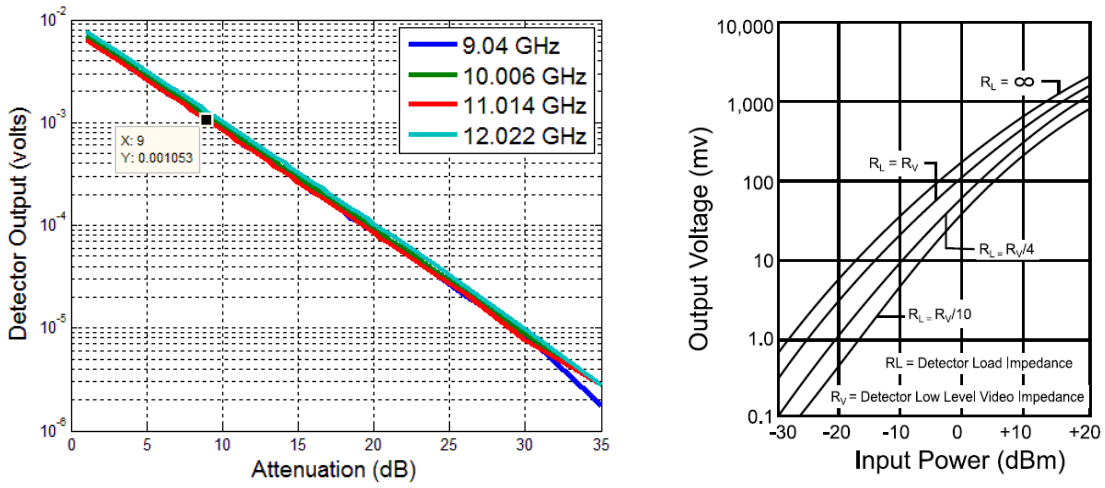

Figure 2.11. Krytar Schottky detector characteristics measured (left, only 4 frequency values are shown) and from datasheet [21] (right).

As seen from the measured data shown for four frequency values (Figure 2.11), an attenuation of 9 dB, for instance, results in a detector voltage output of 1.053 mV. Hence, we know the relative power level (and so the relative voltage level) of the actual standing-wave. Using these values to "convert" the measured voltage to the relative power should remove any non-linearity from the measured data. The correction applied on a measured voltage standing-wave using an open ended waveguide radiating into air as the DUT is shown in Figure 2.12.

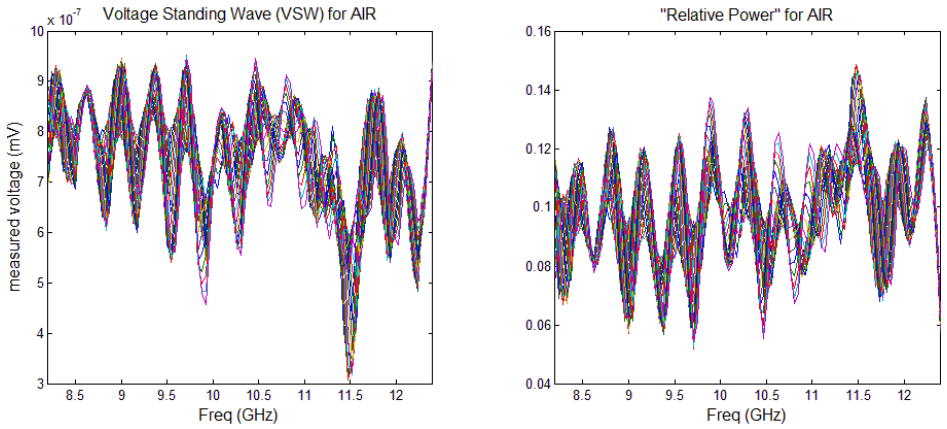

Figure 2.12. Measured voltage and the corresponding converted "relative power" for open-ended waveguide radiating in air (AIR) for all states of the phase-shifter.

3. SYSTEM MODELING AND CALIBRATION

3.1. INTRODUCTION

Three concepts which form the basis of the operation of these one-port VNAs are the standing-wave sampling, phase-shifting and the estimation of Γ. Their explanation, system modeling and factors affecting the performance of these phase-shifter based one-port VNAs are discussed in this section.

3.2. CALCULATION OF Γ BASED ON PHASE SHIFT

To understand and illustrate the concept of Γ calculation by phase shifting the signal, standing-wave voltage was measured using a diode detector fixed in an X-band (8.2 – 12.4 GHz) waveguide for a source frequency of 10.5 GHz. Standing-wave "movement" or phase shift was achieved using a movable short. Using the equations derived in [6], and measurements with 2 mm spacing (3 points per set) Γ was calculated analytically, as shown in Figure 3.1.

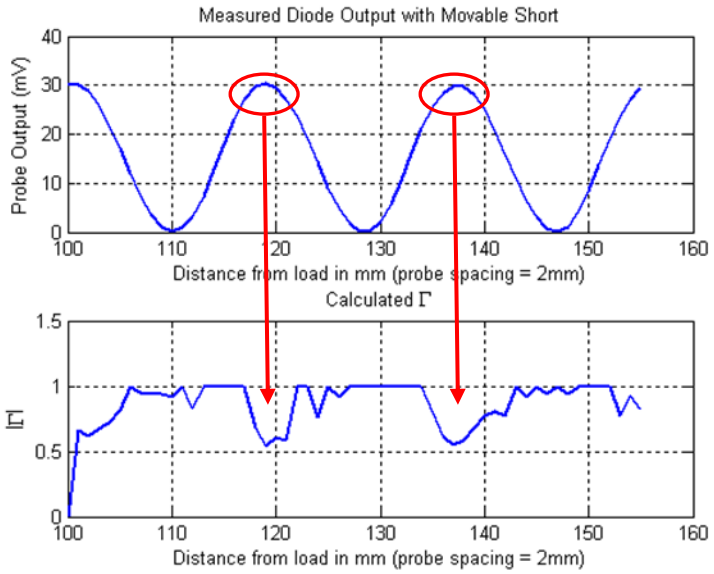

Figure 3.1. Measured standing-wave and calculated Γ.

As explained in [6], the higher the magnitude of measured power (standing-wave voltage), more is the sensitivity of Γ calculation to any measurement error (or operator error). Consequently, for a high-reflection load like the one used in this case – short (|Γ| = 1), the measurement near the standing-wave maximum results in an incorrect estimate of Γ – as clearly seen in Figure 3.1. Detailed results are shown in Appendix A. Automating the measurement system, using a phase-shifter and iterative estimation of Γ in place of the three-point based calculation described above is expected to remove such errors.

3.3. ITERATIVE Γ ESTIMATION

These one-port VNAs have three main components: an RF Source, an RF detector (Schottky diode) and a relatively low-loss electronic phase-shifter providing sufficient (>45º one way) phase shift. All of these components need to be wideband. Iterative estimation of Γ using this system requires modeling the standing-wave pattern inside the waveguide. This model is formed using S-parameter measurement as explained in the following section.

3.3.1. System Model. Measuring all S-parameters of a system or device is termed characterization because by using these measured S-parameters, all other standing-wave parameters can be accurately modeled. Theoretically, a system with any number of ports can be modeled using its S-parameters. But practically, developing models for parameters in a system with more than 2 ports requires extensive calculations to simplify the signal flow graph unless simplifying assumptions are used as discussed below. A general three-port device which makes up the one-port VNA can be modeled as shown in Figure 3.2.

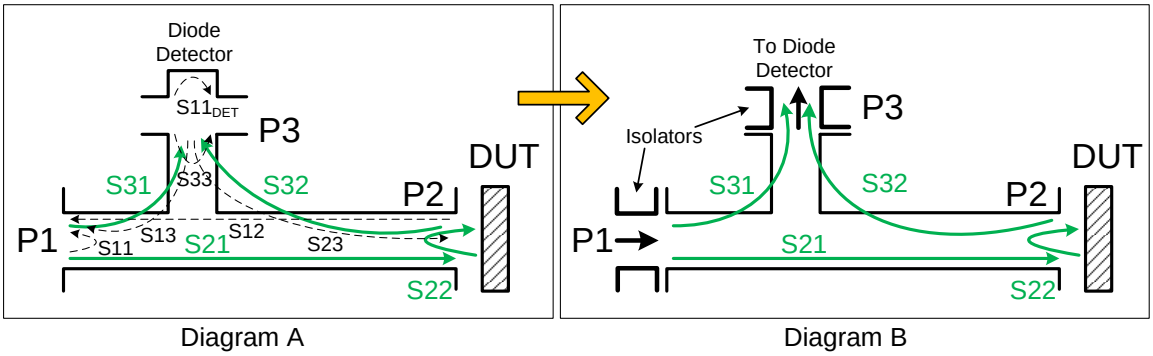

Figure 3.2. S-parameters of: (A) general three-port system, and (B) the simplified version as a result of using isolators.

Diagram A represents the generic or complete system model and shows all the S-parameters of the three-port device (total 9) and S11 of detector. A set of these 9 three-port S-parameters are measured for each of the different phase-shifter states. Diagram B is the reduced model and shows the effect of adding isolators to port 1 & 3 (P1 & P3). These isolators remove the effect of all parameters except Γ, S21, S22, S31 and S32. The signal flow graphs for Diagram A and Diagram B in Figure 3.2 are shown in Figure 3.3.

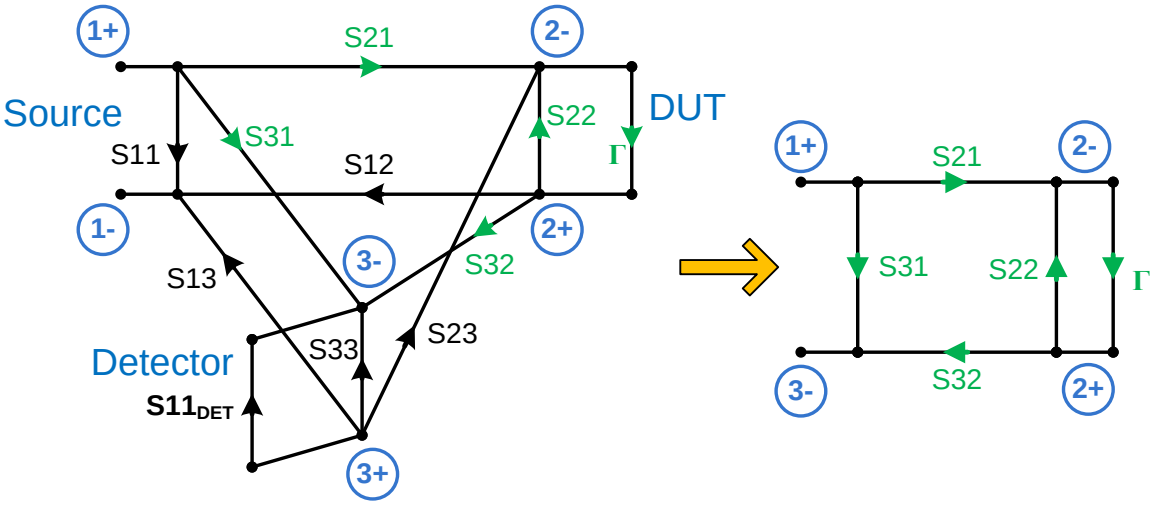

Figure 3.3. S-parameter signal flow graphs for system of Figure 3.2.

These flow graphs can be simplified by applying Mason's Gain Rule to obtain the equivalent S-parameter (Seq) at the detector port (port 3), as shown below:

Solution of the complete three-port model:

$$LHS = \left(1 - S11^{DET}\ S33\ \right)\left(\left(1 - \Gamma\ S22\right)\left(1 - S11\ S^{ISO}\right) - \Gamma\ S12\ S21\ S11^{ISO}\right)$$

$$RHS = S11^{DET}\left(S31\ S11^{ISO}\left(\Gamma\left(S12\ S23 + S13\ S22\right) - S13\right) + \Gamma\ S32\left(\left(S21\ S13 - S11\ S23\right)S11^{ISO} + S23\right)\right)$$

$$Seq = \frac{S31\left(1 - \Gamma\ S22\right) + S21\ S32\ \Gamma}{LHS - RHS} \qquad (1)$$

or,

$$Seq = \frac{S31\ \left(1 - \Gamma\ S22\right) + S21\ S32\ \Gamma}{\left(1 - S11^{DET}\ S33\right)\left(\left(\ 1 - \Gamma\ S22\right)\left(\ 1 - S11\ S11^{ISO}\right) - \Gamma\ S12\ S21\ S11^{ISO}\right) - S11^{DET}\left(S31\ S11^{ISO}\left(\Gamma\left(S12\ S23 + S13\ S22\right) - S13\right) + \Gamma\ S32\left(\left(S21\ S13 - S11\ S23\right)S11^{ISO} + S23\right)\right)}$$

Solution of the simplified model:

$$Seq = S31 + S21\ S32\ \frac{\Gamma}{1 - S22\ \Gamma} \qquad (2)$$

Here, apart from Sij, the three-port S-parameters of the VNA, S11 of the detector ($S11^{DET}$) and S11 of the isolator at port-3 ($S11^{ISO}$) have also been included. These two models can be used to predict the precise standing-wave voltage measured at port-3 for a known value of Γ of DUT. These models also include the phase-shifter and so, all the S-parameters are measured for each phase shift forming an S-parameter matrix. For each such measured S-parameter matrix, a unique Seq is obtained (Γ remains the same in all). The standing-wave voltage (V_{SW}) at port 3 (P3 in Figure 1.4) is proportional to Seq. But the diode detector output is proportional to the power of the standing-wave. Hence;

$$V_{SW} \propto Seq \qquad (3)$$

As described earlier, output of the diode detector is proportional to the power of this signal and is modeled as:

$$P_{SW} \propto \left|V_{SW}\right|^2 \Rightarrow P_{SW} = C\left|Seq\right|^2 \qquad (4)$$

Here, C is proportionality constant called the power scaling constant. So, two models of this standing-wave are obtained – the complete model and a simplified model. If the assumption of isolation (no reflections) at P1 and P3 holds, the simplified model can be used for all practical purposes.

3.3.2. Testing with Several DUTs. To test and see the functionality of the calibration-free one port VNA system described thus far, numerous measurements were performed. Eight X-band microwave loads were used for the analysis: a short, three shims (3 mm, 5 mm and 9 mm), a matched load, an attenuated short with frequency dependent attenuation, a wideband 3 dB attenuated short and an open-ended waveguide radiating into air, as shown in Figure 3.4.

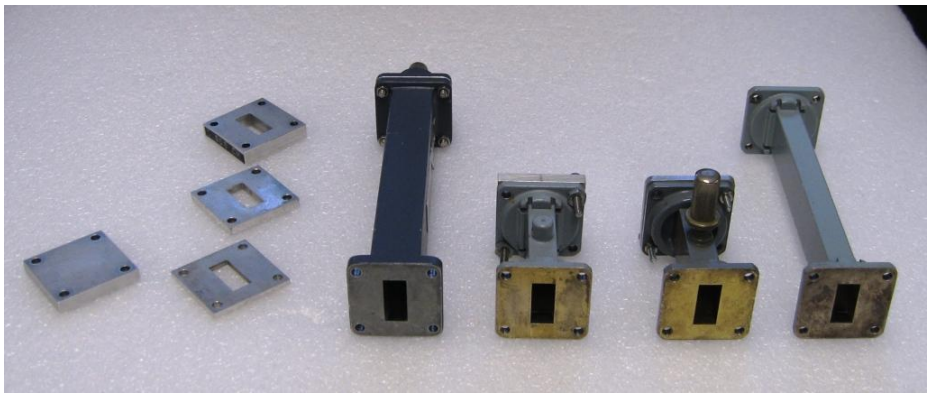

Figure 3.4. The Calibration loads and DUTs used to test the X-band VNA - in order: short, shims (3 mm, 5 mm and 9 mm), matched load, two attenuated shorts (variable and 3 dB) and an open-ended waveguide radiating into air.

The reflection coefficients (S11) of these eight devices were measured using a commercial VNA (HP8510C), as shown in the complex plane in Figure 3.5.

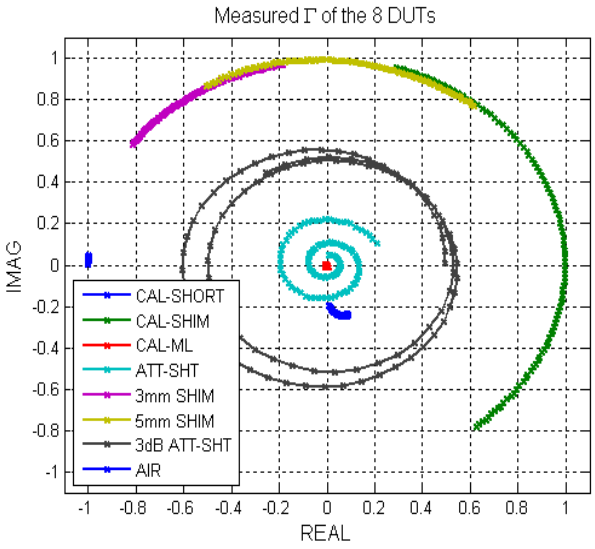

Figure 3.5. Measured reflection coefficients of the eight DUTs using an HP8510C VNA.

The results show that these eight DUTs together span a broad range of Γ values across the entire complex plane (in terms of both magnitude and phase). One of these loads, the variable attenuated short (ATT-SHT), has a Γ with a wide magnitude variation across X-band (-25 dB to -13 dB). This particular Γ has been used as the primary parameter to compare different techniques and measurements. Its magnitude and phase are shown separately in Figure 3.6.

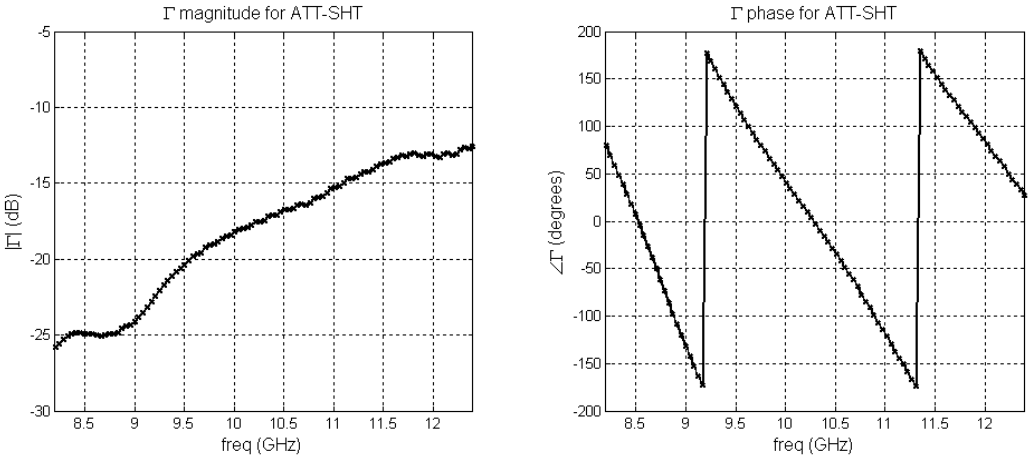

Figure 3.6. Measured magnitude and phase of the variable attenuated short.

3.3.3. Estimation of Γ. Reflection coefficient Γ is estimated by comparing the system model of equation 4 to the measured standing-wave using an iterative process. The S-parameter measurement (characterization) for system modeling needs to be performed only once using a coherent VNA system. It can then be used with any of the DUT standing-wave measurements to estimate Γ. Moreover, these DUT standing-wave measurements may be performed with an altogether different microwave source because a coherent VNA is not required for standing-wave measurements. Since these measurements are performed at different instances and may use different microwave sources, the input power level and hence the standing-wave voltages may vary. Hence, a power scaling constant, "C" is used to scale the measurements. To calculate the value of this constant, one DUT with a known Γ needs to be used. If the phase shifter introduces *n* number of discrete and consecutive phase shifts, the corresponding *n* measurements made using the Schottky detector, form a standing-wave. If the Γ of DUT is known, using the system S-parameter model described in equation 4, *n* values of P_{SW} are obtained. The corresponding ratios of these *n* values for a matched load are shown in Figure 3.7.

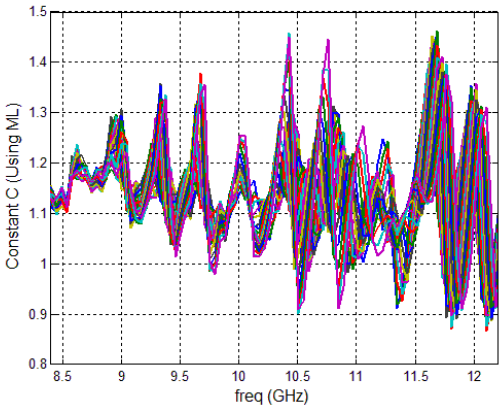

Figure 3.7. Calculated constant "C" using measured Matched Load voltages for all states of the phase-shifter.

Ideally, these *n* values shown in Figure 3.7 should be exactly same since they are the ratios of measured standing-wave and its corresponding model but inaccuracies in the measurement and system model cause them to be slightly different. These inaccuracies

higher with high-reflective loads (Short and Shim) and so, for this calculation, a matched load or some other DUT with a low |Γ| should be used. The average of these *n* values for each frequency point is used as C.

To estimate an unknown Γ, the same two sets of values, i.e., measured standing-wave for the DUT and C × modeled value are compared iteratively using error-minimization to estimate Γ. The estimation results for the eight DUTs of Figure 3.5 are shown in Figure 3.8.

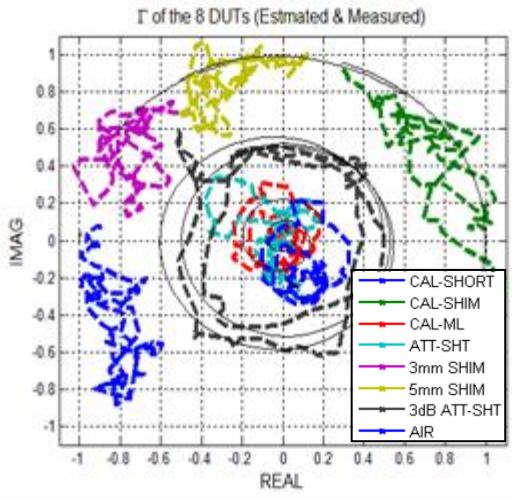

Figure 3.8. Reflection coefficients of the eight DUTs on a complex plane (thin black curves show the corresponding measured Γ).

Even though a full characterization was used for this X-band VNA system, estimation results are clearly erroneous. Although, the estimates are not entirely random and they lie relatively close to the HP8510C VNA measurements, the error in estimation is large and its cause or origin is not clear. So, the well-known three-term calibration procedure [19] is applied on these results to see whether the errors seen above are deterministic.

3.4. CALIBRATION

The three-term calibration procedure models all the errors present the system as three terms of error adapter shown in Figure 3.9.

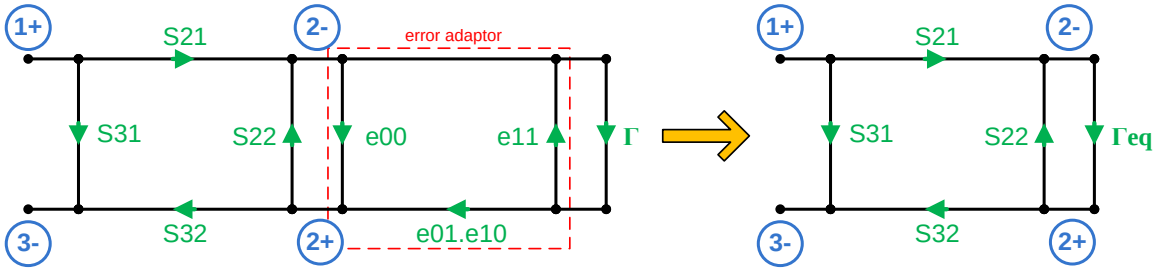

Figure 3.9. Equivalent signal flowchart showing the S-parameters, the fictitious error adapter and its equivalent.

These three error terms are known as directivity (e00), port-match (e11) and tracking (e01.e10). As shown in [19], and similar to the "simplified system model" of the previous section, the signal flow graph of Figure 3.9 can be simplified using Mason's gain rule to obtain:

$$\Gamma eq = e_{00} + e_{10}e_{01}\frac{\Gamma}{1 - e_{11}\Gamma} \tag{5}$$

simplifying,

$$e_{00} + e_{11}\Gamma(\Gamma eq) - \Gamma\Delta_e = \Gamma eq \tag{6}$$

where,

$$\Delta_e = e_{00}e_{11} - e_{10}e_{01} \tag{7}$$

Equation (6) is a linear equation with three unknowns: e_{00}, $e_{11}$and Δ_e. Mathematically, if we have three sets of values for Γ and Γeq, (total of six known Γ values) we can find these three unknown variables or "error-terms" as shown in the following matrix equation:

$$A\ X = B \tag{8}$$

where,

$$A = \begin{pmatrix} 1 & \Gamma_1\Gamma eq_1 & \Gamma_1 \\ 1 & \Gamma_2\Gamma eq_2 & \Gamma_2 \\ 1 & \Gamma_3\Gamma eq_3 & \Gamma_3 \end{pmatrix}; X = \begin{pmatrix} e_{00} \\ e_{11} \\ \Delta_e \end{pmatrix} \text{ and } B = \begin{pmatrix} \Gamma eq_1 \\ \Gamma eq_2 \\ \Gamma eq_3 \end{pmatrix}$$

Practically, this means using three loads with known reflection coefficients (Γ). In these phase-shifter and the waveguide-based one-port VNA systems, the calibration loads used are: short, shim of a known length and a matched load. Equivalent or apparent reflection coefficient, Γeq is found for each of these loads using the estimation procedure described in the previous section. Using these six known Γ values, the three unknown error-terms can be deduced as shown in Figure 3.10 and the system is ready for measurement of any unknown load.

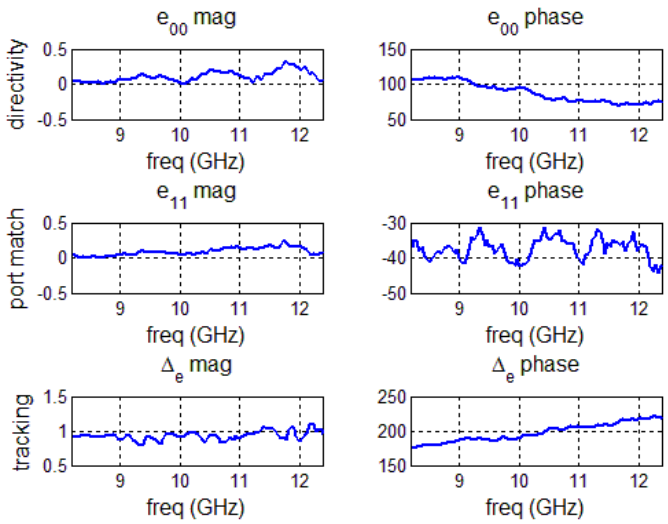

Figure 3.10. The three error terms found using measurements of the three "calibration loads" (i.e., short, 9 mm shim and matched load).

Applying these three error-terms, to correct the estimated results of Figure 3.8, the corrected or calibrated Γ values shown in Figure 3.11 are obtained.

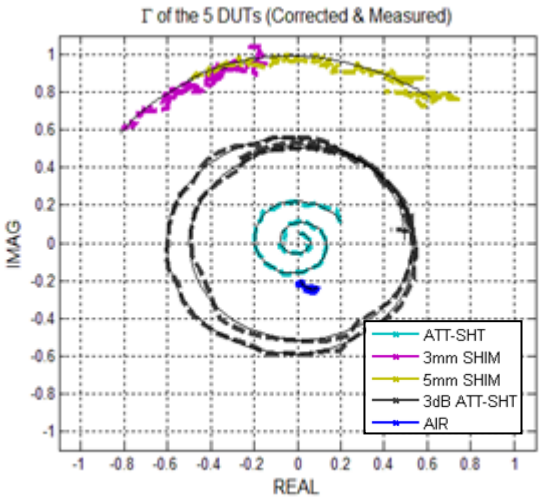

Figure 3.11. Corrected and measured Γ of the five DUTs shown on a complex plane.

In Figure 3.11, the three "calibration loads" are not shown as they will match perfectly. Details and individual steps of this estimation and calibration (correction) process are shown in Appendix C.

Despite the expectation of a calibration-free system, this X-band system works well only when calibrated, as shown here. The objective of this research has been to remove the need of this calibration entirely or limit it to the measurement of just one freely available load i.e., air - making the one-port VNA system calibration-free. By removing the need for calibration, these errors will not vanish from the system. They will just be included in a more precise characterization model of the system. The addition of two isolators at ports 1 and 3, converting all the ports to waveguide so that a complete three-port calibration can be performed and a number of simulations and measurements described in the following sections are all steps taken towards achieving this aim.

3.5. FACTORS AFFECTING PERFORMANCE

The performance of this one-port VNA depends on the following seven major factors described in [8]:

i. detector measurement noise floor and sensitivity,
ii. repeatability and accuracy of detector characterization,
iii. losses in phase-shifter and the overall system,
iv. DUT characteristics, i.e., low and high reflection coefficients,

v. repeatability in producing phase shifts,
vi. number of phase shifts and,
vii. total phase shift and increments between consecutive shifts,

The effect of increments between consecutive phase shifts and their total number are not analyzed in this thesis and can be found in [8]. All other parameters have been analyzed as explained below.

Signal-to-noise ratio (SNR) is the ratio of signal power to noise power. Like every other electronic instrument, the Schottky detector has a noise floor which is essentially the power level below which it cannot distinguish between a signal and noise (thermal noise, phase noise, etc.). This noise floor can be lowered or reduced, by averaging in certain cases, like that of thermal noise. If power of the signal coupled into the detector is close to its noise floor (due to either low signal coupling or a high noise floor), it is difficult to distinguish signal from noise and the resulting SNR will be low. Moreover, the variations in noise, being significant compared to the signal power, may also affect the signal itself. Losses in the phase-shifter (its insertion loss), cause the signal level to decrease, moving it closer to the detector noise floor - thereby reducing the SNR. The absolute value of $|\Gamma|$ also affects the estimation. Lower the $|\Gamma|$, smaller the reflected wave is and since a standing-wave is the phasor addition of incident and reflected waves, the variations in standing-wave are less. A numerical analysis highlighting these relationships in a quantitative manner is also shown later in Section 4.

3.6. EFFECT OF LOW PHASE SHIFT

The systems based on the radiating-slot design, as described earlier, suffer from low phase shift in a significant part of their operating range. The cause of poor performance of an earlier VNA designs was established as low phase shift by performing a unique measurement. Having a low phase shift can be a major disadvantage and was one of the considerations while choosing to work at low frequency of X-band for the calibration-free VNA, as described in this thesis. Hence, this setup and the corresponding measurements are explained here. Subsequently, the system of [10] was developed with highly improved performance.

Among the several electronic phase-shifter based one-port VNAs discussed earlier, the system developed in [9] was designed to operate at a single frequency of 35.5 GHz (within Ka-band). In an attempt to make the system wideband, a new phase-shifter similar to the one used in [9] was developed. The corresponding VNA performance was not good. This earlier version of the Ka-band VNA system, with a low phase shift, had seven radiating slots loaded with PIN-diodes on the broad dimension of the waveguide (consequently, eight phase-shifter states). It was optimized during its design stage to minimize insertion loss and maximize the phase shift by making the spacing between the slots non-uniform. The measured maximum and minimum insertion loss (among all eight states) and total phase shift characteristics of this wideband device are shown in Figure 3.12.

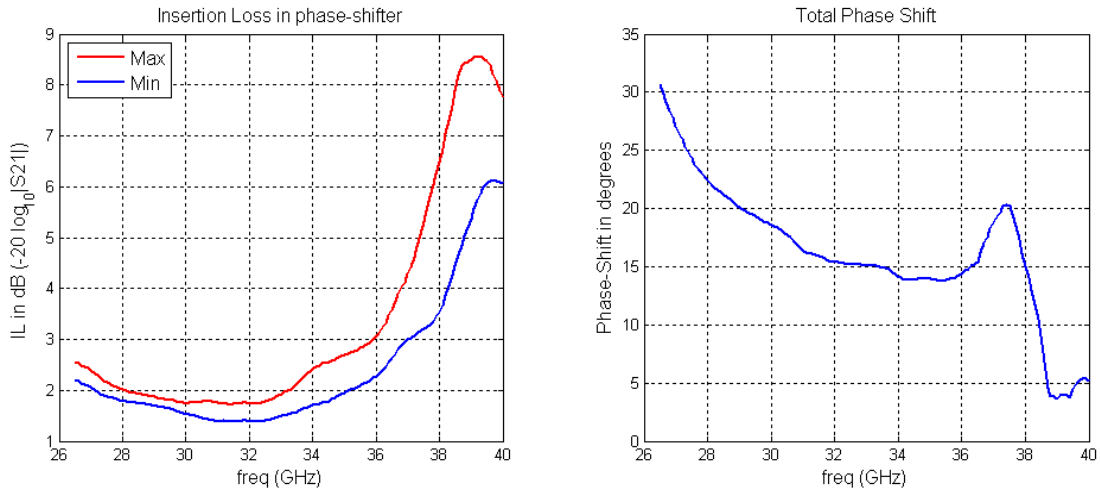

Figure 3.12. Measured loss and total phase shift of the Ka-band phase-shifter based VNA with non-uniformly spaced slots.

It is clear from the figure that the loss in the phase-shifter is relatively high at higher frequencies and the total phase shift provided is low across most of the band. Reflection coefficient Γ of a shorted 3 dB attenuator was estimated using the standing-wave measurements described earlier and the results were compared to measurement using a commercial VNA (Agilent N5245A PNA) as shown in Figure 3.13.

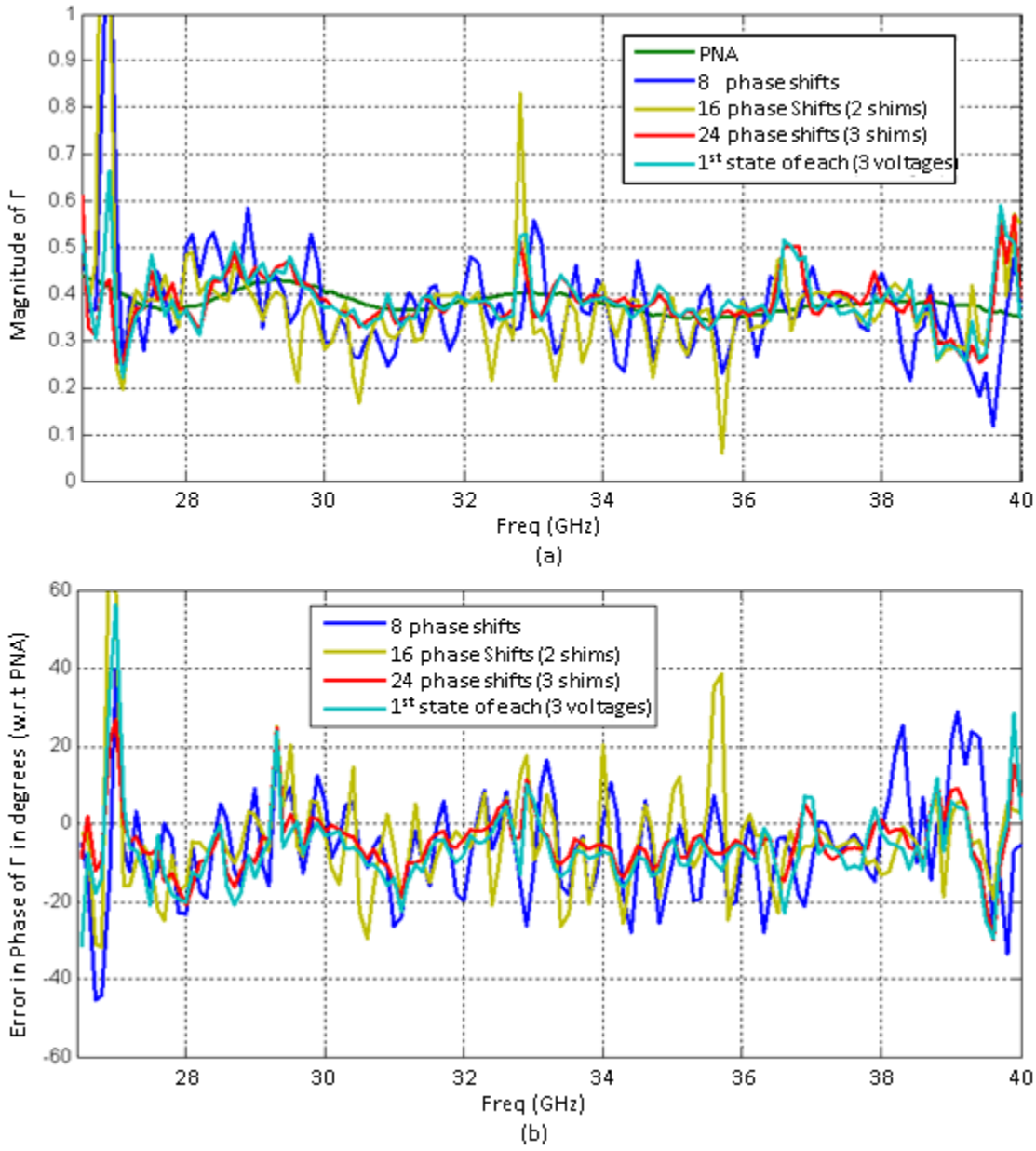

Figure 3.13. (a) Estimated |Γ| and (b) error in ∠ Γ for measurements with the non-standard 4.61 mm shim.

The estimated |Γ| using the eight phase-shifter states (blue) has a relatively high error compared to the actual value - the PNA measurement (green) as seen in Figure 3.13 (a). Figure 3.13 (b) has the corresponding phase errors referenced to the measured phase. As explained in the previous section, many factors can lead to such an error in Γ estimation. To ascertain if low phase shift is the cause of this error, a novel measurement with a non-standard shim was performed.

A shim is inserted between the measurement port (P2) and the DUT, and another set of standing-wave measurements performed. Each one of these new measurements is essentially, the phase-shifted versions of the previous eight measurements. Value of this phase shift is determined by the length of the shim. If these two measurements are combined, a new measurement set with double the old phase shift (sixteen phase shifts) is obtained, i.e., if φ was the total phase-shift provided by the phase-shifter, phase shift in these sixteen new measurements is 2φ, i.e., double the old phase-shift. Also, this shim is easily included in the system model using its electrical length (i.e., $\beta l = 2\pi l/\lambda$, see [20]), where l is the electrical length of the shim, and β is the wavenumber.

Length of these commercially available shims (3 mm, 6 mm at Ka-band) is usually equal to multiples of wavelength (at mid band frequency). In the standing-wave sampling method being used in the one-port phase-shifting VNAs, this corresponds to shifting the standing-wave in multiples of wavelength, i.e., zero phase shift. Hence, a new shim with a non-standard length (4.61 mm) was fabricated as shown in Figure 3.14.

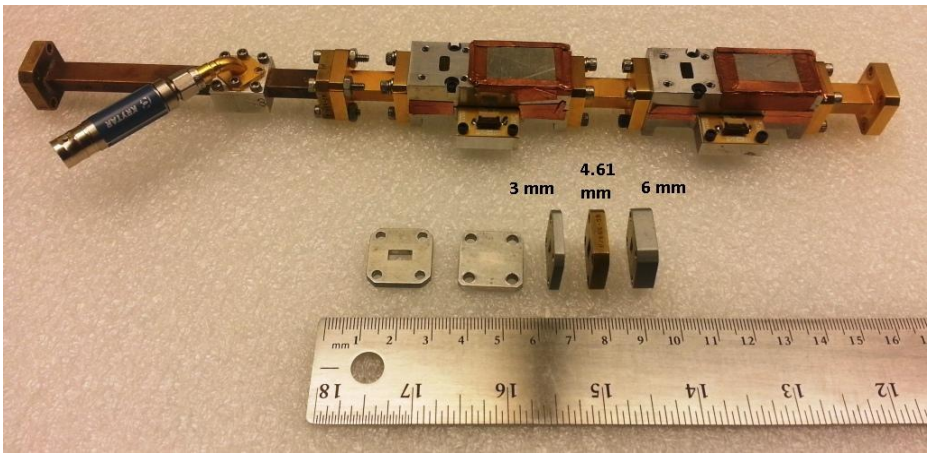

Figure 3.14. Shims used with the Ka-band phase-shifter and coupler.

In Figure 3.13 (a) & (b), yellow plots (16 phase shifts) represent the results with 3 mm shim measurements added and red plots (24 phase shifts) represent the results with the new 4.61 mm shim measurements added. The last graph, blue (1st state of each), uses just 3 measurements – one from each set proving the principle that 3 measurements of standing-wave voltage can be used to estimate Γ [6].

It is clear from results shown in Figure 3.13 that adding the data from the 4.61 mm shim to the old data improves the estimation considerably. Even though this measurement process was time consuming and laborious, it served as the measurement proof that more phase shift will lead to a better estimate of Γ. Based on this analysis, another phase-shifter was built with 9 pin-diode loaded slots and added in series with this phase-shifter. The VNA built using this system (now a total of 17 slots loaded with pin-diodes) was developed and the highly improved results were published in [10] as shown earlier in Figure 1.5.

To analyze the effect of various parameters affecting these one-port VNA systems, a sensitivity study was performed. The results of this study are presented in the following section.

4. SENSITIVITY ANALYSIS

4.1. INTRODUCTION

Sensitivity or error analysis is a study of the effect of error in system parameters on the system output. This analysis is presented for the wideband single-port VNAs, designed based on the non-coherent detection scheme. As described earlier, the cornerstone of this design is the phase-shifter and its properties have a direct impact on the system performance. Simulations were performed to obtain the sensitivity of the systems based on this design, to noise associated with the measured standing-wave voltage. Different levels of error are introduced in the following five parameters of the VNA system: (i) signal to noise ratio (SNR), (ii) insertion loss in phase-shifter (IL), (iii) total phase shift, (iv) scaling constant C, and (v) detector slope. A quantitative analysis of the effect of this error introduction on the output (estimated Γ) is done based on the system model. Results of this analysis were validated by measurements performed using the single-port VNA systems at X-band (8.2 – 12.4 GHz) and Ka-band (26.5 – 40 GHz).

4.2. METHODOLOGY

As described earlier, the voltage standing-wave in these one-port VNA systems can be modeled using S-parameters as:

$$V_{SW} = \left\{ S31 + S21\, S32 \left(\frac{\Gamma}{1 - S22\, \Gamma} \right) \right\} \tag{9}$$

The detector output is proportional to the power of this signal and is modeled as:

$$P_{SW} = C\left|V_{SW}\right|^2 + \text{Noise} \tag{10}$$

Three different cases of this S-parameter model have been considered: (1) purely theoretical model - without using any measured data, (2) using measured S-parameters of X-band VNA, and (3) using measured S-parameters of Ka-band VNA [10]. The results

using measured X-band VNA S-parameters (case 2), have been presented here. Corresponding cases 1 and 3, since very similar, are presented in Appendix B.

A modeled standing-wave is obtained by adding white Gaussian noise with noise power (NP) as shown in equations (9) and (10). The noise power is calculated from SNR using equation 11.

$$NP = \frac{\text{mean}\left\{C\left|V_{sq}\right|^2\right\}}{SNR} = \frac{\text{mean}\left\{C\left|V_{sq}\right|^2\right\}}{10^{\frac{SNR_{dB}}{10}}} \tag{11}$$

To analyze and compare the effect of different error levels, three parameters based on the DUT reflection coefficient were studied: error vector magnitude (EVM), normalized magnitude error and standard deviation of phase error defined as:

$$\text{Error vector magnitude} = \frac{\left|\Gamma_{ACT} - \Gamma_{ESTM}\right|}{\left|\Gamma_{ACT}\right|} \tag{12}$$

$$\text{Magnitude error} = \left|\frac{\left|\Gamma_{ACT}\right| - \left|\Gamma_{ESTM}\right|}{\left|\Gamma_{ACT}\right|}\right| \tag{13}$$

$$\text{St.Dev. of phase error} = \text{std}\left(\text{angle}\left(\frac{\Gamma_{ESTM}}{\Gamma_{ACT}}\right)\right) \tag{14}$$

Both Γ_{ACT} and Γ_{ESTM} are the reflection coefficients of DUT - Γ_{ACT} is measured apriori using a commercial VNA (HP 8510C for X-band measurements) and Γ_{ESTM} is found by applying the optimization process, explained in Section 3, on the modeled standing-wave. Mean of magnitude error and standard deviation of phase error are common and straightforward parameters. Error vector magnitude is a parameter which combines the influence of both magnitude and phase errors. It is the magnitude of the *vector difference* between the actual and estimated Γ, observed on a complex plane and normalized to the actual magnitude $|\Gamma_{ACT}|$. The methodology to find Γ_{ACT} and Γ_{ESTM} is now explained in detail for case 2, i.e., using measured S-parameters of X-band VNA.

From system modeling equations (9) and (10), it is expected that noise in the measured standing-wave voltage and properties of the system S-parameters contribute to errors in the estimated Γ through the optimization process. The "ideal" or noise-less power standing-wave (I_{PSW}) corresponds to DUT reflection coefficient Γ_{ACT} and Γ_{ESTM} comes from the "noisy" power standing-wave (N_{PSW}). As explained previously, the X-band phase-shifter creates eleven successive phase shifts (the Ka-band VNA has eighteen). Using a known test-value of reflection coefficient Γ_{ACT}, standing-wave voltage and the corresponding P_{SW} is obtained for each of the eleven phase shifts, together forming the ideal I_{PSW}. Noise with a standard normal distribution and magnitude NP (n_1, n_2, … n_{11}) was added to this I_{PSW} (using MATLAB's randn function) resulting in the noisy N_{PSW}:

$$N_{PSW} = I_{PSW} + \text{Noise} \tag{15}$$

in Matrix form,

$$\begin{pmatrix} N_{PSW}^{1} \\ N_{PSW}^{2} \\ \vdots \\ N_{PSW}^{11} \end{pmatrix} = \begin{pmatrix} I_{PSW}^{1} \\ I_{PSW}^{2} \\ \vdots \\ I_{PSW}^{11} \end{pmatrix} + \begin{pmatrix} n_1 \\ n_2 \\ \vdots \\ n_3 \end{pmatrix} \tag{16}$$

To obtain Γ_{ESTM}, a random guess value of Γ_{ESTM} is used with the eleven S-parameter sets and P_{SW} model to form another power standing-wave. By changing Γ_{ESTM} iteratively to minimize the error between this and N_{PSW}, the Γ_{ESTM} corresponding to minimum error is obtained (using Levenberg-Marquardt algorithm in MATLAB's fsolve function). Each of these "noisy" simulations was performed for 25 values of |Γ|. Furthermore, to calculate each of these magnitude error points, Γ estimates for 72 phase shift values between –180º to 180º, as shown in Figure 4.1, were averaged.

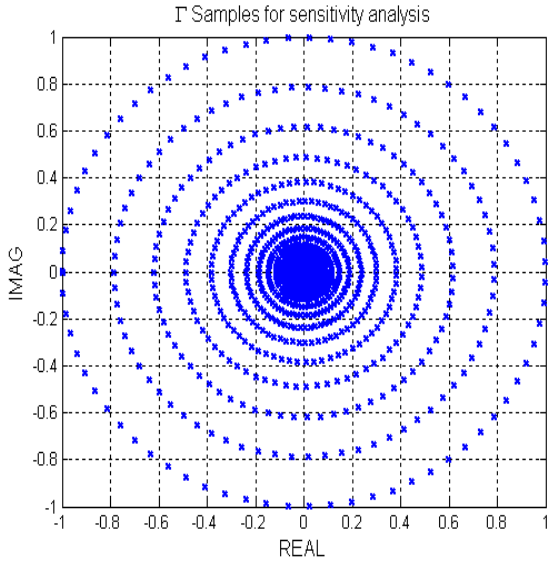

Figure 4.1. Complex Γ test-points (25x72). Results from 72 values of phase (1 complete circle) were averaged for each | Γ | in the simulation.

In this way, the Γ estimation process was tested with a broad range of test reflection coefficients spanning the whole area of the unit circle for each of the noise levels shown in results.

4.3. SIMULATION AND ANALYSIS

4.3.1. Signal-to-Noise Ratio (SNR). As described earlier, standing-wave voltage is measured using a Schottky diode detector. The output of this detector is a voltage proportional to the standing-wave power. Signal-coupling factor to the detector port (port 3), in the transmission line between ports 1 & 2, is designed to be low (<-10 dB for Ka band and -20 dB for X band) for minimum standing-wave perturbation. Consequently, the output of the detector can be close to its noise floor especially for the measurements around standing-wave nulls with highly-reflective loads (lowest power level) - resulting in a low SNR. Simulations with different SNR values were performed, using NP (equation 10) and the measured S-parameters of the X-band VNA. Signal to noise ratios between 0 dB to 85 dB were simulated. Results in Figure 4.2 (a)-(c) show

that the error in estimating the reflection coefficient is higher for lower reflection coefficient values of the DUT.

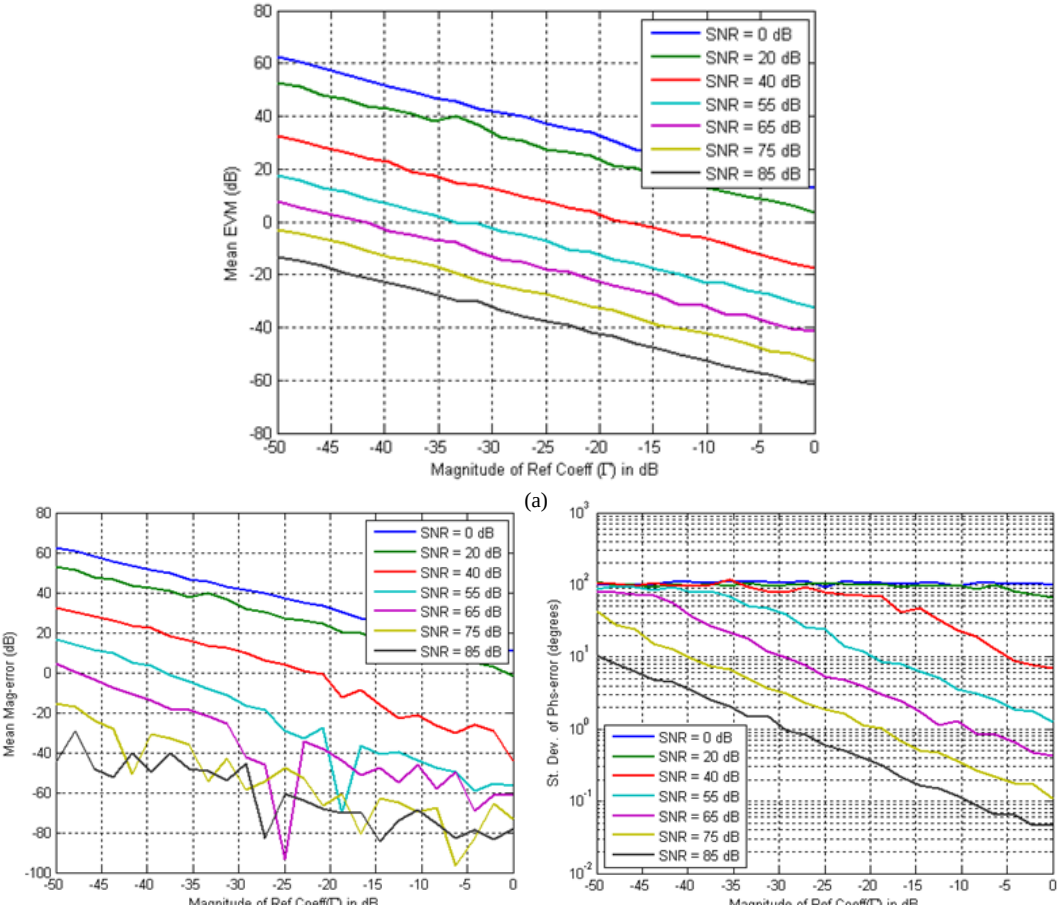

Figure 4.2. Sensitivity w.r.t Signal-to-Noise Ratio.

Furthermore, this error rapidly increases for SNR values lower than 55 dB. For example, for an SNR of 55 dB, and a maximum EVM requirement of -20 dB, we may not be able to measure any |Γ| below -12 dB reliably. Accordingly, the magnitude error becomes less than -40 dB and the phase error becomes less than 4 degrees. Considering that the typical power detector can provide a maximum dynamic range of 55 dB [15], these graphs can provide an insight on the performance of such a system.

4.3.2. Loss in Phase-Shifter. The phase-shifter of the X-band VNA uses a low loss phase-shifter IC. However, the phase shifter exhibited an insertion loss (PS loss) upto 9 dB as described earlier (for the Ka band VNA of [10], it is upto 10 dB). Also, in these one port VNAs, impedance mismatches in the waveguide transmission line cause multiple reflections. In other words, a small part of signal is always lost and this loss changes depending on phase-shifter state. Loss is simulated only in S21 & S32 since their signal flow path crosses the phase-shifter (Figures 1.6 and 2.1). Their values are modified by the "PS loss" value and using these 'reduced' S-parameters, an N_{PSW} is created for a test SNR of 65 dB, as explained earlier. Simulation results are shown in Figure 4.3 (a)-(c).

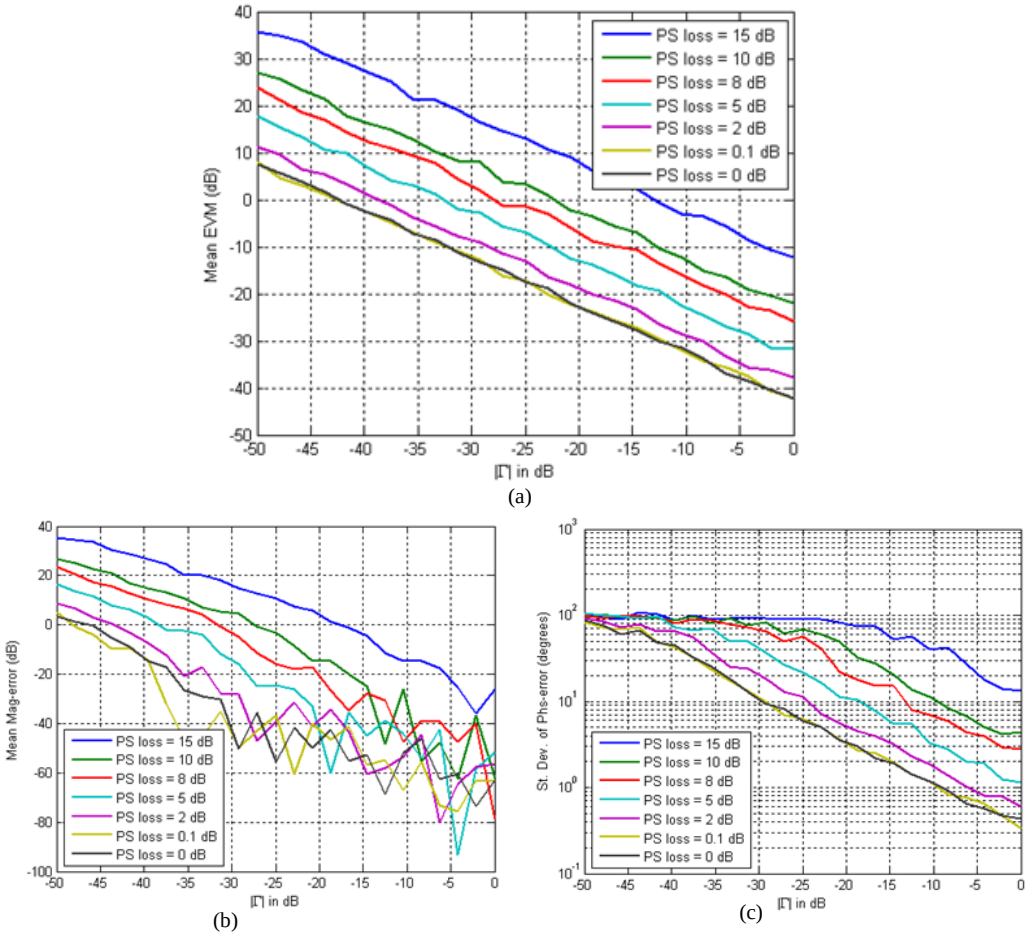

Figure 4.3. Sensitivity w.r.t phase-shifter loss (SNR = 65 dB).

Figures 4.3 (a)-(c) show that for a simulated SNR of 65 dB, the phase-shifter loss below 5 dB (considering phase error below 4º for this example) may be tolerable. Beyond that, the phase-shifter loss becomes the major contributor of error in the estimated reflection coefficient.

4.3.3. Total Phase Shift. Although the X-band system can provide a large phase shift (greater than 360º), the Ka-band system is limited in this respect because as discussed earlier, for larger phase shift, the insertion loss becomes high causing performance degradation. Phase-shifters used in these two systems provide discrete phase shifts, all of which are combined to get the total phase shift. To simulate the variation in this total phase shift, five equal phase-shifter states (each providing one-fifth of total phase shift) were considered. Also, a purely theoretical model of the system was used with a test SNR of 45 dB and phase-shifter insertion loss as 5 dB. Results of this simulation are shown in Figures 4.4 (a)-(c).

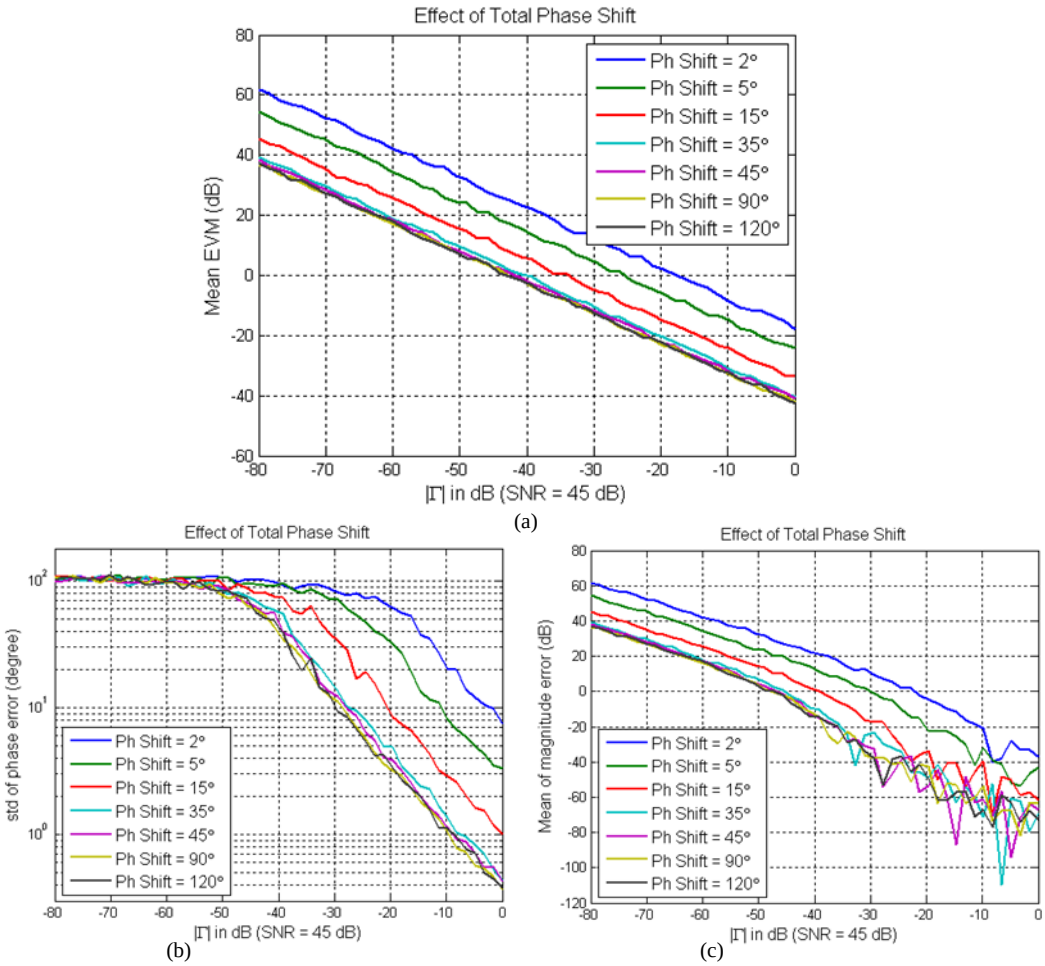

Figure 4.4. Sensitivity w.r.t total phase shift (SNR = 45 dB).

Figures 4.4 (a)-(c) show that as the total phase shift is increased, the errors in estimated reflection coefficient decrease, which is an important conclusion when designing such systems (i.e., more phase shift is better). In other words, this analysis relates the available total phase shift to the expected accuracy in estimated Γ. These graphs show that there is no noticeable improvement in the measurement errors when the phase shift is 45º or larger. However it also shows that even a 35º total phase shift may be sufficient.

4.3.4. Scaling Constant C. The power scaling constant C is used to scale the modeled standing-wave (I_{PSW}) to the level of the measured voltage standing-wave (V_{SW}). These standing-waves are a collection of 'n' points – the phase-shifting states of VNA, i.e., 18 states in Ka-band version [10] and 11 states in X-band version. The corresponding

ratios of each of these n points vary a little and constant C, per frequency point, is the mean of these n ratios. Consequently, this ratio may vary slightly between measurements. The effect of such a variation was simulated and its effect investigated based on the results shown in Figure 4.5.

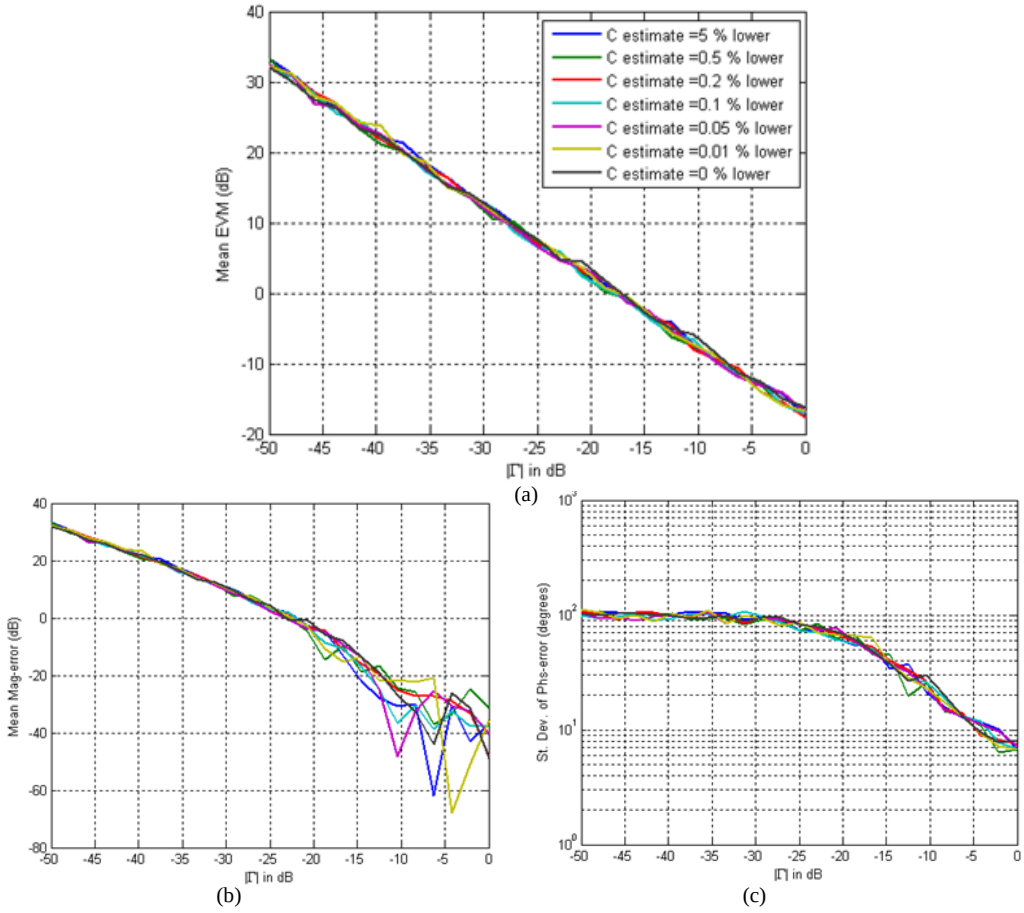

Figure 4.5. Sensitivity w.r.t scaling constant C (SNR = 40 dB).

Similar to the other parameters and as expected, a higher error magnitude can be seen for lower |Γ|. Γ estimation error increases by a significant amount only when the C estimate is 50% lower (Appendix B). So, unlike other parameters, minor errors in estimating C do not affect the estimated reflection coefficient.

4.3.5. Detector Slope. The RF Schottky detector used in these reflectometers follows the square law, i.e., the output voltage of the detector is proportional to the square of standing-wave voltage. Typically the detector characteristics (input-output relation) is measured and compensated for. However, an offset or error in frequency (signal source error), for example, can cause a shift in detector characteristics. Figure 4.6 shows the unique setup used for this simulation using the X-band system and the HP8510C VNA as both a source and a detector.

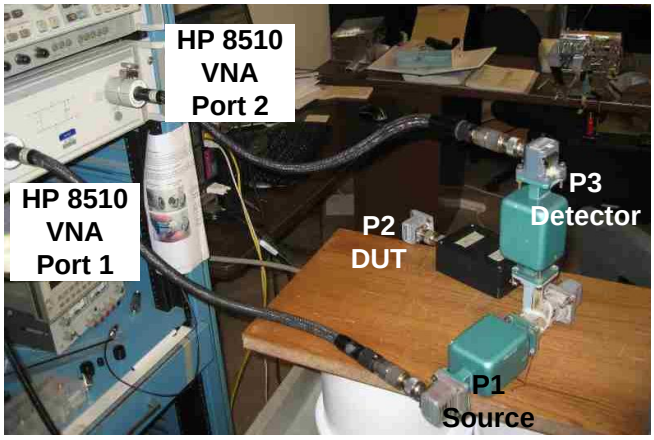

Figure 4.6. Unique setup for detector slope analysis at X-band

Although the source being used in this case is a very accurate one, i.e., a commercial VNA (HP8510) and an error is unlikely, this simulation was performed in order to leave no stone unturned while looking for the source of error (as discussed later in Section 4). To simulate detector characteristics slope, the measured |S21| from the VNA was distorted using the equation $y = Mx + K$ for different values of M and K. The measured quantity S21 is a normalized voltage. So, $|S21|^2$ has the unit of power and models the output of the Schottky detector (also normalized). Two kinds of errors are possible: slope (M) change and shift in the constant (K). These two possibilities are shown in Figure 4.7.

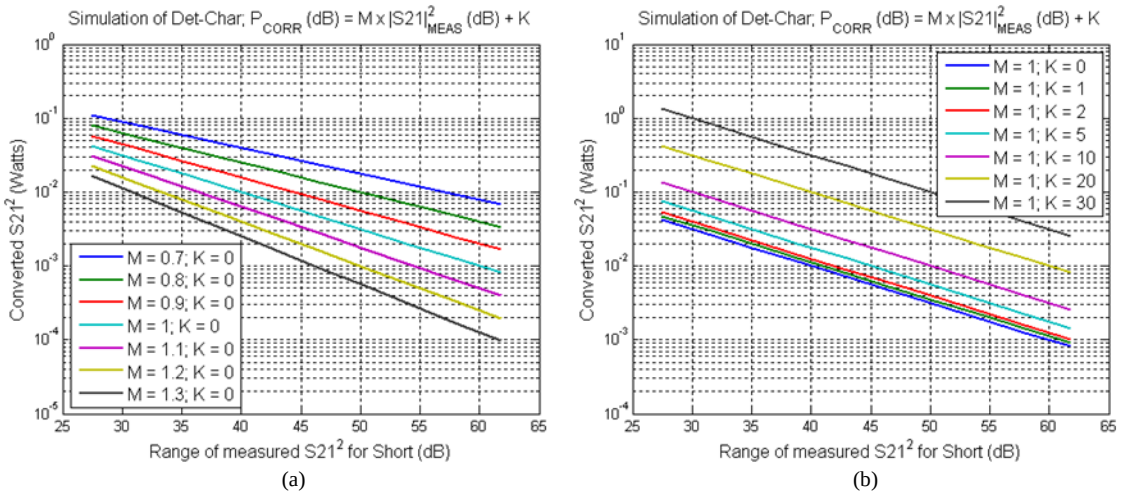

Figure 4.7. Two possible cases of detector characteristic variation (a) slope and (b) constant shift.

The lines corresponding to M = 1; K = 0 (blue lines in Figure 4.7) are the ideal lines, i.e., if we use the horizontal axis as the measured value, the corresponding values on vertical axis will be the same. But for all other lines, the y-axis values (converted values) will be different. Hence, after passing through this 'conversion' process a measured standing-wave will become distorted. This distorted standing-wave represents the erroneous measurement. The standing-wave is used to back-calculate Γ_{ESTM}. The result comparison with Γ_{ACT} in black and the corresponding Γ_{ESTM} in red for the three standard loads – short, quarter wavelength shim and matched load is shown in Figure 4.8.

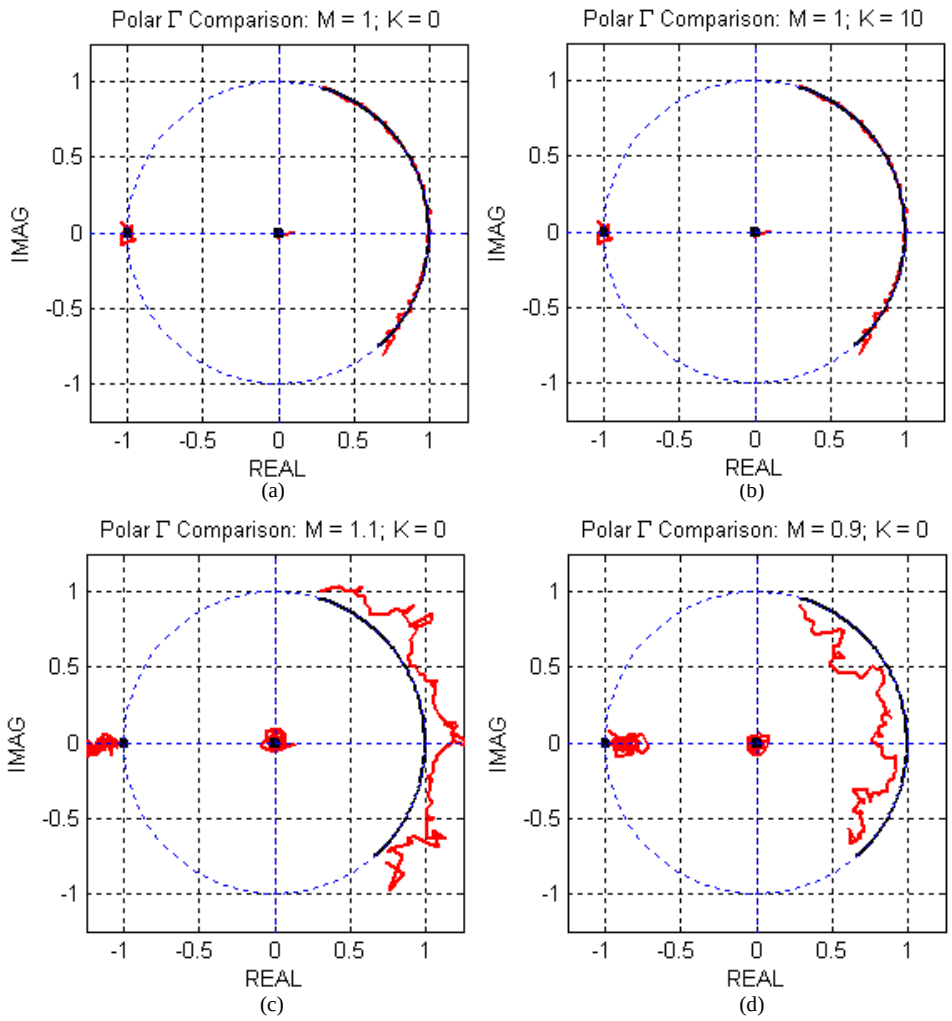

Figure 4.8. Results of detector-slope simulation for three standard loads (short, shim and matched load).

It is clear that even a slight slope change has a big impact on Γ_{ESTM} while a constant shift has no impact on it. Moreover, this effect is very recognizable on highly reflective loads (in this case short and shim). Lower slopes tend to underestimate Γ_{ESTM} while higher slopes tend to overestimate Γ_{ESTM}.

4.4. PERFORMANCE COMPARISON WITH COMMERCIAL VNA

The sensitivity analysis results of this X-band VNA are compared with commercially available handheld VNAs system (Agilent FieldFox microwave VNAs

N99XX series). The corresponding magnitude and phase comparisons are shown in Figure 4.9.

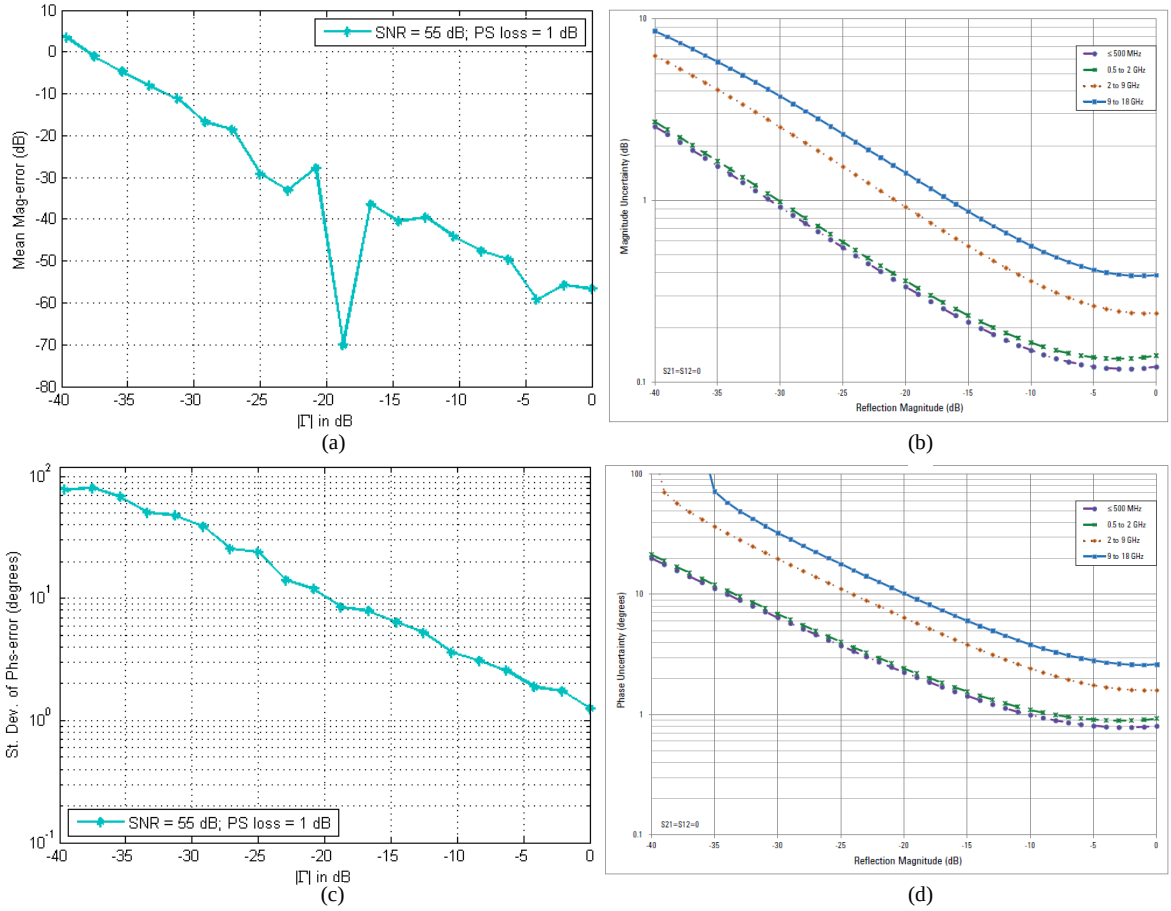

Figure 4.9. Comparison of the Ka-band VNA with a commercial handheld VNA.

Since the sensitivity analysis of the X-band VNA was performed at 10.3 GHz, its results, i.e., Figures 4.9 (a) and (c) are compared to the blue lines (9 to 18 GHz) in the Figures 4.9 (b) and (d). For a typical SNR value of 55 dB and phase-shifter loss of 1 dB, although the errors in phase are similar but the errors in magnitude are much lower for the X-band system. Hence, the performance of this X-band VNA system, which is a strong function of SNR and phase-shifter loss is comparable if not better compared to the commercial handheld VNA within the |Γ| test range of -40 dB to 0 dB.

4.5. SUMMARY

From the results shown in Figures 4.2 – 4.9 we clearly see the achievable limit of accuracy in estimating Γ using these reflectometer systems for a wide range of SNR, phase-shifter loss, total phase shift and C values. For example if for a particular imaging application, a mean magnitude-error of 3 dB is acceptable, for a SNR of 55 dB, a one-port reflectometer with these characteristics can measure Γ from 0 dB to -35 dB satisfactorily (see Figure 4.2). The sensitivity required in the measurement instrumentation is highly application specific. In other words, even though this is not acceptable for precise signal integrity applications, it is useful in applications like imaging and non-destructive testing and evaluation where the level of accuracy required may be lower. Trends in variation of the parameters can be used to identify sources of error in system, for example, a frequency offset or variation in a RF source will have a distinct effect on highly reflective loads like a shim. This study also provides the system designer with design parameters such as phase-shifter loss and required SNR. If these parameter values are not achievable, a more accurate standing-wave model like the one described in Section 3, may be used.

5. MEASUREMENTS

5.1. INTRODUCTION

Using the designed one-port X-band VNA measurement system, its S-parameter model and the estimation processes described earlier, Γ was estimated, and then corrected, for the eight DUTs, using the three-term calibration technique explained in Section 3. A Schottky diode - Krytar 202B [21], was used as the detector and a short, a 9 mm shim and a matched load were used as the three calibration standards for correction. The estimated and corrected Γ values for the eight X-band loads are shown in Figure 5.1.

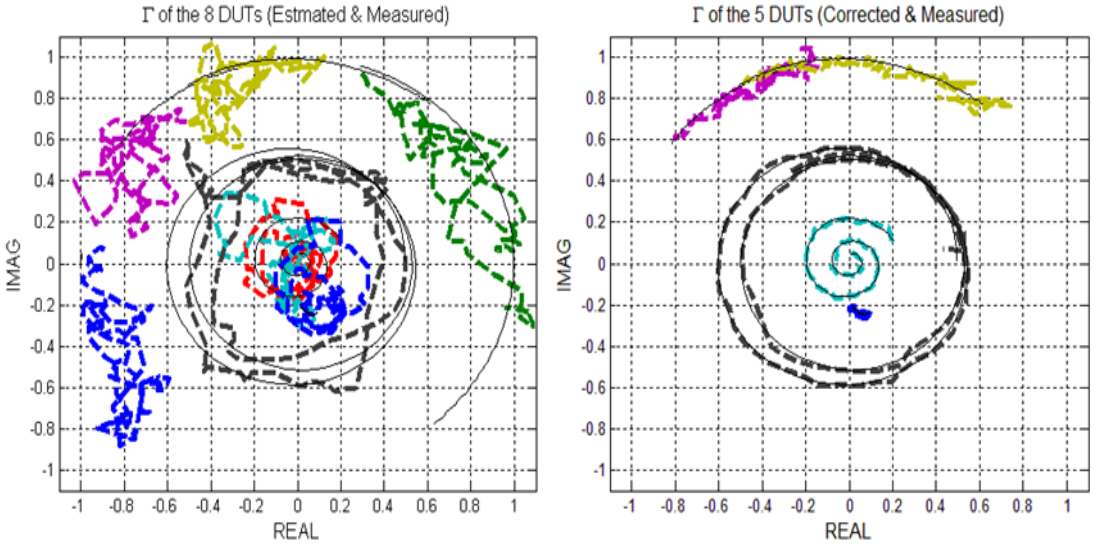

(a) (b)

Figure 5.1. Krytar detector results: the estimated and corrected Γ values for the DUTs. The thin black curves show the S11 values measured using a commercial VNA.

The corresponding complete set of results is in Appendix C. The fact that calibration removes the errors from the estimated Γ shows that errors are deterministic and it should be possible to include them in the characterization. A thorough three-port characterization of the phase-shifter is already included in the system model, and since the diode detector is not included in the 3-port characterization, the same process was

repeated with other detectors. Also, other data acquisition systems (DAQ) were used in place of the NI DAQ card used in this case.

5.2. ALTERNATIVE DETECTION AND DAQ METHODS

In the VNA system, the NI DAQ card performs a dual function – it controls the phase shift (analog output) and reads the voltage from the RF detector (analog input). Due to the shared ground connection, error may be introduced in either of these voltages affecting either the phase shift or the measured standing wave voltage. Further, there is a small (0.5 mV) bias on the analog input channel which shows variations when the grounds (return paths) of these two signals are shorted. With the aim of detecting and removing any unforeseen errors being introduced by the detection or the DAQ systems, both of these systems were replaced. A log detector was used for measuring the standing-wave voltage, since its output varies linearly with the square of input power (or power in dB). Also, instead of using the NI DAQ card for reading the output from this RF detector, a Fluke multi-meter (8840A) was used. The corresponding Γ estimation results are shown in Figure 5.2.

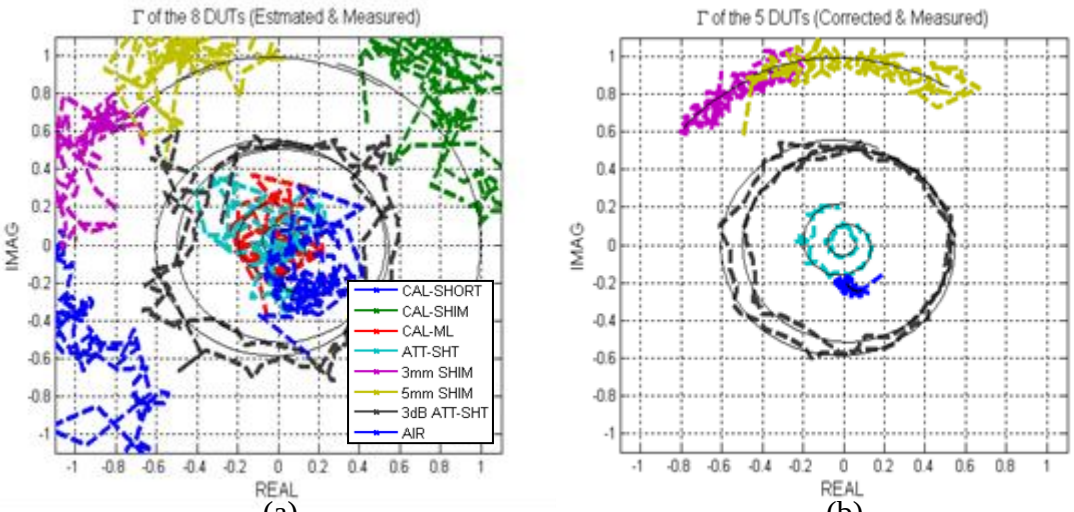

(a) (b)

Figure 5.2. Log detector results: The estimated and corrected Γ values for the DUTs. The thin black curves show the S11 values measured using a commercial VNA.

The results from these measurements are very similar to the Krytar Schottky diode measurements using NI DAQ and they also need the three-term calibration. In fact, the results are slightly worse indicating that the Krytar diode and NI DAQ system is more accurate and introduces less noise in the signal. Detailed results are shown in Appendix E.

Hence, in a methodical process to realize this calibration-free VNA, and in an attempt to determine the source(s) of this still-present "error", a thorough step-by-step testing approach was devised and followed. To this end, the effect and stability (or instability) of every system parameter, i.e., each of the phase-shifter control input, phase shift, data acquisition system, diode detector and even the stability of HP8510C VNA source was tested individually and thoroughly.

As the first step, to remove the whole issue of "power conversion" using the diode or the log detectors, the complete detection system was removed from the X-band VNA and it was replaced by the HP8510C VNA.

5.3. HP8510C VNA USED AS DETECTOR

Before describing the use of the HP8510C VNA for standing-wave detection, a brief review of S-parameters is presented. As mentioned earlier, the diode output is proportional to the square of standing-wave voltage. A commercial VNA, on the other hand, directly measures the incident, reflected and transmitted voltages by down-converting the RF signal. All of the S-parameters are defined using the ratios of these measured voltages. Specifically, the parameter S21 is defined as *b2/a1* where *a1* is the voltage wave incident at the DUT from port-1 and *b2* is the wave transmitted through the DUT and measured at port-2. As shown in Figure 5.3, if ports P1 and P3 of the X-band VNA are connected to the port1 and port-2 of the HP8510C VNA respectively, the measured parameter S21 (with DUT connected at P2) is actually the measurement of the standing-wave voltage.

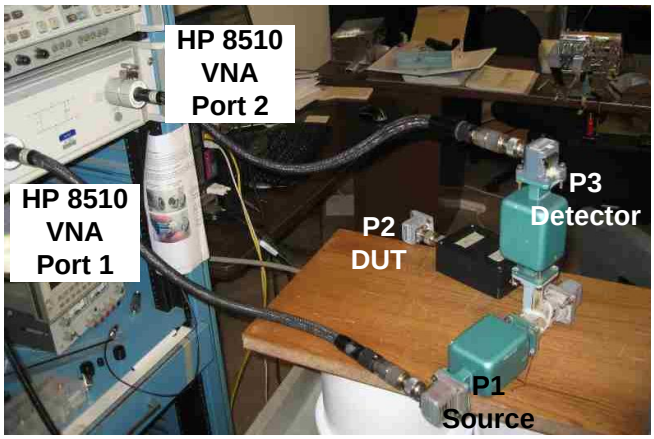

Figure 5.3. Unique setup for simulating the detection system using the HP8510C VNA.

Also, unlike the case of the diode detector, this measurement is the standing-wave voltage itself (normalized) and not a quantity proportional to power. To move a step further, the term *b2* can be read directly from the HP8510C VNA. This is the raw or un-normalized standing-wave voltage. The accuracy of the measurement using this HP8510C VNA can be enhanced by calibrating it. Three types of calibration-states are possible: full 2-port calibration, response calibration and no calibration (or un-calibrated). Measurements were made with the HP8510C VNA for each of these calibration types and with and without the isolators at P1 and P3 and the results are presented in the following sections.

5.3.1. HP8510C VNA with Full 2-port Calibration. Performing a full 2-port calibration on any VNA system removes or compensates for all errors due to mismatch and losses in cables and connectors. This is a more complete version of the one-port calibration explained in Section 3 and was performed on the HP8510C VNA instead of the one-port X-band VNA. So, the two ports of this HP8510C VNA, i.e., the source at P1 and the detector at P3 are both ideal and since the X-band system is completely characterized beforehand, all system parameters are known and accounted for. S21 measurements are made for the previously described attenuated short (with frequency dependent attenuation) and the three standard “calibration loads” (short, shim, matched load) X-band loads. The reflection coefficient of the attenuated short was iteratively estimated and also corrected (calibrated) using the three calibration loads. These results,

with and without the isolators at P1 and P3, are shown in Figures 5.4 to 5.6 with direct S11 measurement made by HP8510C VNA used as a reference (Black).

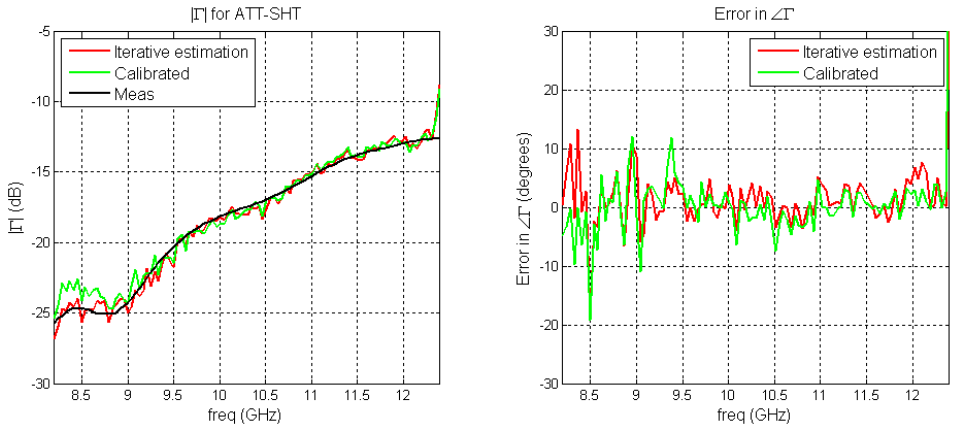

Figure 5.4. Magnitude and phase error of Γ for X-band system with no isolator and full 2-port calibration of HP8510C VNA.

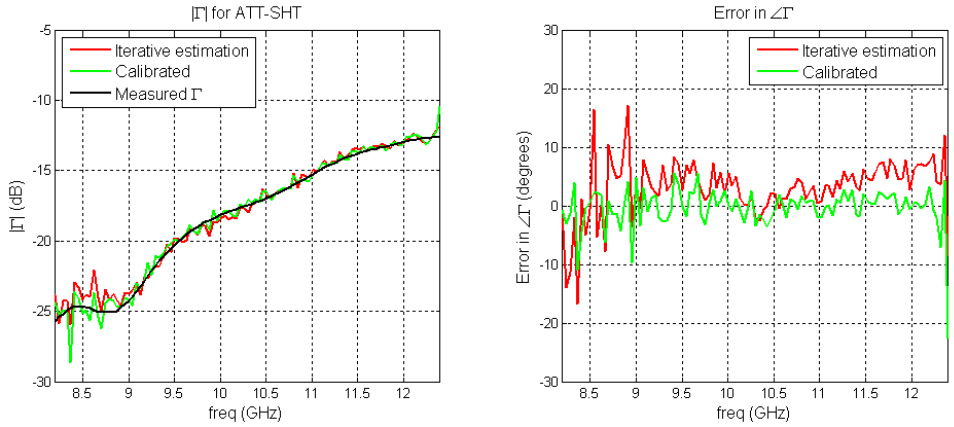

Figure 5.5. Magnitude and phase error of Γ for X-band system with isolator at P1 only and full 2-port calibration of HP8510C VNA.

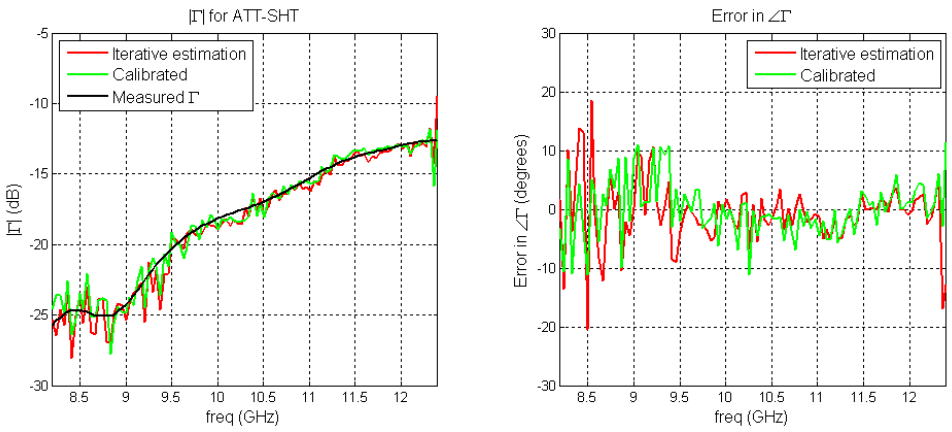

Figure 5.6. Magnitude and phase error of Γ for X-band system with isolators at both P1 & P3 and full 2-port calibration of HP8510C VNA.

Mean and standard deviation of magnitude and phase errors, relative to the measured Γ, is used to quantify and compare the results. The average magnitude and phase errors in each of these three "iterative estimations" are below 0.005 (unit-less) and 3º and the standard deviations are below 0.009 and 5.7º, respectively. As expected, the estimated Γ is close to the measured value. An important observation is that the calibration procedure (of the X-band system) does not improve the results. Also, results with isolators are better than the one without showing that mismatch and hence reflections at ports P1 and P3 contribute to errors significantly. This will become more evident in the following sections.

The S21 measurements using HP8510C VNA with full 2-port calibration provides another unique opportunity. From equation 2, we see that instead of squaring S21, we can have a linear equation in Γ:

$$S21^{M} = S31 + S21\,S32\,\frac{\Gamma}{1 - S22\,\Gamma} \tag{17}$$

Solving,

$$\Gamma = \frac{S21^{M} - S31}{S21\,S32 + S22\left(S21^{M} - S31\right)} \tag{18}$$

Here, the current S21 measurement is represented by the superscript 'M' and other terms are the measured 3-port S-parameters. In other words, there is an analytical

solution for Γ which can be used to verify the results of the iterative solution. However, since all terms in the above equation are complex, this approach works only when phase and magnitude of S21 are well-defined, i.e., when HP8510C VNA is calibrated. A tabulated comparison of errors for all these cases is presented at the end of this section.

5.3.2. HP8510C VNA with Response Calibration. In a VNA, a response (or through) calibration scheme only corrects for some of the errors in the measurement setup (transmission or tracking errors). Since the same process of measurement, estimation and calibration is followed as in the previous case, the results are expected to be better than no-calibration case and worse compared to the full 2-port calibration case and are presented in Figures 5.7 to 5.9.

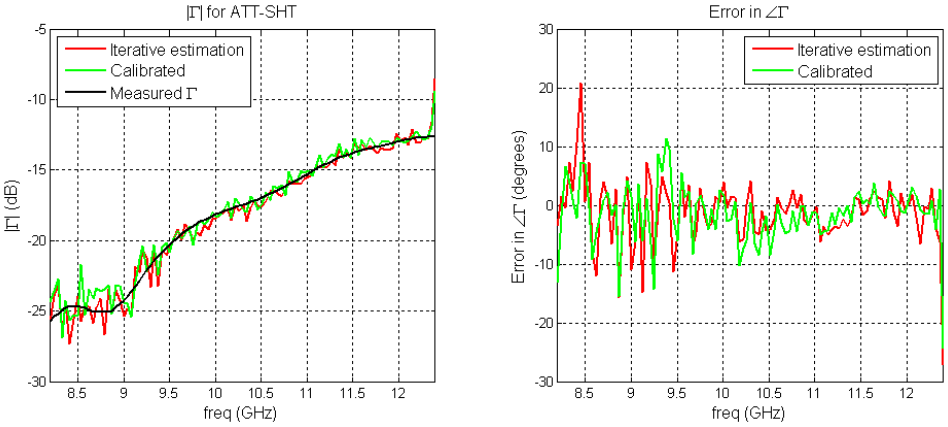

Figure 5.7. Magnitude and phase error of Γ for X-band system with isolators at both P1 & P3 and HP8510C VNA with response calibration.

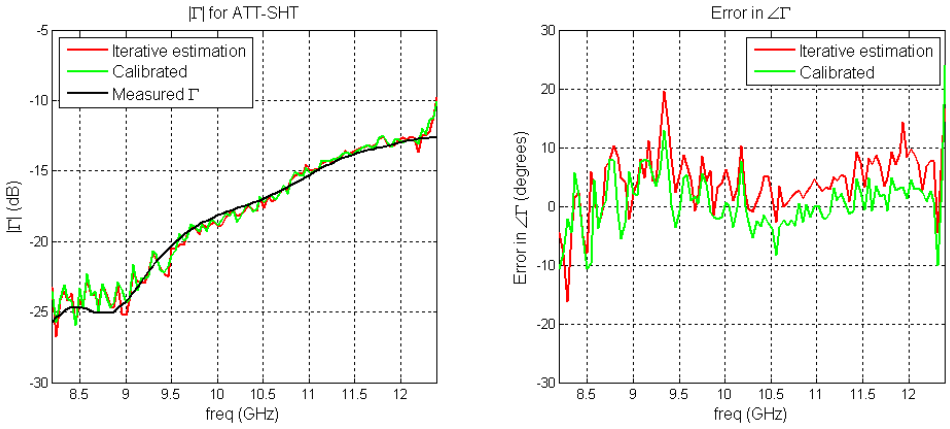

Figure 5.8. Magnitude and phase error of Γ for X-band system with isolator only at P1 and HP8510C VNA with response calibration.

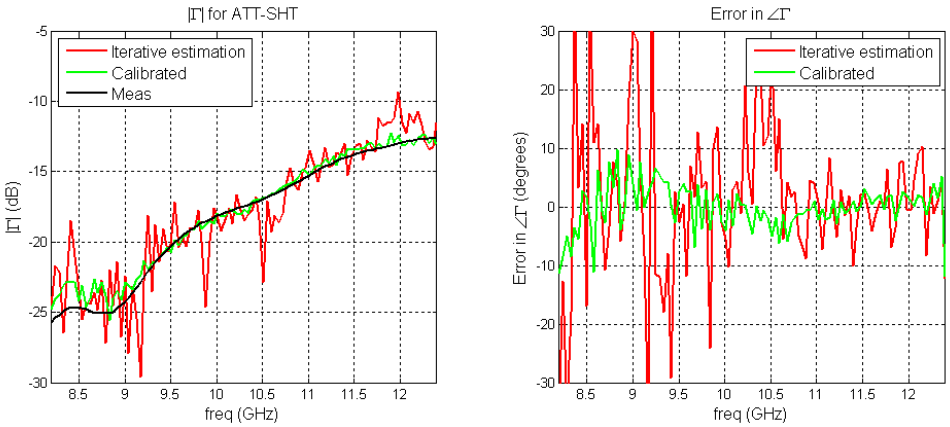

Figure 5.9. Magnitude and phase error of Γ for X-band system with no isolators and HP8510C VNA with response calibration.

In Figures 5.7 and 5.8, it is seen that the estimated and corrected values of Γ are close to the measured value but when the isolator at P1 (source) is removed; the Γ estimation becomes erroneous (Figure 5.9) showing that reflections at source (P1), which the isolator suppresses, are a major contributor towards error. Moreover, this error seems to be deterministic as it is being corrected when the 3-load calibration scheme is applied. The corresponding magnitude and phase errors and standard deviations are tabulated at the end of this section.

5.3.3. HP8510C VNA is Un-calibrated. This is the most important measurement set amongst the three cases being discussed because, here the operating principle is closest to the detection system using a diode. Since the HP8510C VNA is not

calibrated, neither the magnitude nor the phase of the RF signal is known and therefore $(S21)^2$ should be identical to the output of the diode. Results are shown in Figures 5.10 to 5.12.

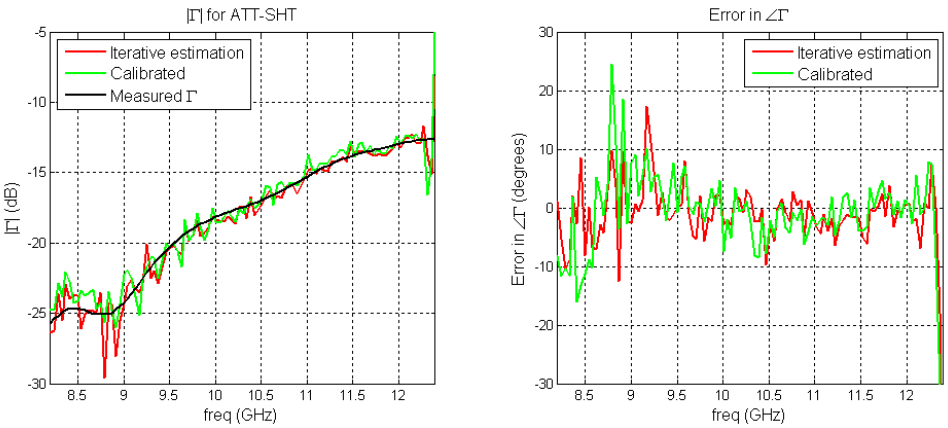

Figure 5.10. Magnitude and phase error of Γ for X-band system with isolators at both P1 & P3; HP8510C VNA is un-calibrated.

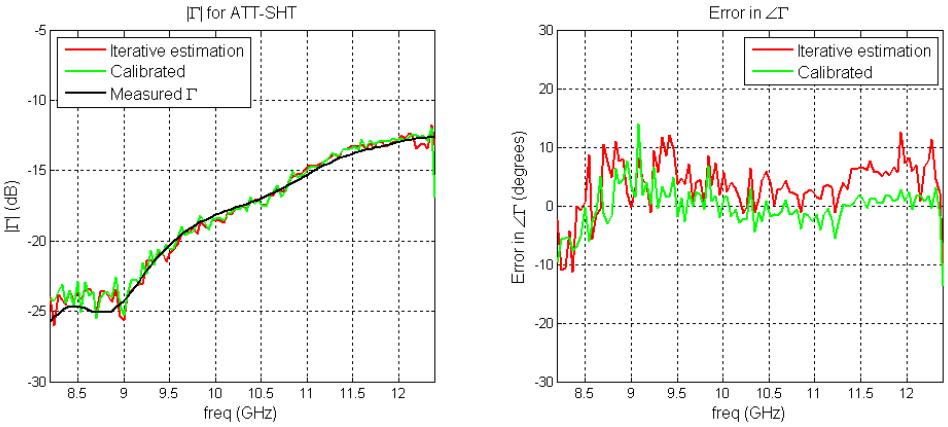

Figure 5.11. Magnitude and phase error of Γ for X-band system with isolator at P1 only; HP8510C VNA is un-calibrated.

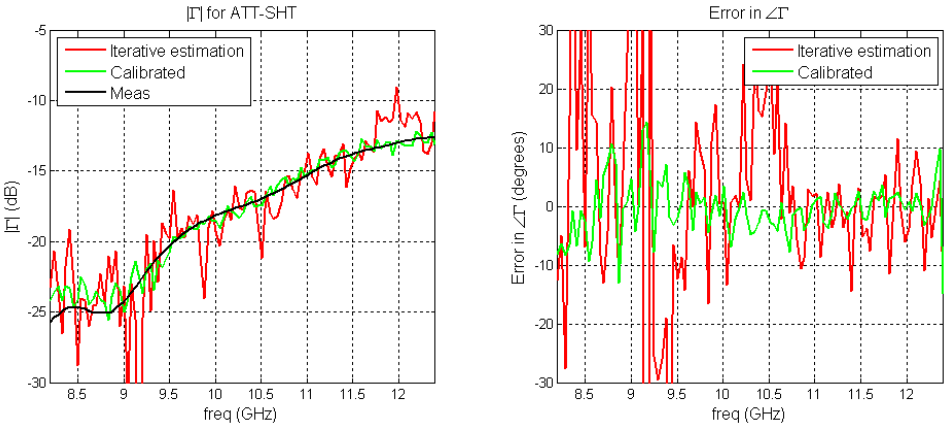

Figure 5.12. Magnitude and phase error of Γ for X-band system with no isolators; HP8510C VNA is un-calibrated.

As shown in Figures 5.10 and 5.11, the estimated and calibrated Γ are both close to the measured value and the "3-load calibration" does not improve the results significantly. On the other hand, the estimated Γ in Figures 5.10 and 5.12 has a large error. To check if a higher signal power improves the results, measurements were performed using HP 83554A RF amplifier at input P1 (pre-amplification) and again using Hittite HMC564 - low noise RF amplifier at output P3 (post-amplification) of the RF signal. The results are shown in Figures 5.13 and 5.14.

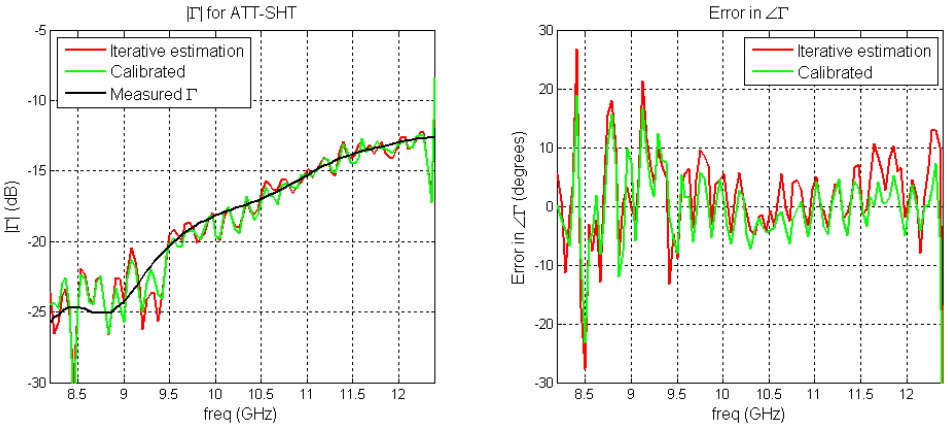

Figure 5.13. Pre-amplification (input at P1 is amplified): magnitude and phase error of Γ for X-band system with isolator only at P1; HP8510C VNA is with response calibration.

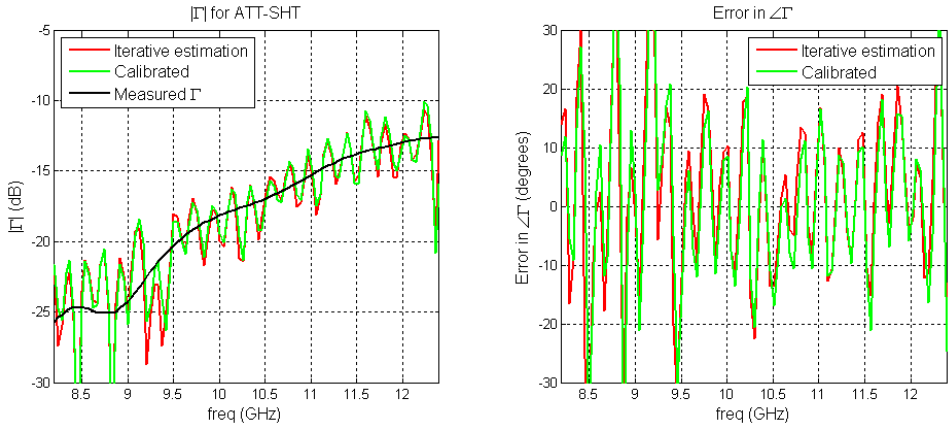

Figure 5.14. Post-amplification (output at P3 is amplified): magnitude and phase error of Γ for X-band system with isolator only at P1; HP8510C VNA is with response calibration.

Instead of improving the Γ estimation, the amplifiers add more errors to the system. This is probably because the losses and mismatches within these devices have not been included in either the system characterization or the HP8510C VNA calibration.

A tabulated comparison of errors for all of these cases is shown in Table 5.1.

Table 5.1. Mean & standard deviation of errors in Γ (ATT-SHT) using S21 measurements.

8.2 to 12 GHz data (ANALYTIC SOLUTION)																							
Cal of 8510		Without Isol				With Isol on P1				With Isol on P1 (Hittite RF amp)				With Isol on P1 (HP 83554A amp)				With Isol(s) on P1 & P3			
		MagMn	MagSD	PhsMn	PhsSD	MagMn	MagSD	PhsMn	PhsSD	MagMn	MagSD	PhsMn	PhsSD	MagMn	MagSD	PhsMn	PhsSD	MagMn	MagSD	PhsMn	PhsSD
Full 2port	est	0.000	0.015	2.020	5.627	-0.004	0.016	2.075	6.987									0.003	0.008	-1.789	4.926
	cor	-0.002	0.015	1.003	5.669	-0.001	0.006	-0.352	2.536									-0.001	0.007	-0.692	3.859
Resp	est	-0.074	0.136	5.978	58.818	-0.067	0.114	12.220	54.472	-0.040	0.075	6.436	38.451	-0.232	0.220	-9.033	89.237	0.003	0.022	0.503	12.756
	cor	-0.003	0.006	0.102	3.427	-0.003	0.021	0.906	8.319	-0.002	0.020	0.852	9.210	-0.002	0.011	-2.083	4.870	-0.003	0.010	-2.444	4.555
Un-cal	est	-2.277	1.407	-2.417	103.414	-2.408	1.965	5.075	104.015	-3.250	1.182	12.052	104.606	-3.573	2.923	11.992	104.289	-2.276	1.341	-1.000	104.864
	cor	-0.002	0.007	-0.372	3.819	-0.003	0.008	-1.179	3.585	-0.002	0.017	-0.056	10.059	-0.004	0.011	0.940	6.722	-0.005	0.039	0.080	13.188

8.2 to 12 GHz data (ITERATIVE SOLUTION)																							
Cal of 8510		Without Isol				With Isol on P1				With Isol on P1 (Hittite RF amp)				With Isol on P1 (HP 83554A amp)				With Isol(s) on P1 & P3			
		MagMn	MagSD	PhsMn	PhsSD	MagMn	MagSD	PhsMn	PhsSD	MagMn	MagSD	PhsMn	PhsSD	MagMn	MagSD	PhsMn	PhsSD	MagMn	MagSD	PhsMn	PhsSD
Full 2port	est	0.000	0.007	0.918	3.978	-0.002	0.006	2.853	4.968									0.004	0.008	-0.564	5.588
	cor	-0.002	0.007	-0.203	4.283	-0.001	0.005	-0.123	2.730									0.000	0.009	-0.230	4.880
Resp	est	-0.005	0.026	1.253	13.558	-0.001	0.008	3.862	5.022	0.000	0.027	1.770	15.247	0.001	0.014	1.777	7.507	0.002	0.008	-0.955	5.216
	cor	-0.004	0.006	-0.238	3.941	-0.002	0.008	0.322	4.381	-0.003	0.027	1.020	14.726	0.002	0.012	-0.156	6.193	-0.003	0.009	-1.335	4.804
Un-cal	est	-0.004	0.028	1.486	22.521	-0.002	0.006	3.449	4.484	-0.003	0.039	-0.847	30.314	-0.003	0.012	1.523	9.019	0.002	0.008	-0.862	4.592
	cor	-0.002	0.008	-0.523	4.541	-0.003	0.007	-0.169	3.525	-0.006	0.038	-0.626	24.112	-0.006	0.013	-0.087	8.574	-0.003	0.010	-0.470	6.186

In Table 5.1, “MagMn” is the mean of magnitude errors for 101 values of |Γ| for frequencies between 8.2 and 12 GHz. “PhsMn” is the corresponding mean of errors in phase while “MagSD” and “PhsSD” are the corresponding standard deviations. As expected, the errors are minimum when HP8510C VNA has a full 2-port calibration. A significant improvement can be observed when an isolator is attached at P1 removing any source mismatch as the standard deviations of errors from un-calibrated HP8510C estimations decreases from 0.028 to 0.006 and from 22.5º to 4.4º for magnitude and phase respectively. This shows the huge effect of reflections from source on the measurements and consequently on Γ.

Compared to the isolator at P1, adding another isolator at P2 (for detector mismatches) also improves Γ estimation but by a less significant amount. This is because the signal coupled to P3 is itself very low (-18 dB). A noteworthy observation is that even when using an un-calibrated HP8510C VNA, the Γ estimation for the third case (using isolators at both P1 & P3) is close to the measured value and more importantly, is not improved by the 3-load calibration. *This shows that the basic principle of a calibration-free VNA, upon which this research was based, works.* However, the addition of two isolators makes the system very big in size, resulting in a lot of cable stresses while performing the characterization of the device. The effect and removal of this is discussed later.

5.3.4. b2 Measurements. As described earlier, measurements of the parameter *b*2, the un-normalized voltage which is closest to the detector measurement, were also performed for the X-band VNA system (with isolators at both P1 and P3). The Γ estimates and its errors, using measurements made with an un-calibrated HP8510C VNA are shown in Figure 5.15.

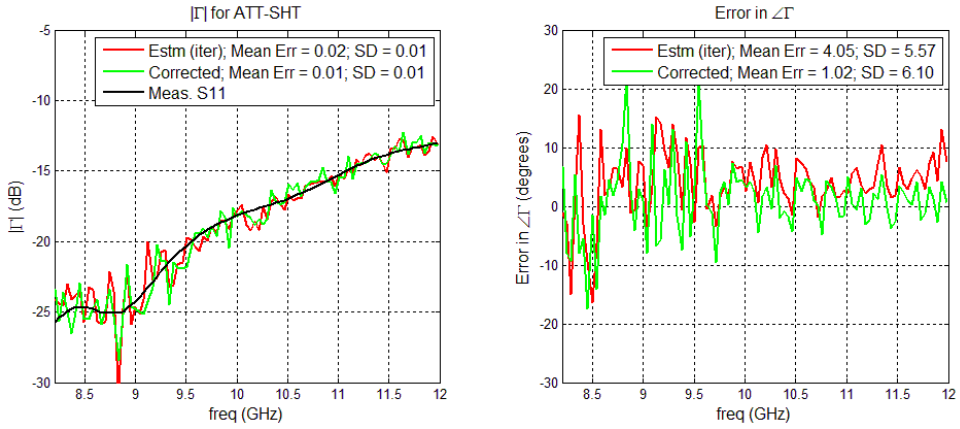

Figure 5.15. "b2" measurements: Magnitude and phase error of Γ for X-band system with isolators at both P1 & P3; HP8510C VNA is un-calibrated.

This estimate of Γ, although having a higher error than the corresponding S21 measurement, again seems not to have any deterministic errors as the three-term calibration does not improve the results. Although using an expensive commercial VNA like the HP8510C for building the one-port X-band VNA is not a feasible design, this analysis provides a measurement based proof that such a device is possible.

As discussed in the previous sections, the calibration-free VNA works as designed. Even though standing-wave measurements using a power detector could not be used towards this end, the principle of operation of the VNA and design is validated. Yet, the results in Table 5.1 show that correction (using three-load calibration) does improve these estimation results slightly. For such a slight improvement in accuracy, "*air*" or open-ended waveguide radiating into air is proposed as a standard.

5.3.5. Air as a Standard. Instead of using three expensive precision calibration standards (for correction) to achieve a slight improvement in accuracy (Table 5.1), it is possible to use air (open ended waveguide radiating into air) as a standard. Reflection coefficient magnitude |Γ|, for air is about – 13 dB and port 2 of the VNA can be pointed towards any non-reflective open space for its measurement. Towards this end, and since the finite nature of the waveguide flange and the screw-holes affect this measurement significantly, measurement and simulations (using CST) were performed to find the complex reflection coefficient of an open ended waveguide radiating into air. The

simulation results and their comparison to the actual measurements are shown in Figures 5.16 and 5.17.

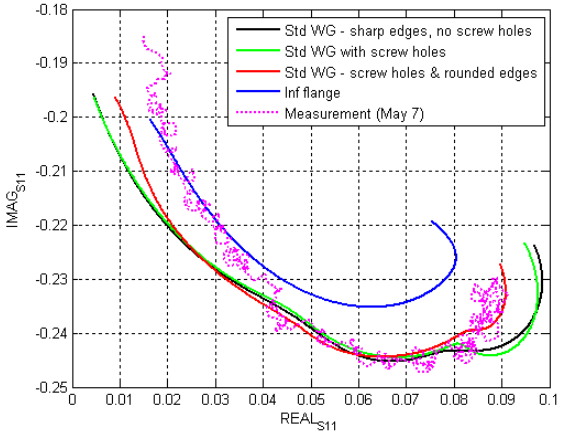

Figure 5.16. Complex Γ of waveguide radiating into air - simulations and measurement.

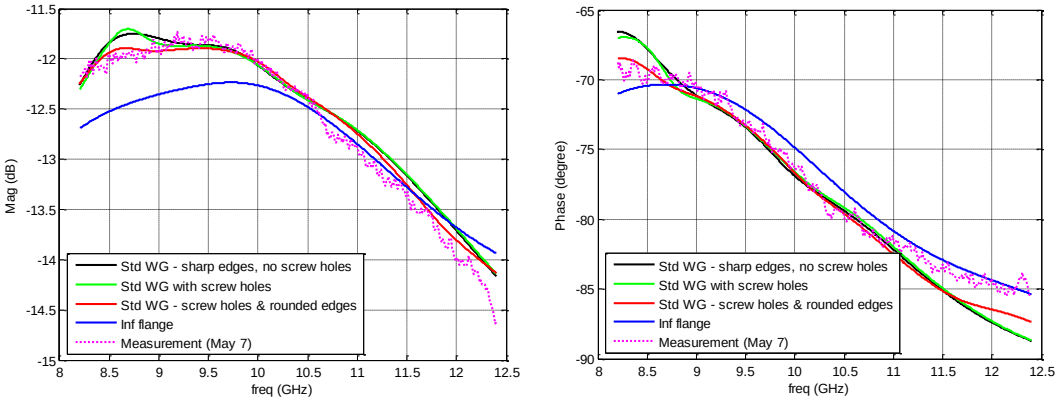

Figure 5.17. Magnitude & Phase of waveguide radiating into air - simulations and measurement.

The simulations were done for four cases: (i) standard X-band waveguide flange with sharp rectangular edges and no screw holes, (ii) standard X-band waveguide flange with screw holes (iii) standard X-band waveguide flange with screw holes and tapered, rounded edges and (iv) infinite flange. As we can see, the simulation result of case (iii), which is also closest to a practical radiating waveguide, is very similar to the measured

reflection coefficient. At higher frequencies, the phase starts to deviate but through most of the X-band, this simulation model matches the measurement.

5.3.6. S-parameter Correction and Verification. Addition of isolators to the system makes it bulky. The characterization of this bulky three-port device is done using a calibrated two port VNA, i.e., the HP8510C. This requires three separate two-port measurements with the third port "matched" in every case. The nine three-port S-parameters are found by combining data from these measurements. Practically, this process requires moving or re-orienting both the X-band system and the connecting cables of the calibrated HP8510C VNA. One of these orientations is shown in Figure 5.18.

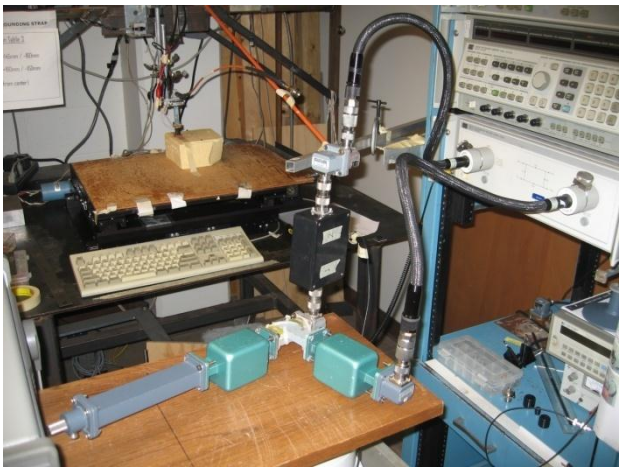

Figure 5.18. System orientation during the characterization process illustrating cable stresses.

The process of VNA calibration removes the errors due to mismatches which are a strong function of orientation and bends in connecting cables especially at higher frequencies. Consequently, for the orientations like the one shown in Figure 5.18, the measurement (of S-parameters) may have errors which should be identified and minimized.

The S21 measurements using a full 2-port calibration on the HP8510C VNA can be used to verify and correct these measured S-parameters. Considering equation 14

describing S21 and equation 5 of calibration from Section 1, it is observed that they are in the same format as shown below.

Measured S21: $$S_{21}^{M} = S_{31} + S_{21}S_{32}\frac{\Gamma}{1 - S_{22}\Gamma}$$

Error terms for calibration: $$\Gamma eq = e_{00} + e_{10}e_{01}\frac{\Gamma}{1 - e_{11}\Gamma}$$

Hence, the "three-known-load" based error-term solution described in Section 3 can be applied to find three S-parameters, i.e., S31, S22 and S21×S32. Since S21 and S32 are always used together (as a product) so, this case also has three overall unknowns and this solution is viable. It should be noted that this calculation is only possible for S21 measurements made using the HP8510C VNA with a full 2-port calibration since both the phase and magnitude of measured S21 need to be known correctly. The advantage of this method of "inferring" the S-parameters is that since the setup itself is not moved, and the only movement is of three different loads being placed at the DUT port - P2, cable stresses and the corresponding errors can be avoided. A comparison of measured and "inferred" S-parameter (S31) is shown in Figures 5.19 and 5.20.

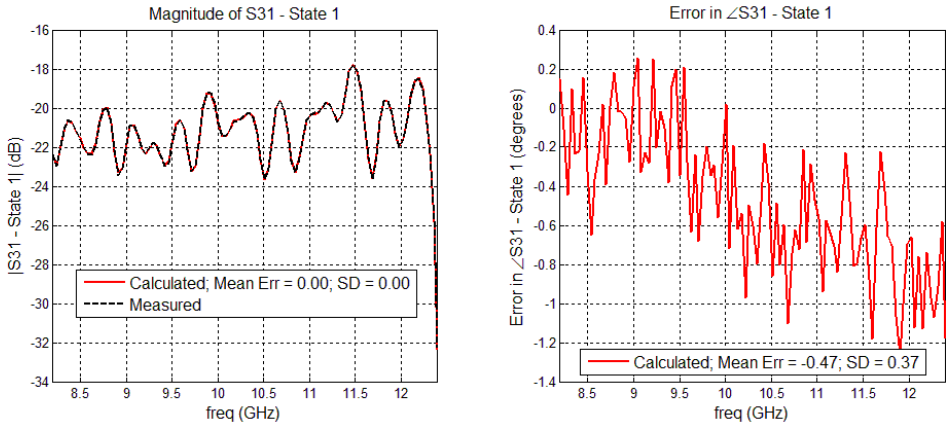

Figure 5.19. Measured and inferred (calculated) S-parameter: S31 of the 1-port VNA system.

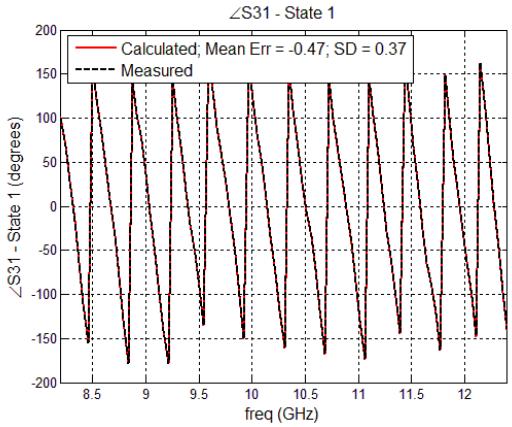

Figure 5.20. Measured and inferred (calculated) phase of S-parameter: S31 of the 1-port VNA system.

The most prominent effect of the cable errors can be seen on the phase of S-parameter S31 in the form of a phase error increasing with frequency as shown in Figure 5.19. The overall monotonically increasing nature of this error suggests that this is due to cable bends which has a greater effect on higher frequencies. The effect on other S-parameters is shown in Appendix D. Apart from providing a much less cumbersome way of measuring the three-port S-parameters, these measurements serve a dual purpose – they provide a way of quantifying the errors being introduced due to cable bends etc. in the S-parameter measurements. This is important since each and every source of error needs to be identified and minimized. Secondly, although these inferred S-parameters are very similar to the measured ones, they are being used for a small improvement in accuracy in the previous sections.

The aim of this research has been to build a calibration-free VNA system using only the standing-wave voltage measurements from an inexpensive diode. Having determined that both normalized (S21 from HP8510C VNA) and raw (b2 from HP8510C VNA) standing-wave voltage measurements can be used to get a good estimate of the reflection coefficient Γ, different ways were considered to measure power similar to a diode. Thermistors have traditionally been used for accurate RF power measurements [24]. Hence, they were considered but the available models could not operate at the low power levels available. Hence, another instrument which can measure RF power accurately, i.e., the spectrum analyzer was used.

5.4. SPECTRUM ANALYZER AS DETECTOR

A spectrum analyzer is an instrument used to measure signal amplitude as a function of frequency. In case of the X-band VNA, it operates through X-band (8.2 to 12.4 GHz) and the input frequency is set by the user. Hence, a spectrum analyzer can be used to accurately measure the RF power level at any set frequency. Agilent's 8563E spectrum analyzer was used for standing-wave measurement in the configuration shown in Figure 5.21.

Figure 5.21. Setup to measure signal power using a spectrum analyzer.

The setup for these measurements is exactly same as the previous cases, except in place of the detector system, the spectrum analyzer is connected. Making the measurements itself, is slightly more complicated. Having set the source (HP8510C VNA) to a specific frequency, a peak-search is done on the spectrum analyzer keeping the "span" set to 20 KHz (constant) and a very wide resolution bandwidth (RBW) of 300 Hz. Setting the center frequency to this maximum-power point, the RBW is reduced and the same process is repeated till a RBW of 1Hz is reached. At this point, an almost flat power waveform is captured from the instrument and the average of these values is saved as the power corresponding to the standing-wave measurement. A similar sweep of span is also performed (20 KHz to 100 Hz). The entire process was automated using NI's LABVIEW software. A time delay (750 ms) is provided after each setting to account for the instrument settling time. Upon repeating the process of Γ estimation using these

measured values for the eight DUTs, the results are found to be very similar to those with the Schottky detector, in the sense that the process of 3-load calibration improves them substantially. The results are shown in Figures 5.22 and 5.23.

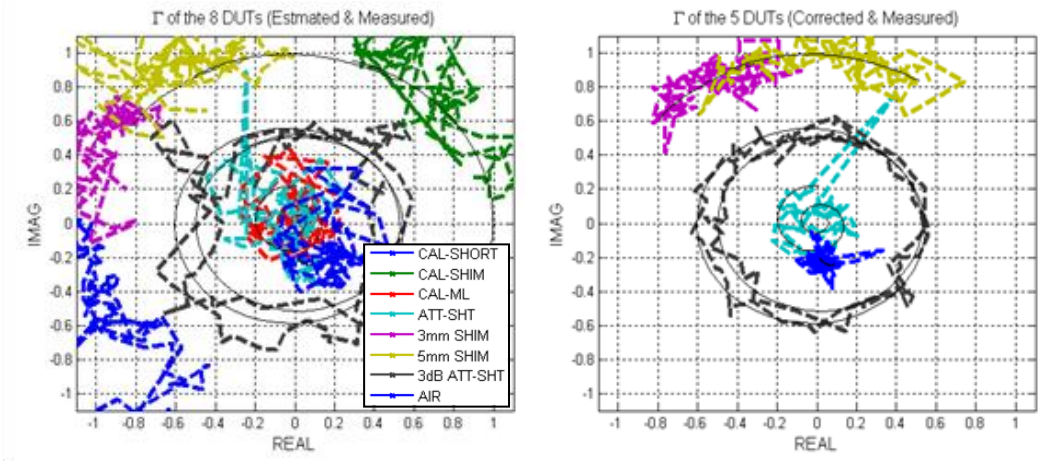

(a) (b)

Figure 5.22. Spectrum analyzer measurements: estimated & corrected Γ values for the eight DUTs. The thin black curves show the S11 values measured using a commercial VNA.

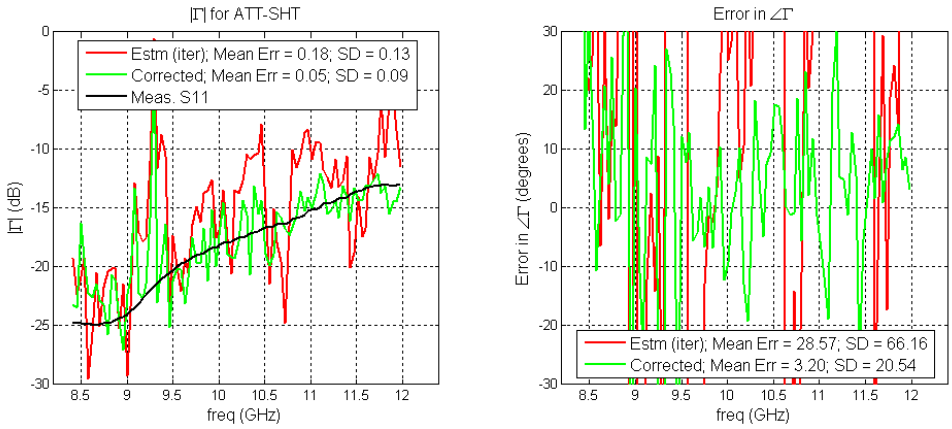

Figure 5.23. Magnitude & phase plots: estimated and corrected Γ values for the variable attenuated short.

Detailed results of these measurements are shown in Appendix E. For ruling out error introduction due to measurement or data acquisition (DAQ) style, the same

measurement was performed using GPIB as the control protocol, using linear and log scales on the spectrum analyzer and again using the video output on the spectrum analyzer for DAQ. The results were found to be very similar with all these cases and required the three-term based calibration. As mentioned earlier, the frequency stability of even the HP8510C VNA was tested using this spectrum analyzer as described in the next section.

5.4.1. Frequency Stability of the VNA. Spectrum analyzer is also used to measure "spectrum" or the frequency characteristics of an RF signal. A vector network analyzer by itself is a very accurate instrument. Yet, the HP8510C VNA used for measurements has not been "company calibrated" for many years. Hence, its frequency stability was tested using the spectrum analyzer system. While performing the repeated power measurements with the setup described earlier, the peak frequency was also measured in every step. The VNA's frequency was found to be quite stable and accurate. The results are shown in Appendix F.

5.5. GROUND NOISE REMOVAL AND MAGIC-T MEASUREMENTS

National Instruments's (NI) DAQ and control-hardware controls two system parameters – the analog control voltage of the phase-shifter and the measurement of the standing-wave voltage measured by detector. There is a small (~5 mV) DC bias in the NI DAQ analog inputs system which may vary due to grounding noise and the same may introduce errors in the detector output and analog control input to the phase-shifter. Based on electromagnetic compatibility (EMC) expert Dr. David Pommerenke's advice, to remove any such noise, the whole system was connected to a common ground using an Aluminum foil as shown in Figure 5.24 and the measurements repeated.

Figure 5.24. Metal foil for ground-noise removal.

There was no improvement in the results using this setup and so effect of ground noise was discarded as a possible cause of error.

All the measurements for Γ estimation described earlier can be categorized in two generic groups: (1) the measurements using VNA as detector, measuring S21 – these do not need calibration, hence proving the theoretical basis of the present work and (2) power measurements using various detection schemes which require calibration. Each of these two groups of measurements requires a different setup. A measurement setup using a "Magic-T" was envisaged which enables both these measurements to be carried out at the same time as shown in Figure 5.25.

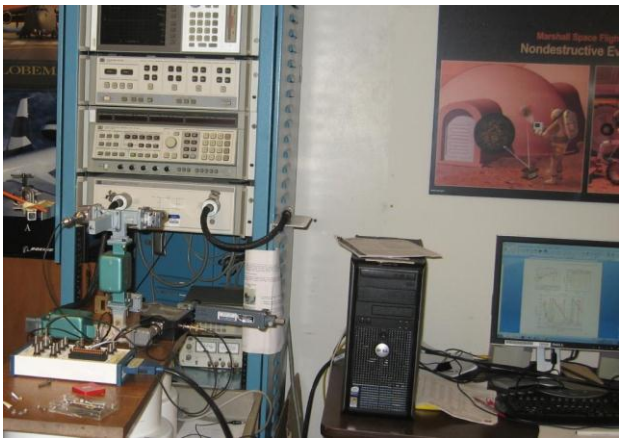

Figure 5.25. Setup to perform measurements using a Magic-T.

Magic T is a waveguide based hybrid coupling device. Attached at the detector port (P3) of the VNA, it is used to split the coupled signal into two equal parts. Due to symmetry, output at each of these ends is symmetric and hence, can be measured with different detection schemes described above. A new three-port characterization was performed to include the Magic-T in the system model. The S21 measurements from one end result in good Γ estimation while the same at the other end using a Schottky detector require calibration as illustrated in Figures 5.26 and 5.27 for the variable attenuated short as the DUT.

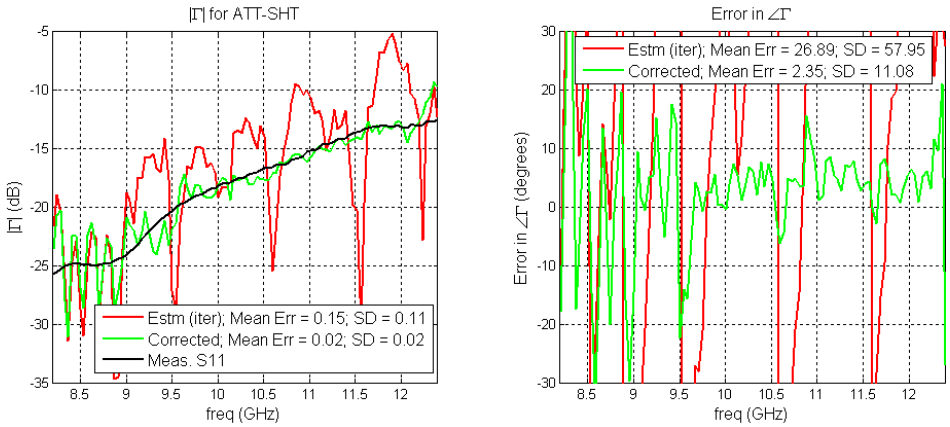

Figure 5.26. Estimated and corrected Γ using Schottky detector measurements.

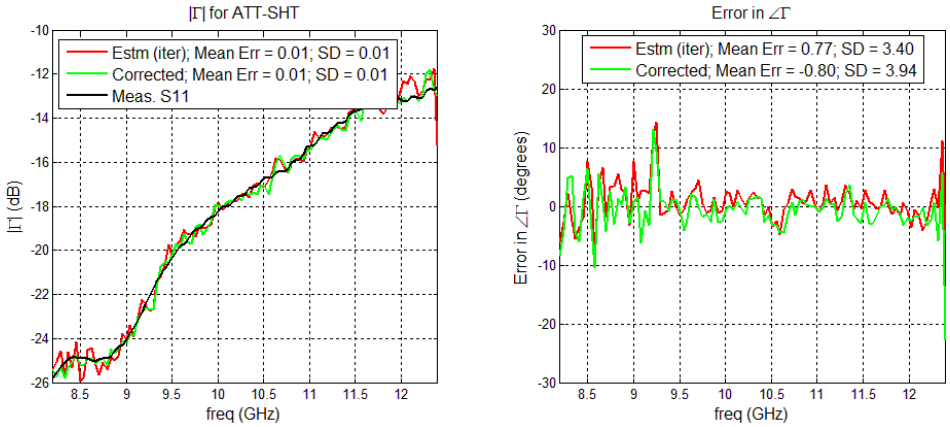

Figure 5.27. Estimated and corrected Γ using un-calibrated S21 measurements.

Detailed results for these two cases are shown in Appendix G. In this setup every parameter is the same for the two measurement cases except the detection method.

Hence, these measurements using the Magic T were conclusive in proving that the errors are not in the measurement methodology or system characterization.

5.6. FURTHER INVESTIGATION OF THE SOURCE OF ERROR

As is clear from the measurements using the Magic-T, the measurements made using any kind of power measurement scheme (Schottky diode, spectrum analyzer, log detector, etc.) require a three-term calibration procedure to correct the Γ estimation results. In order to better understand the "correction" being brought using the calibration procedure, T-parameters were used. Using the conversion to T-parameters illustrated in Figure 5.28, the errors were merged into the S-parameters resulting in the new equivalent or corrected S-parameters (shown in red color).

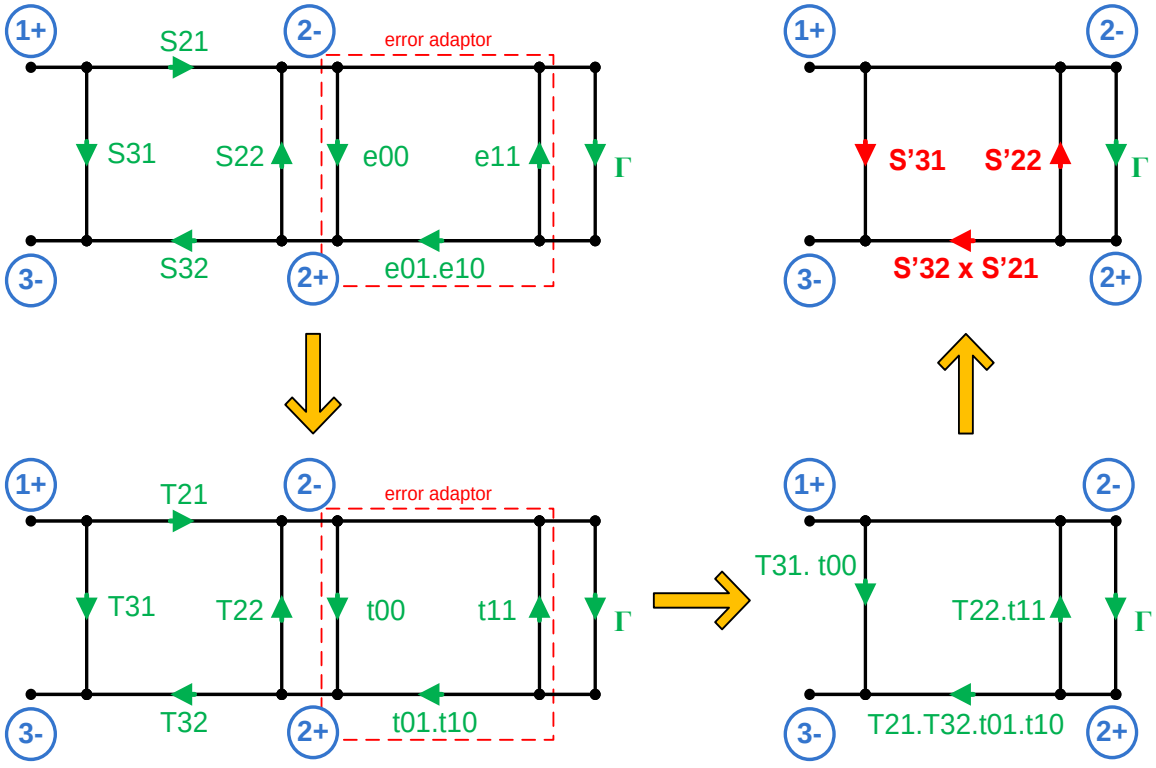

Figure 5.28. Use of T-parameter equivalence for error investigation.

This conversion enables the one-to-one comparison of the measured S-parameters and the calculated or equivalent system S-parameters. It may be used to locate the cause of error. The comparison of these equivalent S-parameters with the measured S-parameters along with the calculated error terms is shown in Figures 5.29 to 5.34.

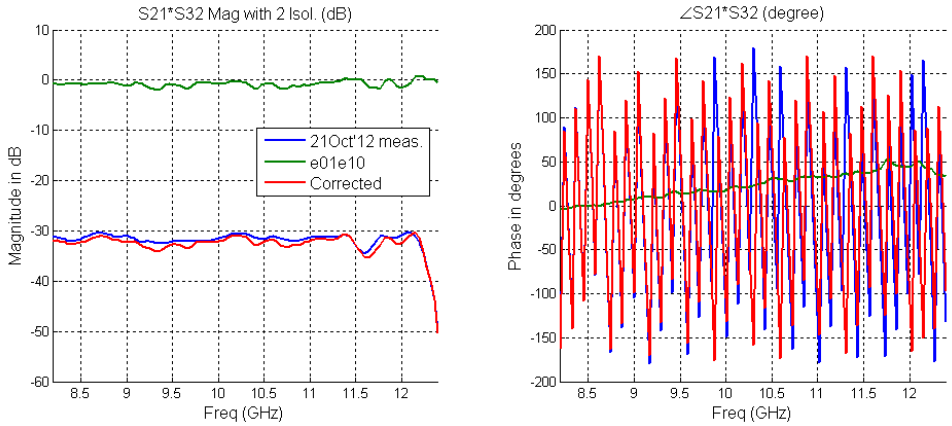

Figure 5.29. Measured and corrected S21xS32 term: magnitude and phase.

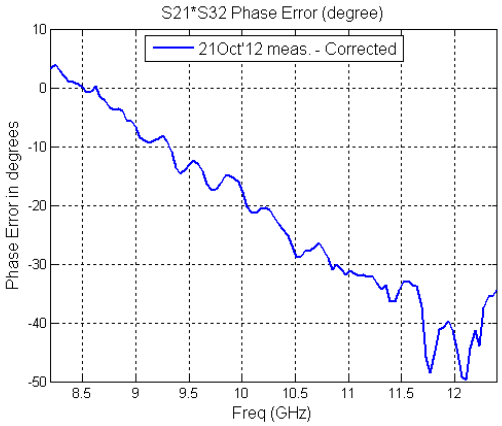

Figure 5.30. Measured and corrected S21xS32 term: phase error.

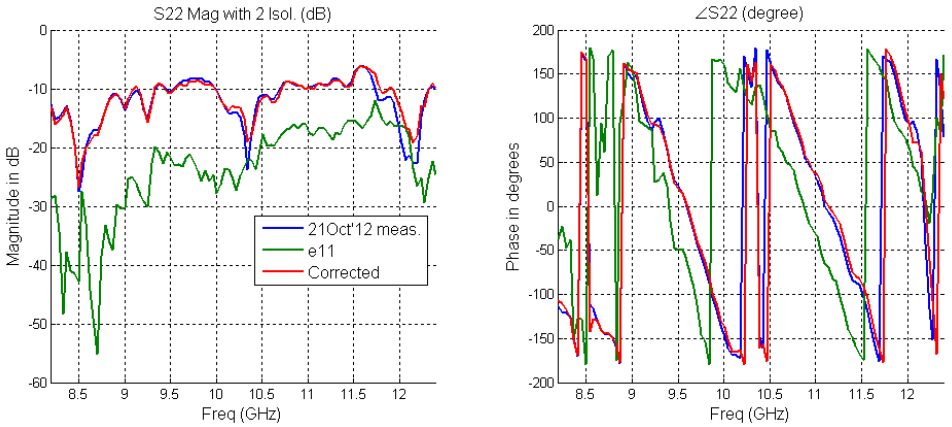

Figure 5.31. Measured and corrected S22 term: magnitude and phase.

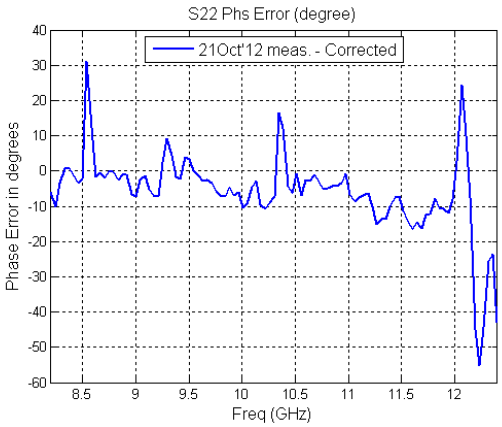

Figure 5.32. Measured and corrected S22 term: phase error.

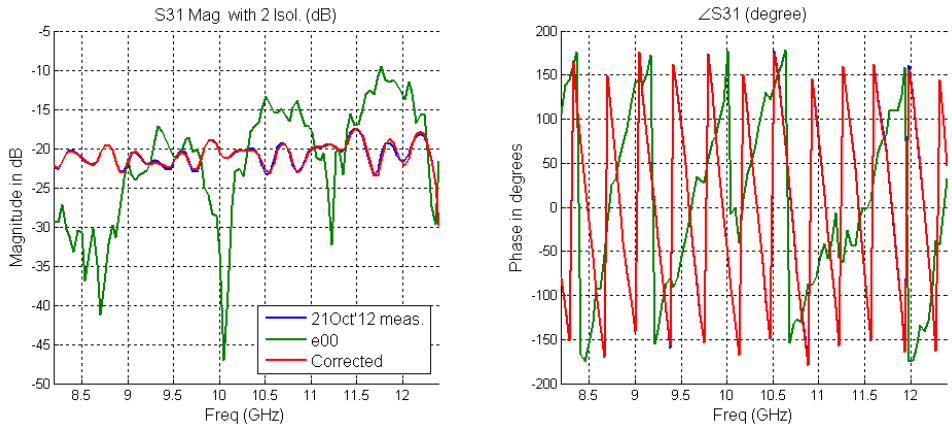

Figure 5.33. Measured and corrected S31 term: magnitude and phase.

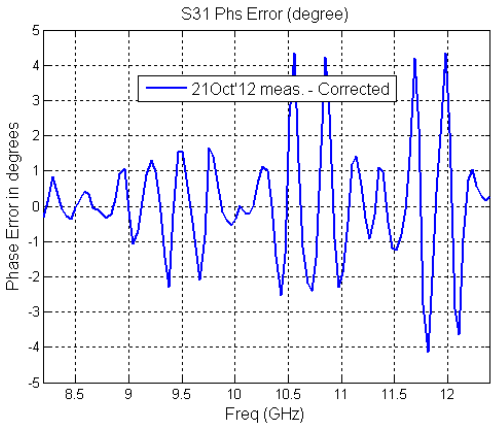

Figure 5.34. Measured and corrected S31 term: phase error.

Except for the phase-error in S21×S32 (Figure 5.30), all other magnitude and phases show relatively less deviation. The significant phase-error of Figure 5.30 can be approximated by a straight line, i.e., a phase error increasing linearly with frequency as shown in Figure 5.35.

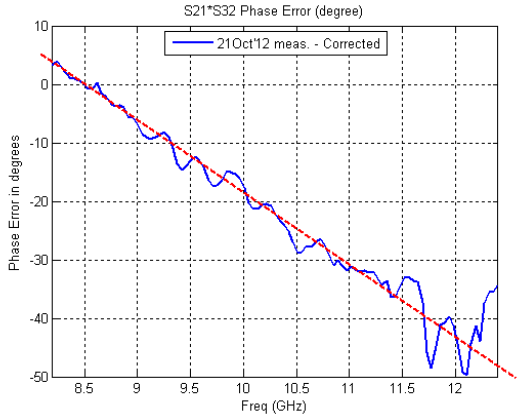

Figure 5.35. Approximate line fitted to the phase error.

The line in Figure 5.35 looks like a shim of 2.8 mm placed in the transmission line at the detector port. These corrected S-parameters, if used in place of the measured system model, give the accurate or the "corrected" result shown in the above figures. In other words, if a theoretical bias can be found to explain the origin of these new S-parameters or this "2.8 mm shim" error, the VNA system becomes calibration-free.

6. CONCLUSION

This X-band VNA was able to achieve the proposed calibration-free result only when another VNA (un-calibrated & without phase reference) was used as a detector. Various other power detection schemes were used for the standing-wave measurement but the Γ estimation always requires a three-load calibration. This indicates that some deterministic errors still remain in the system and are being fixed by this process of calibration. Although a theoretical bias could not be found, the precise correction required to make the VNA calibration-free was determined experimentally. Moreover, even though the proposed VNA system could not be built with a power detector, each and every aspect beginning from system modeling using Matlab and CST, sensitivity analysis of system and analysis of the detection and data acquisition system was performed thoroughly – a learning exercise which would not have been accomplished otherwise. This thesis was a detailed description of all the different measurements and simulations performed with the aim of finding this remaining source of error.

APPENDIX A
ANALYTICAL CALCULATION OF REFLECTION COEFFICIENT (Γ)
(CALDECOTT'S METHOD)

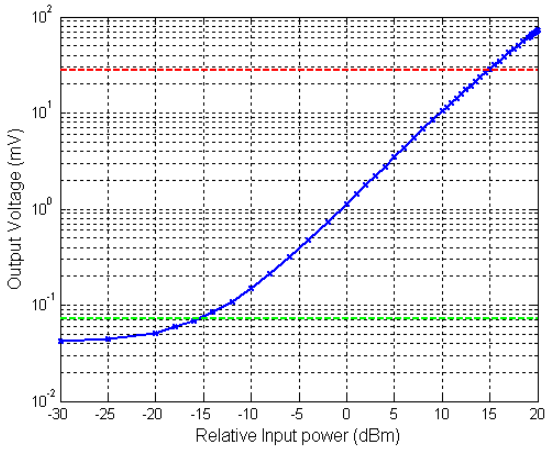

Characterization of the Schottky diode detector showing maximum (red) and minimum (green) voltage measured.

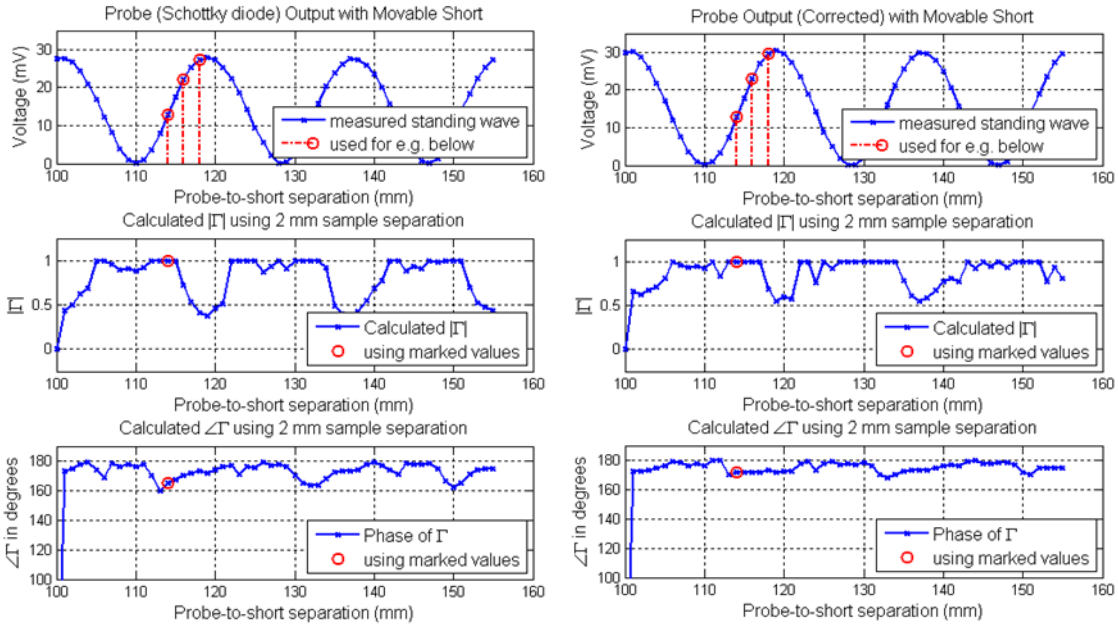

Γ calculation using three points as described by Caldecott in [6]

APPENDIX B

SENSITIVITY ANALYSIS RESULTS FOR KA-BAND SYSTEM & FOR THE PURELY THEORETICAL MODEL

Sensitivity analysis results for Ka-band system (using measured S-parameters of the Ka-band system):

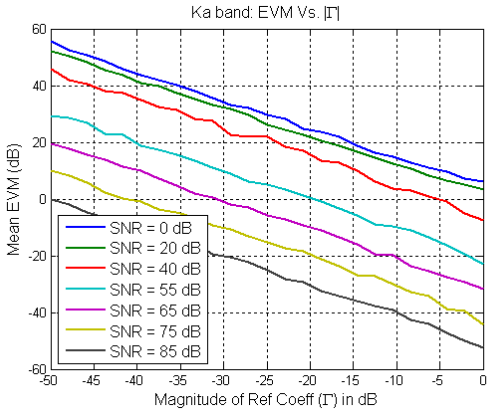

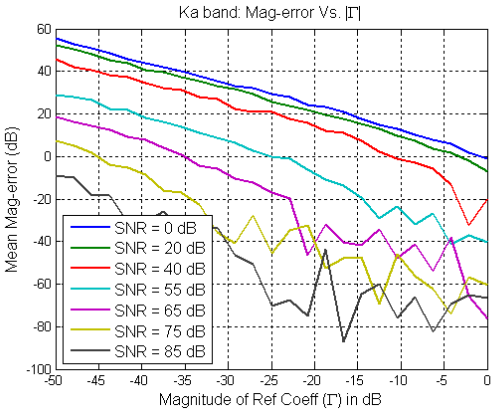

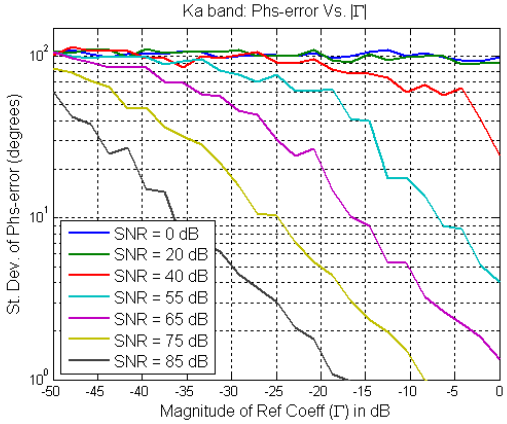

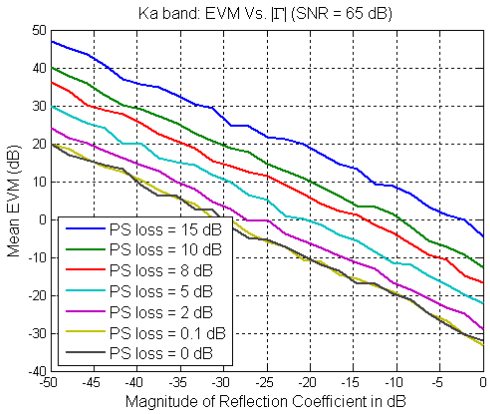

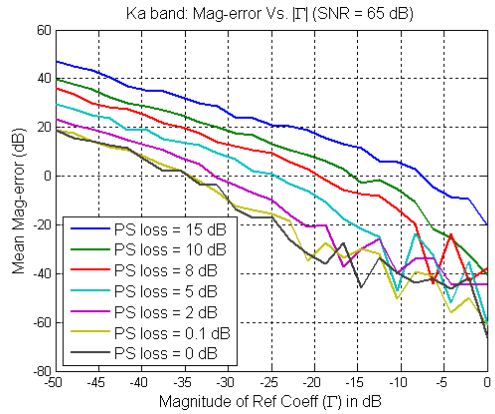

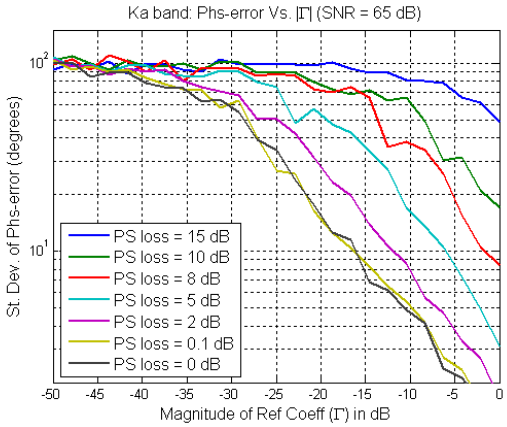
Ka band: Phs-error Vs. |Γ| (SNR = 65 dB)
St. Dev. of Phs-error (degrees)
Magnitude of Ref Coeff (Γ) in dB
PS loss = 15 dB
PS loss = 10 dB
PS loss = 8 dB
PS loss = 5 dB
PS loss = 2 dB
PS loss = 0.1 dB
PS loss = 0 dB

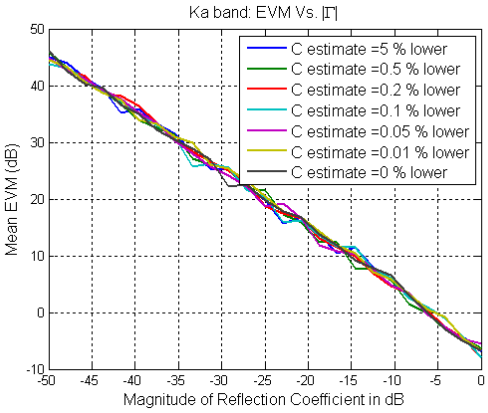
Ka band: EVM Vs. |Γ|
Mean EVM (dB)
Magnitude of Reflection Coefficient in dB
C estimate =5 % lower
C estimate =0.5 % lower
C estimate =0.2 % lower
C estimate =0.1 % lower
C estimate =0.05 % lower
C estimate =0.01 % lower
C estimate =0 % lower

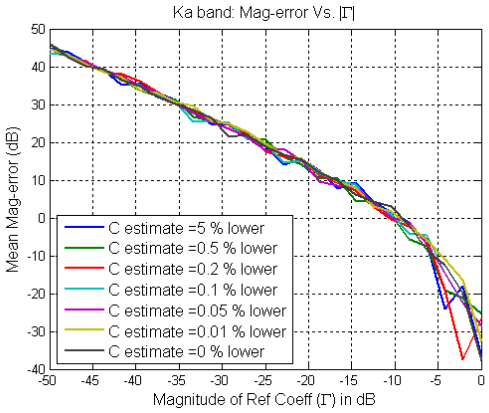
Ka band: Mag-error Vs. |Γ|
Mean Mag-error (dB)
Magnitude of Ref Coeff (Γ) in dB
C estimate =5 % lower
C estimate =0.5 % lower
C estimate =0.2 % lower
C estimate =0.1 % lower
C estimate =0.05 % lower
C estimate =0.01 % lower
C estimate =0 % lower

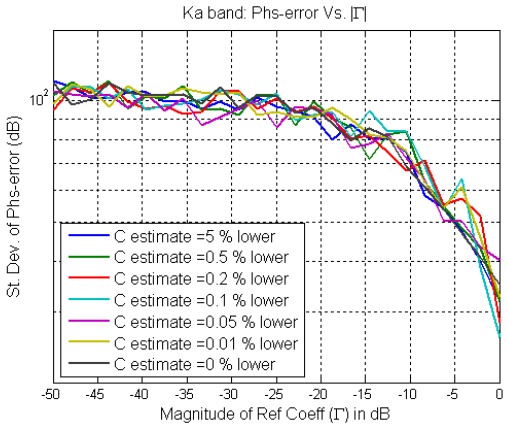
Ka band: Phs-error Vs. |Γ|
St. Dev. of Phs-error (dB)
Magnitude of Ref Coeff (Γ) in dB
C estimate =5 % lower
C estimate =0.5 % lower
C estimate =0.2 % lower
C estimate =0.1 % lower
C estimate =0.05 % lower
C estimate =0.01 % lower
C estimate =0 % lower

Sensitivity analysis results for purely theoretical model - without using any measured data:

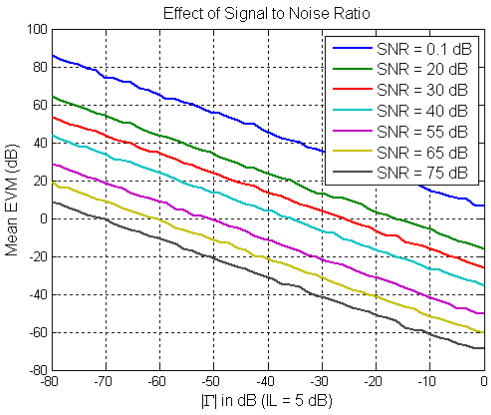

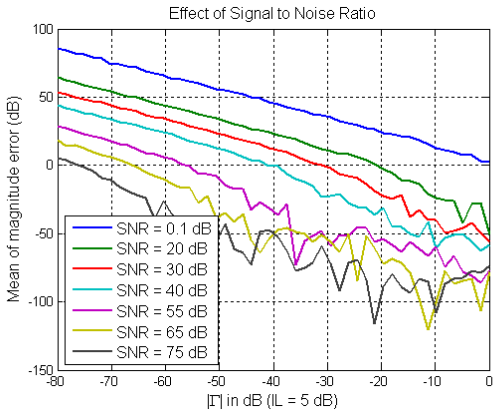

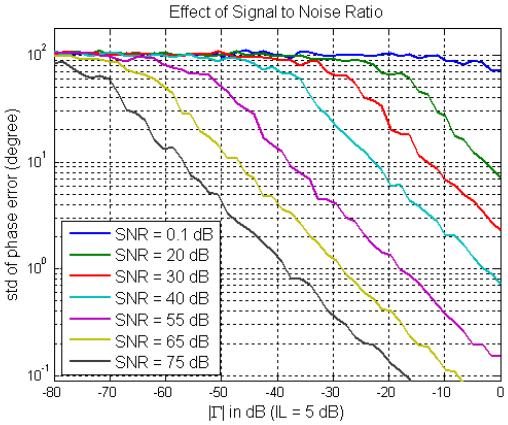

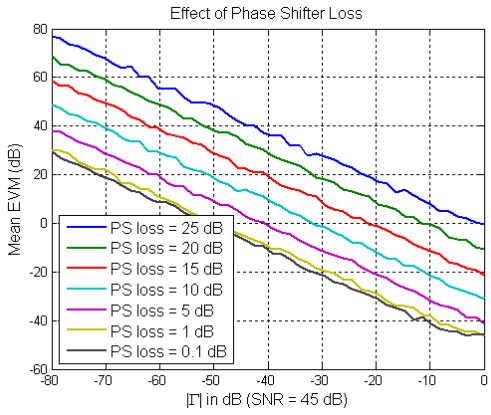

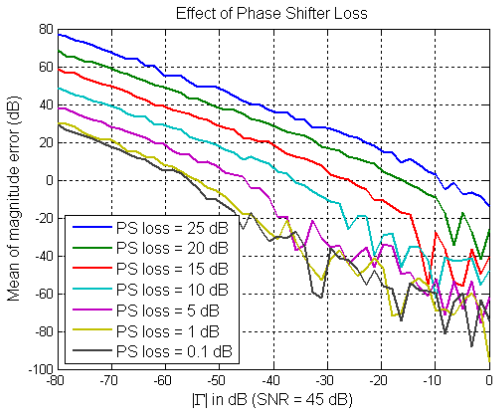

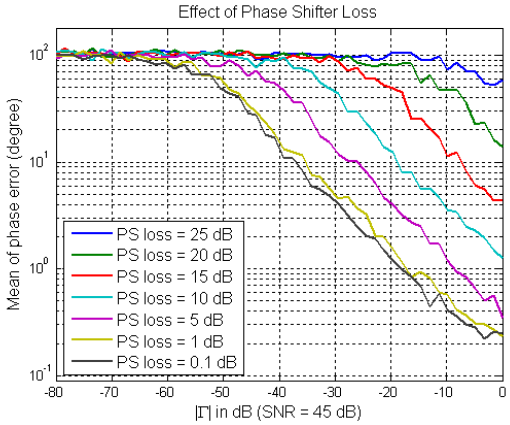
Effect of Phase Shifter Loss
Mean of phase error (degree)
|Γ| in dB (SNR = 45 dB)
PS loss = 25 dB
PS loss = 20 dB
PS loss = 15 dB
PS loss = 10 dB
PS loss = 5 dB
PS loss = 1 dB
PS loss = 0.1 dB

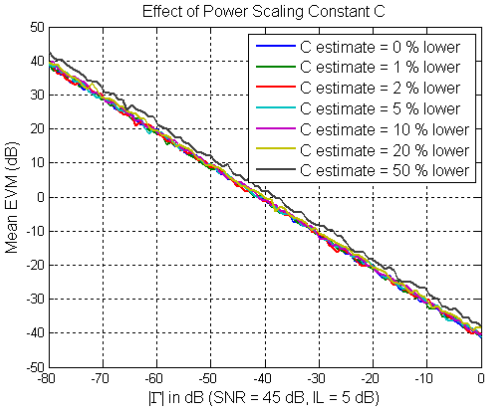
Effect of Power Scaling Constant C
Mean EVM (dB)
|Γ| in dB (SNR = 45 dB, IL = 5 dB)
C estimate = 0 % lower
C estimate = 1 % lower
C estimate = 2 % lower
C estimate = 5 % lower
C estimate = 10 % lower
C estimate = 20 % lower
C estimate = 50 % lower

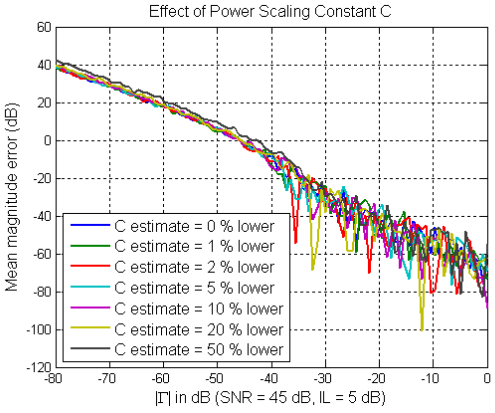
Effect of Power Scaling Constant C
Mean magnitude error (dB)
|Γ| in dB (SNR = 45 dB, IL = 5 dB)
C estimate = 0 % lower
C estimate = 1 % lower
C estimate = 2 % lower
C estimate = 5 % lower
C estimate = 10 % lower
C estimate = 20 % lower
C estimate = 50 % lower

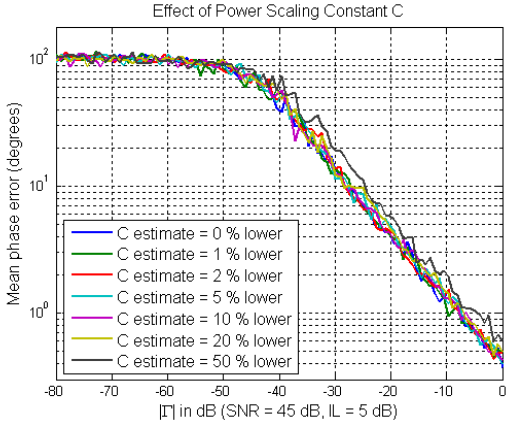
Effect of Power Scaling Constant C
Mean phase error (degrees)
|Γ| in dB (SNR = 45 dB, IL = 5 dB)
C estimate = 0 % lower
C estimate = 1 % lower
C estimate = 2 % lower
C estimate = 5 % lower
C estimate = 10 % lower
C estimate = 20 % lower
C estimate = 50 % lower

APPENDIX C

COMPLETE Γ ESTIMATION PROCESS USING KRYTAR SCHOTTKY DETECTOR

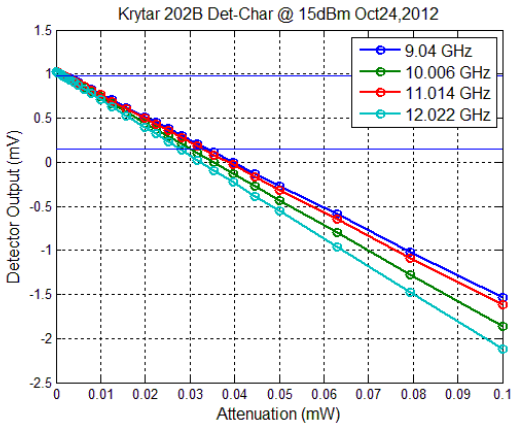

Detector characterization.

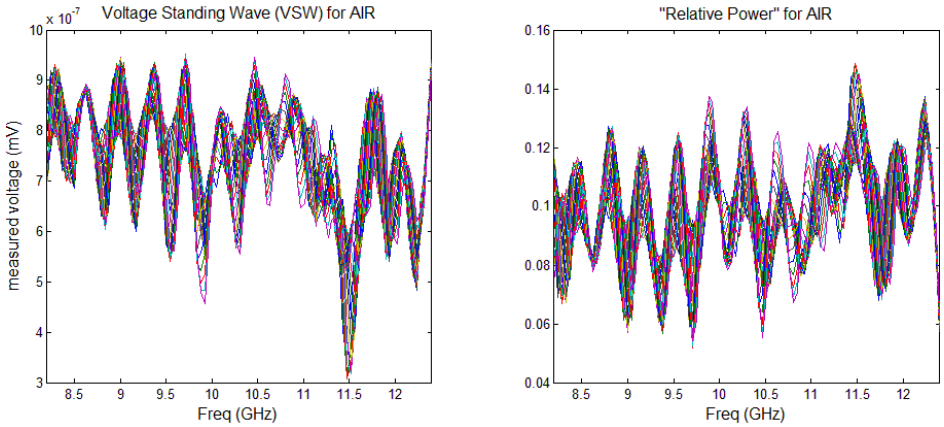

Measured voltage and the corresponding converted "relative power" for open-ended waveguide radiating in air (AIR) for all states of the phase-shifter.

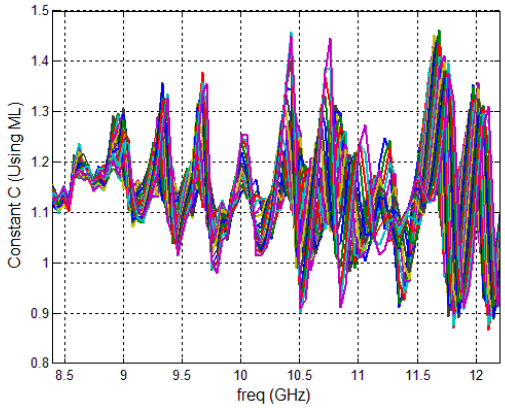

Calculated constant 'C' using measured Matched Load voltages for all states of the phase-shifter.

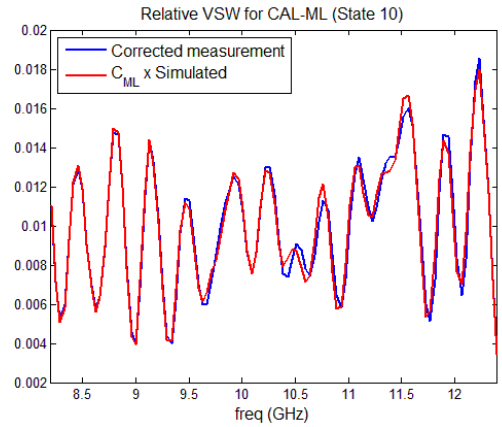

Comparison of measured and simulated voltages as a function of frequency for state 10 (10^{th} phase shift) of the phase-shifter.

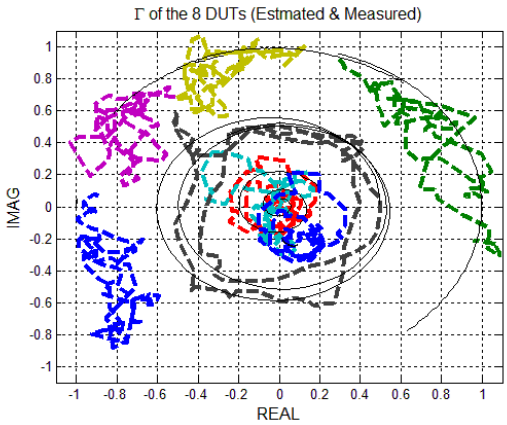

Reflection coefficients of the eight DUTs on a complex plane (thin black curves show the corresponding measured Γ).

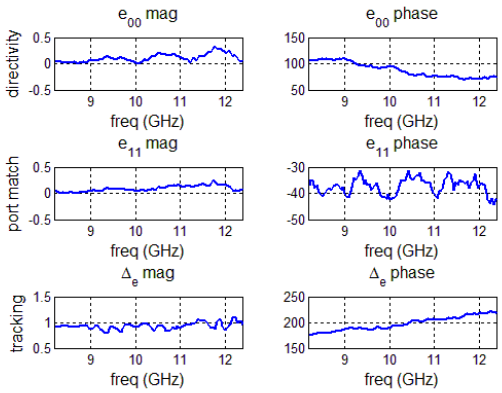

The three error terms found using measurements of the three "calibration loads" i.e., short, 9 mm shim and matched load.

The magnitudes, phases and phase-errors of the estimated, calibrated (corrected) and measured reflection coefficients (Γ) for each of the five DUTs, i.e., attenuated short with variable attenuation (ATT-SHT), 3 mm shim, 5 mm shim, 3 dB attenuated short and open-ended waveguide radiating into air (AIR):

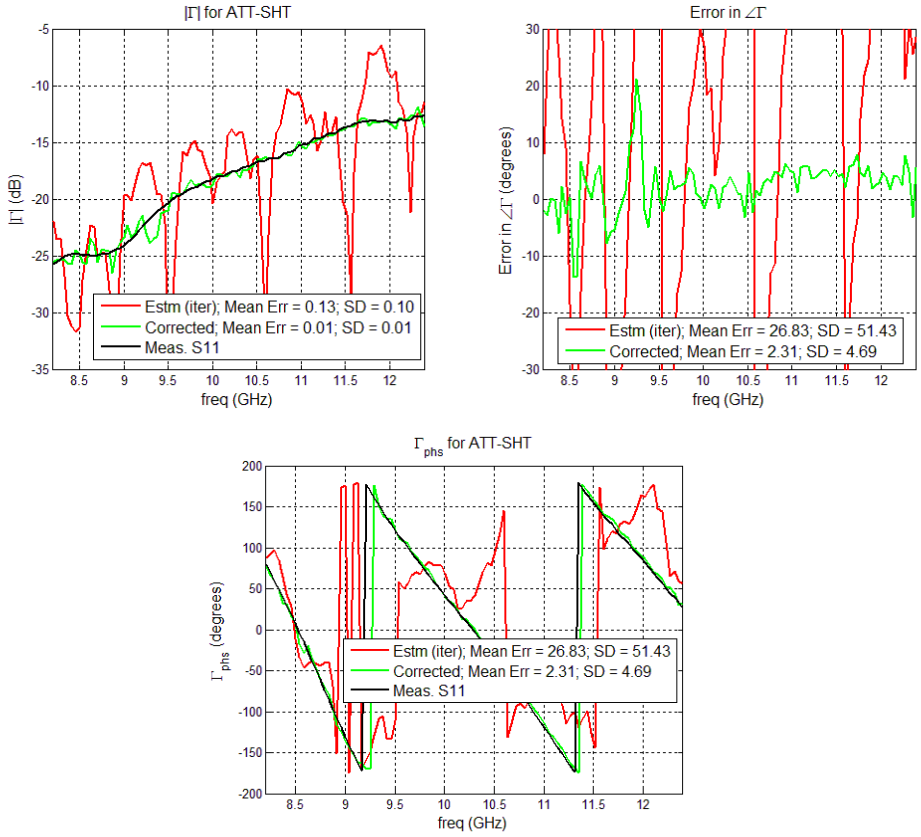

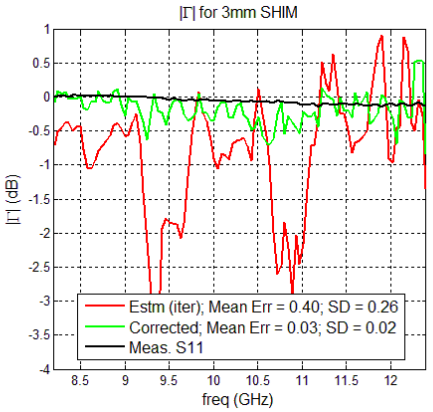
|Γ| for 3mm SHIM
|Γ| (dB)
freq (GHz)
Estm (iter); Mean Err = 0.40; SD = 0.26
Corrected; Mean Err = 0.03; SD = 0.02
Meas. S11

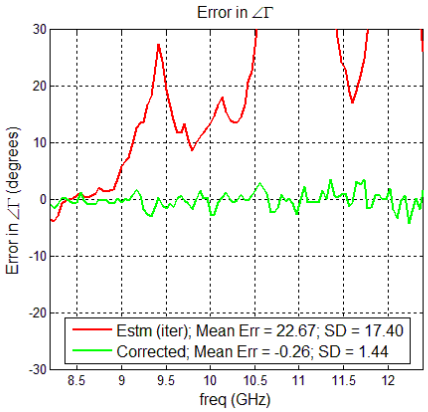
Error in ∠Γ
Error in ∠Γ (degrees)
freq (GHz)
Estm (iter); Mean Err = 22.67; SD = 17.40
Corrected; Mean Err = -0.26; SD = 1.44

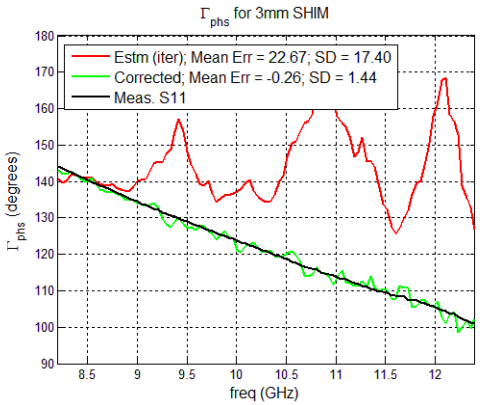
Γphs for 3mm SHIM
Γphs (degrees)
freq (GHz)
Estm (iter); Mean Err = 22.67; SD = 17.40
Corrected; Mean Err = -0.26; SD = 1.44
Meas. S11

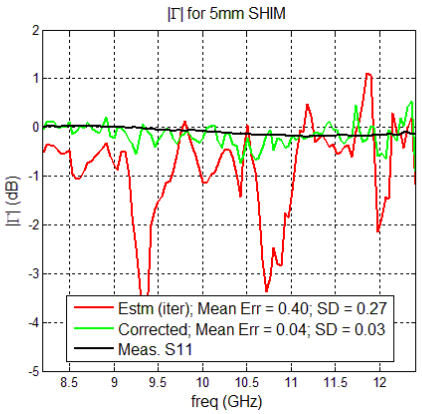
|Γ| for 5mm SHIM
|Γ| (dB)
freq (GHz)
Estm (iter); Mean Err = 0.40; SD = 0.27
Corrected; Mean Err = 0.04; SD = 0.03
Meas. S11

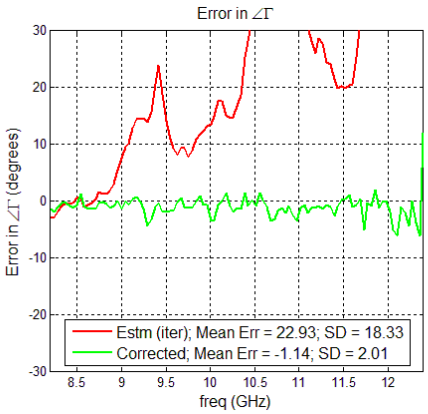
Error in ∠Γ
Error in ∠Γ (degrees)
freq (GHz)
Estm (iter); Mean Err = 22.93; SD = 18.33
Corrected; Mean Err = -1.14; SD = 2.01

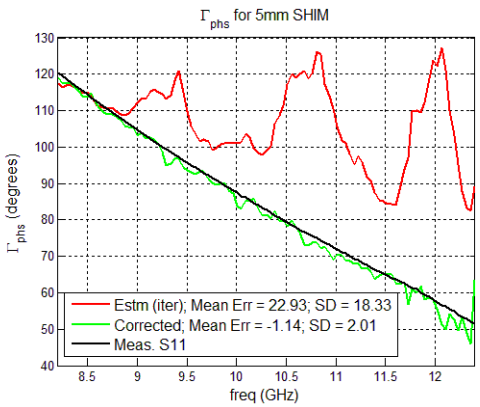
Γphs for 5mm SHIM
Γphs (degrees)
freq (GHz)
Estm (iter); Mean Err = 22.93; SD = 18.33
Corrected; Mean Err = -1.14; SD = 2.01
Meas. S11

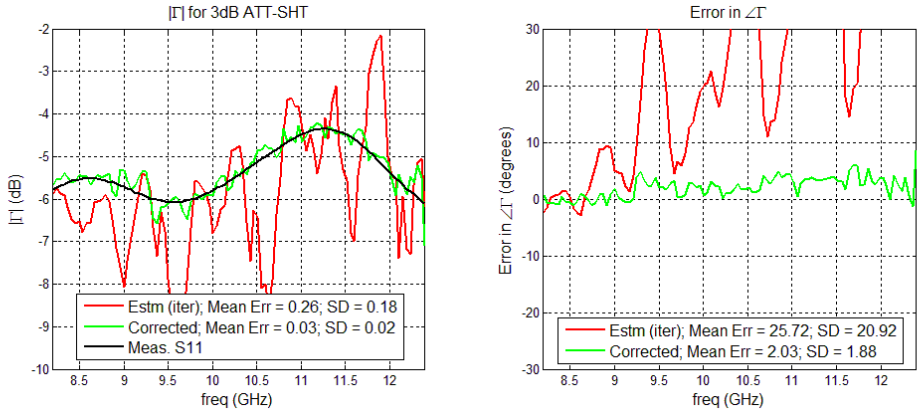
|Γ| for 3dB ATT-SHT
|Γ| (dB)
freq (GHz)
Estm (iter); Mean Err = 0.26; SD = 0.18
Corrected; Mean Err = 0.03; SD = 0.02
Meas. S11
Error in ∠Γ
Error in ∠Γ (degrees)
freq (GHz)
Estm (iter); Mean Err = 25.72; SD = 20.92
Corrected; Mean Err = 2.03; SD = 1.88

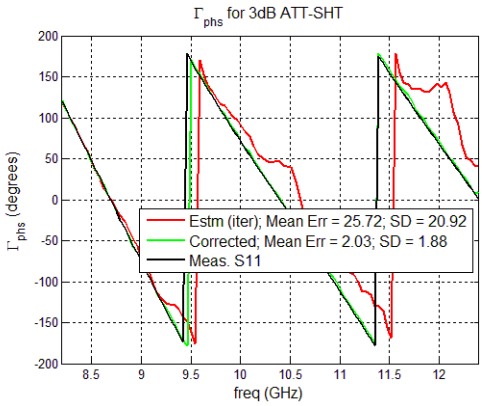
Γphs for 3dB ATT-SHT
Γphs (degrees)
freq (GHz)
Estm (iter); Mean Err = 25.72; SD = 20.92
Corrected; Mean Err = 2.03; SD = 1.88
Meas. S11

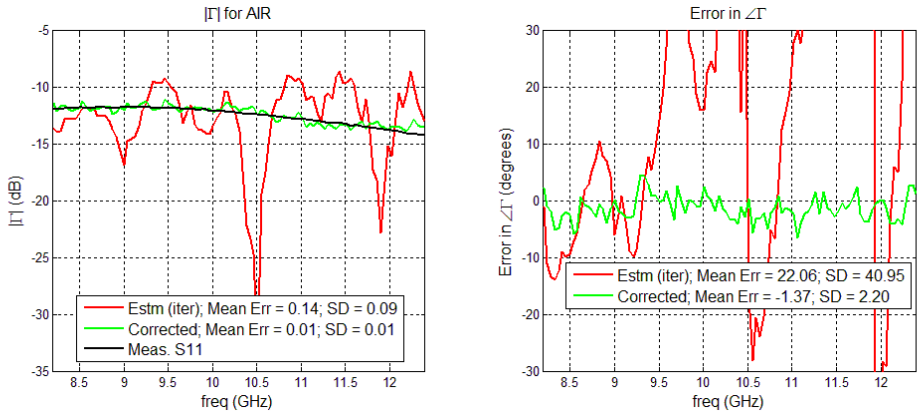
|Γ| for AIR
|Γ| (dB)
freq (GHz)
Estm (iter); Mean Err = 0.14; SD = 0.09
Corrected; Mean Err = 0.01; SD = 0.01
Meas. S11
Error in ∠Γ
Error in ∠Γ (degrees)
freq (GHz)
Estm (iter); Mean Err = 22.06; SD = 40.95
Corrected; Mean Err = -1.37; SD = 2.20

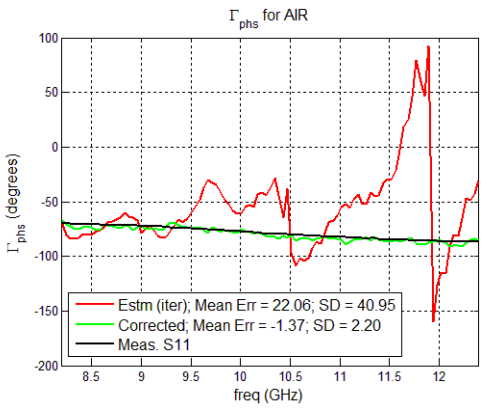
Γphs for AIR
Γphs (degrees)
freq (GHz)
Estm (iter); Mean Err = 22.06; SD = 40.95
Corrected; Mean Err = -1.37; SD = 2.20
Meas. S11

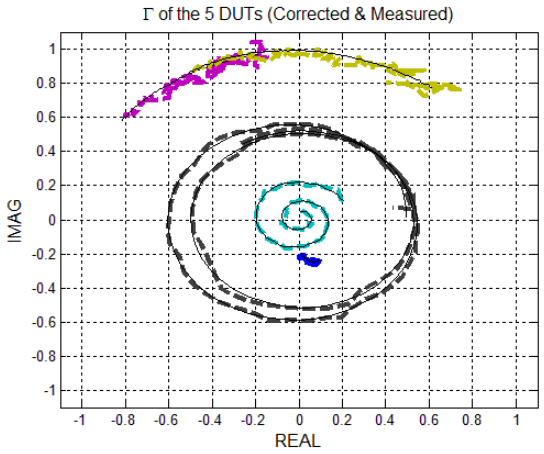

Corrected and measured Γ of the five DUTs shown on a complex plane.

APPENDIX D

CORRECTION AND VERIFICATION OF THREE-PORT S-PARAMETERS OF THE ONE PORT VNA SYSTEM

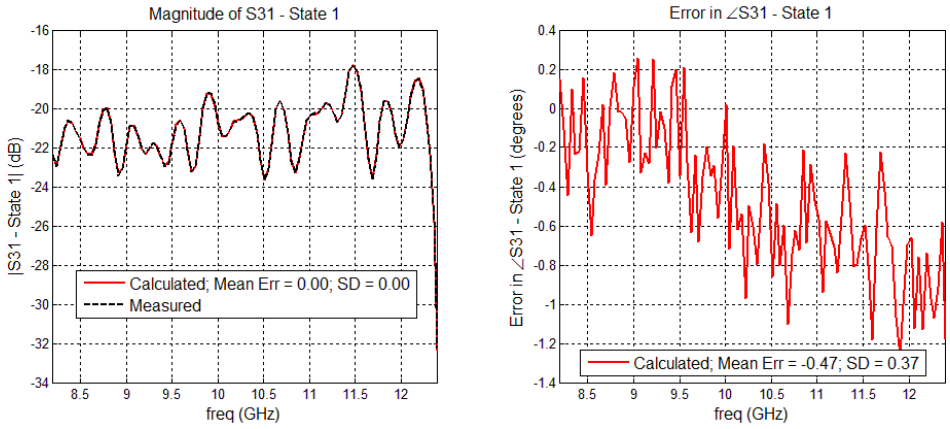

Measured and inferred (calculated) S-parameter S31 of the one-port VNA system.

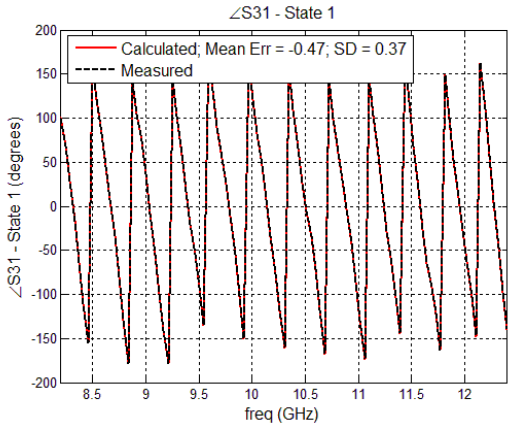

Measured and inferred (calculated) phase of S-parameter S31 of the one-port VNA system.

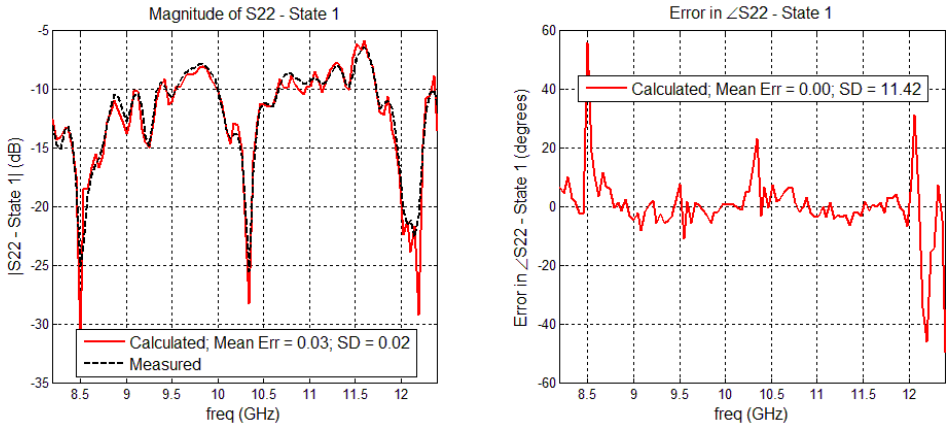

Measured and inferred (calculated) S-parameter S22 of the one-port VNA system.

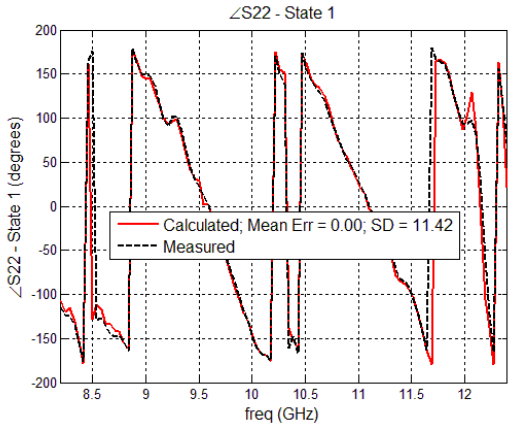

Measured and inferred (calculated) phase of S-parameter S22 of the one-port VNA system.

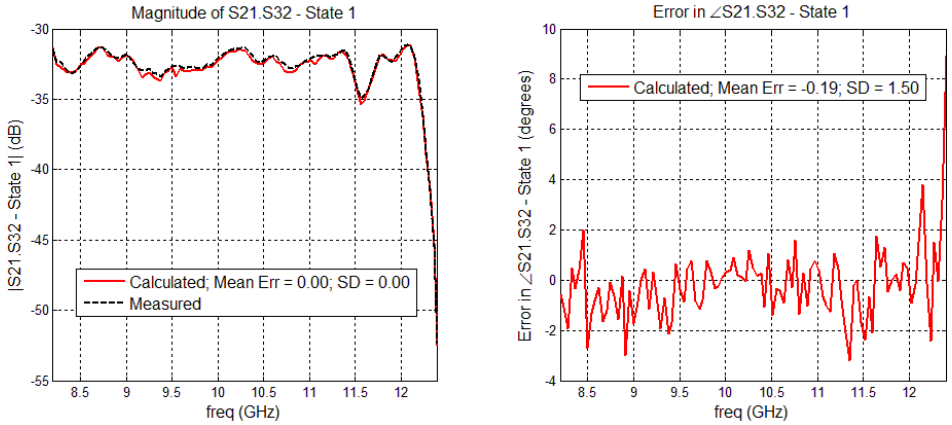

Measured and inferred (calculated) S-parameter S21xS32 of the one-port VNA system.

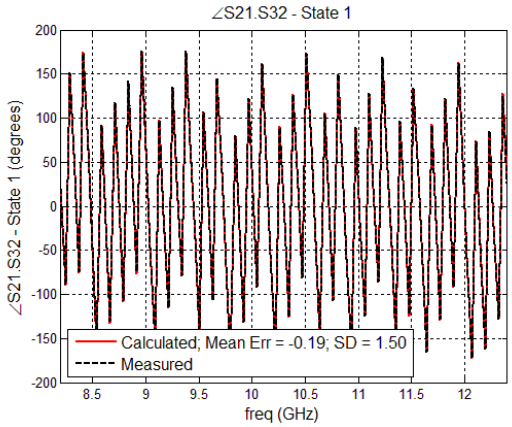

Measured and inferred (calculated) phase of S-parameter S21xS32 of the one-port VNA system.

APPENDIX E

REFLECTION COEFFICIENT ESTIMATION USING ALTERNATIVE MEASUREMENT METHODOLOGIES

Measurements and results using a Fluke multi-meter for measurement of Schottky detector output:

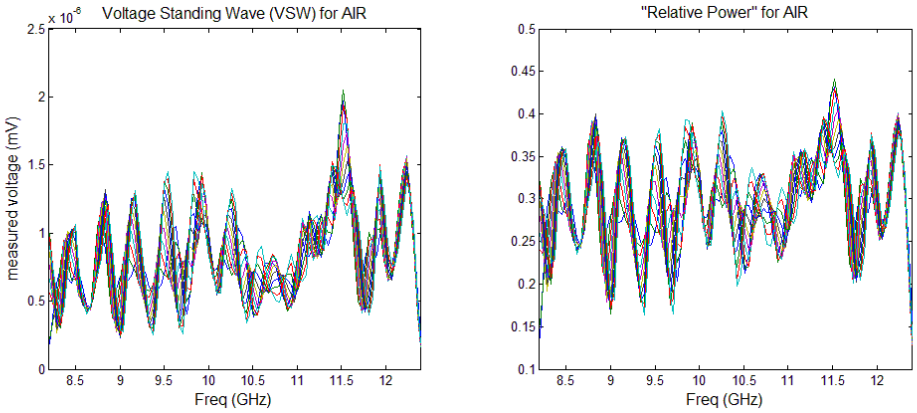

Measured and corrected voltages measured from the standing wave as a function of frequency.

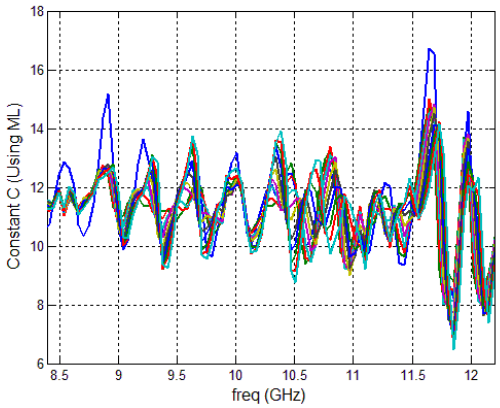

Calculation of the constant C using the 11 phase shifts. C is the average of these measured values.

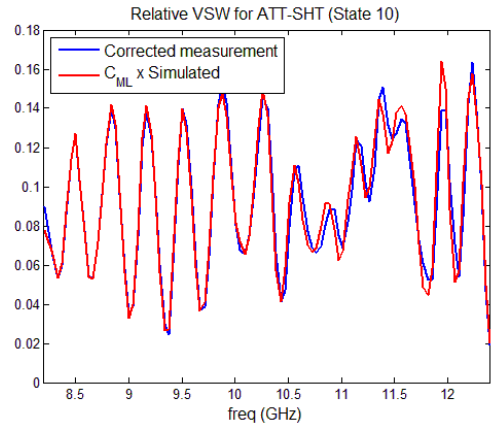

Matching the corrected standing wave measurement and the modeled voltages using the constant C.

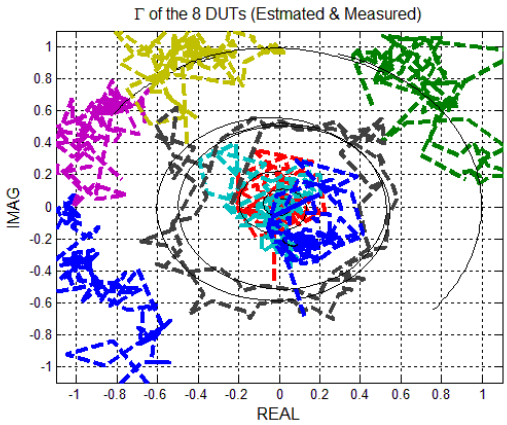

Estimated Γ for the eight DUTs.

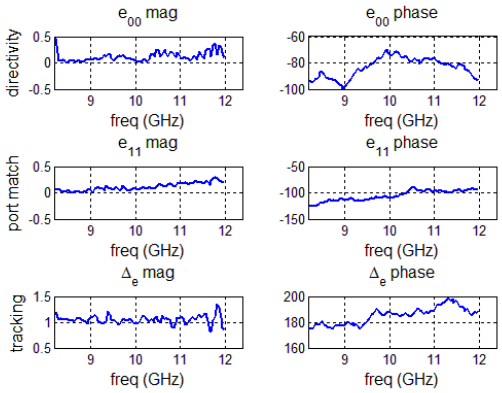

The three error terms calculated form measured and estimated reflection coefficients.

Comparing the measured, estimated and corrected Γ values and the corresponding errors for each of the five "non-calibration" loads:

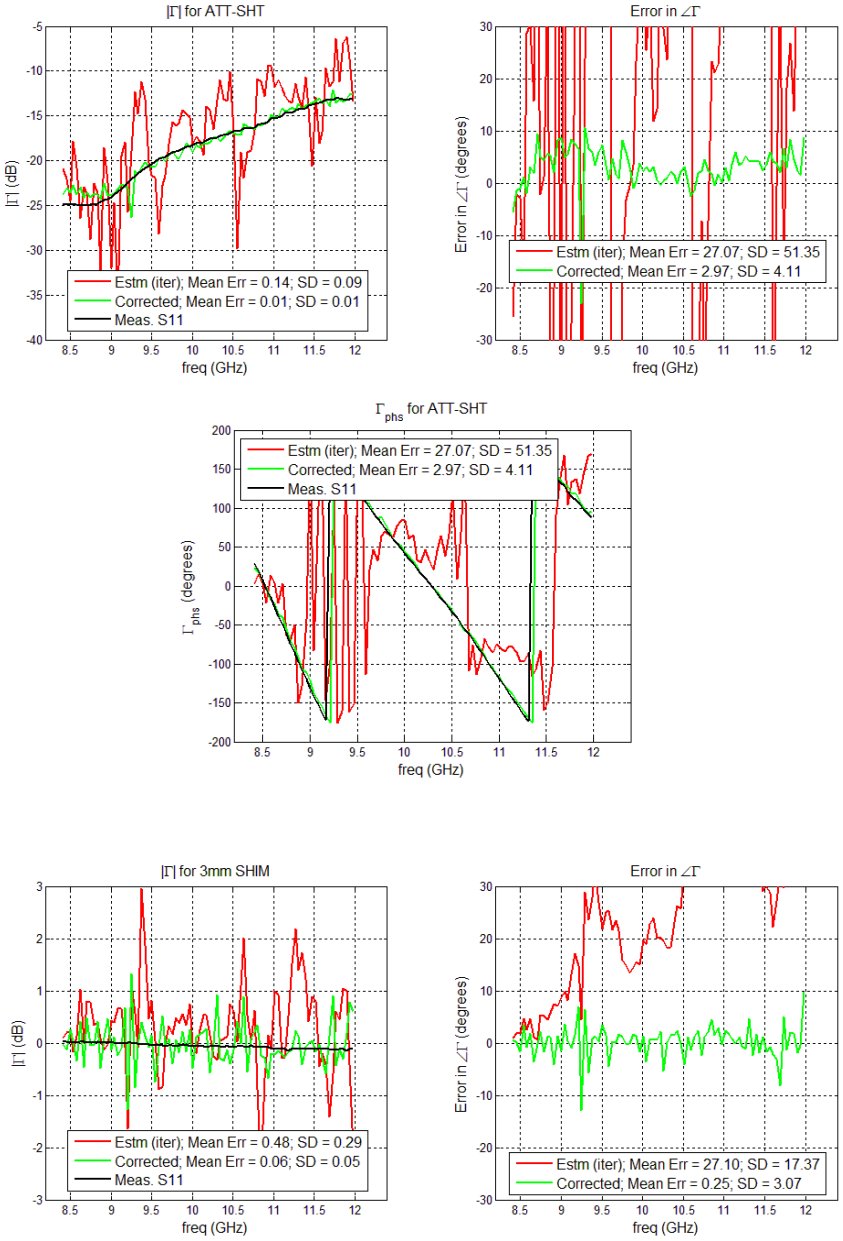

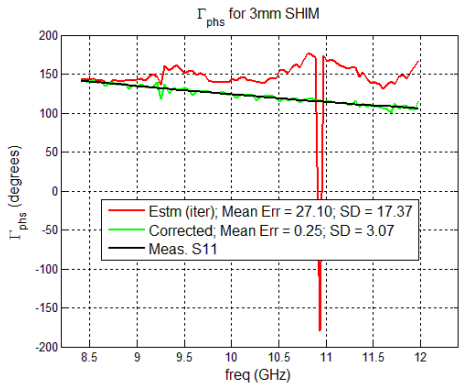
Γphs for 3mm SHIM
Γphs (degrees)
freq (GHz)
Estm (iter); Mean Err = 27.10; SD = 17.37
Corrected; Mean Err = 0.25; SD = 3.07
Meas. S11

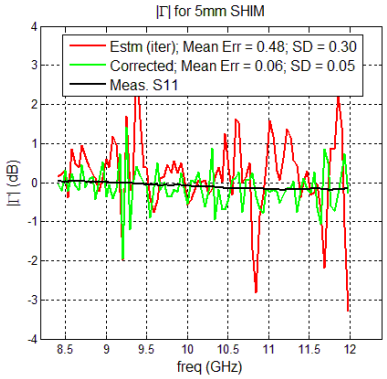
|Γ| for 5mm SHIM
|Γ| (dB)
freq (GHz)
Estm (iter); Mean Err = 0.48; SD = 0.30
Corrected; Mean Err = 0.06; SD = 0.05
Meas. S11

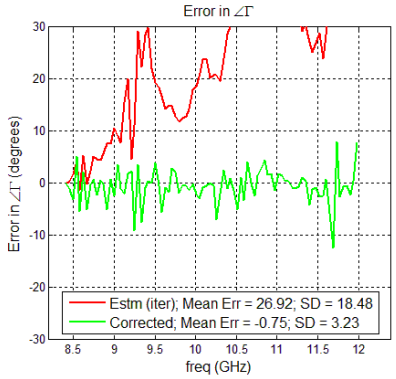
Error in ∠Γ
Error in ∠Γ (degrees)
freq (GHz)
Estm (iter); Mean Err = 26.92; SD = 18.48
Corrected; Mean Err = -0.75; SD = 3.23

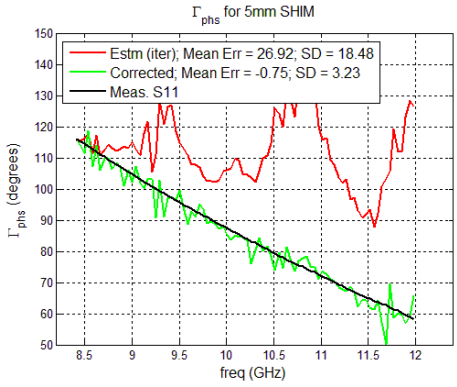
Γphs for 5mm SHIM
Γphs (degrees)
freq (GHz)
Estm (iter); Mean Err = 26.92; SD = 18.48
Corrected; Mean Err = -0.75; SD = 3.23
Meas. S11

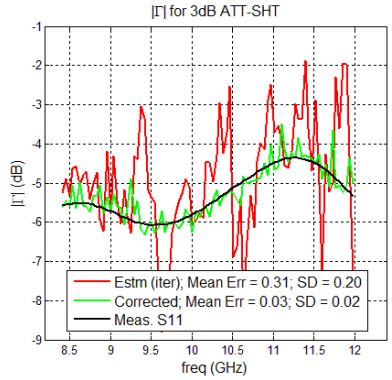
|Γ| for 3dB ATT-SHT
|Γ| (dB)
freq (GHz)
Estm (iter); Mean Err = 0.31; SD = 0.20
Corrected; Mean Err = 0.03; SD = 0.02
Meas. S11

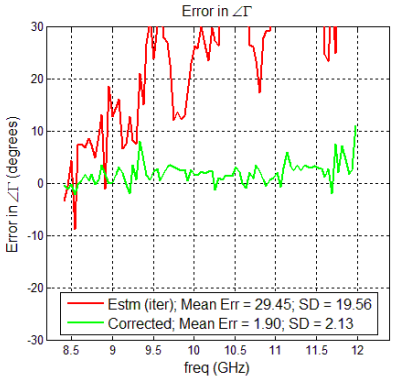
Error in ∠Γ
Error in ∠Γ (degrees)
freq (GHz)
Estm (iter); Mean Err = 29.45; SD = 19.56
Corrected; Mean Err = 1.90; SD = 2.13

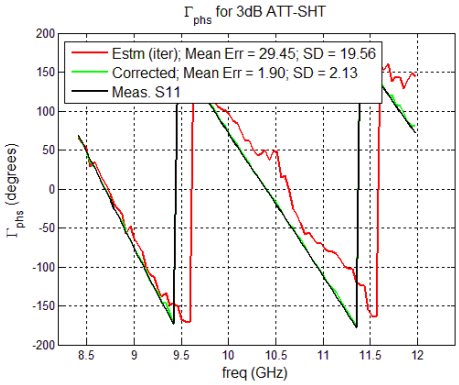
Γphs for 3dB ATT-SHT
Γphs (degrees)
freq (GHz)
Estm (iter); Mean Err = 29.45; SD = 19.56
Corrected; Mean Err = 1.90; SD = 2.13
Meas. S11

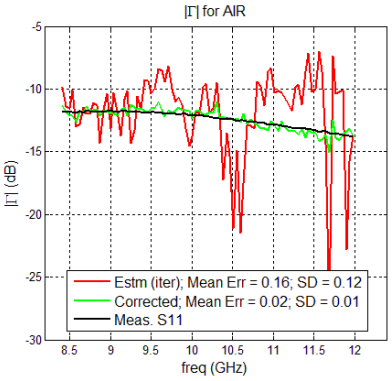
|Γ| for AIR
|Γ| (dB)
freq (GHz)
Estm (iter); Mean Err = 0.16; SD = 0.12
Corrected; Mean Err = 0.02; SD = 0.01
Meas. S11

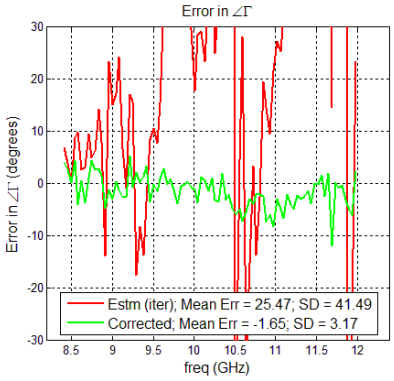
Error in ∠Γ
Error in ∠Γ (degrees)
freq (GHz)
Estm (iter); Mean Err = 25.47; SD = 41.49
Corrected; Mean Err = -1.65; SD = 3.17

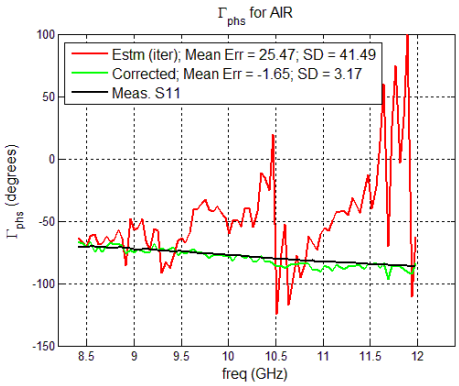
Γphs for AIR
Γphs (degrees)
freq (GHz)
Estm (iter); Mean Err = 25.47; SD = 41.49
Corrected; Mean Err = -1.65; SD = 3.17
Meas. S11

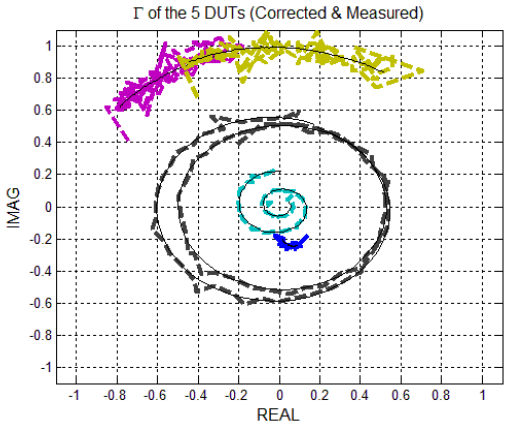

Corrected Γ of the five "non-calibration" DUTs shown on a complex plane.

Measurements and results using a Log-detector for measurement of standing wave voltage (using the Fluke multi-meter for DAQ):

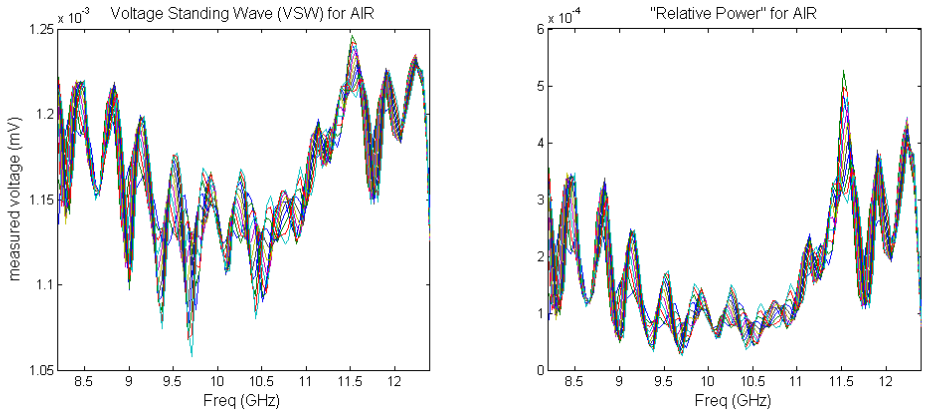

Measured and corrected voltages measured from the standing wave as a function of frequency.

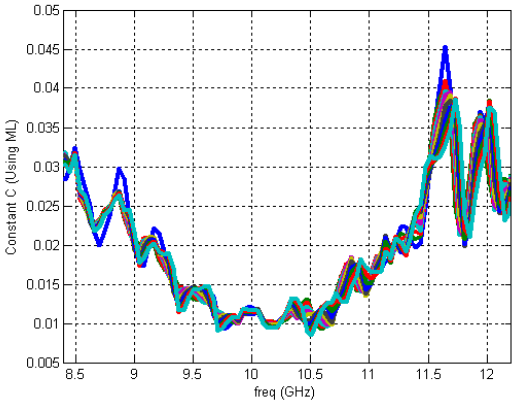

Calculation of the constant C using the 11 phase shifts. C is the average of these measured values.

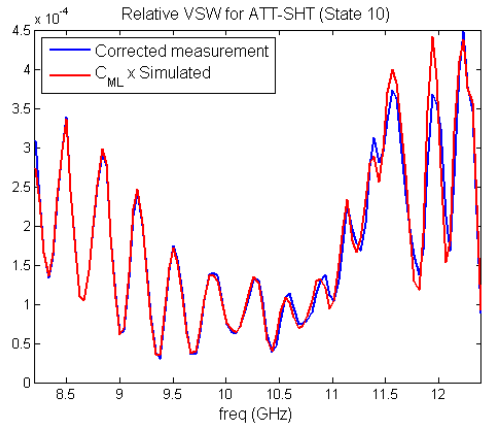

Matching the corrected standing wave measurement and the modeled voltages using the constant C.

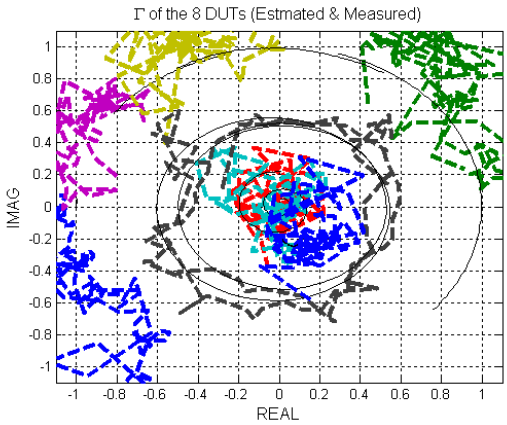

Figure 36. Estimated Γ for the eight DUTs.

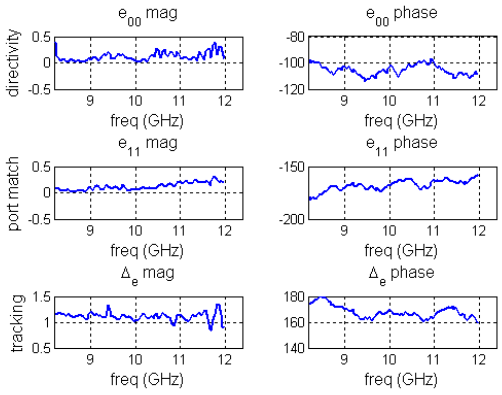

The three error terms calculated form measured and estimated reflection coefficients.

Comparing the measured, estimated and corrected Γ values and the corresponding errors for each of the five "non-calibration" loads:

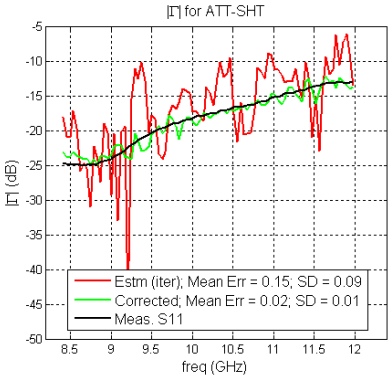

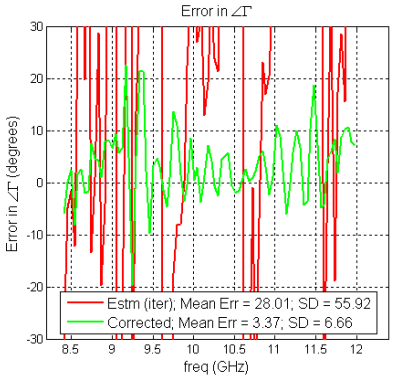

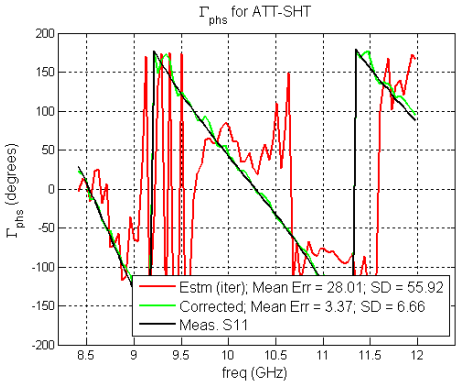

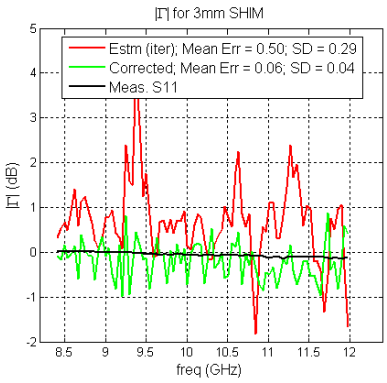

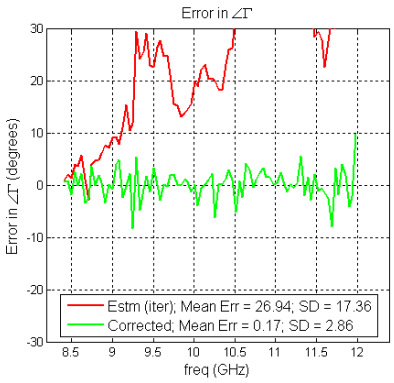

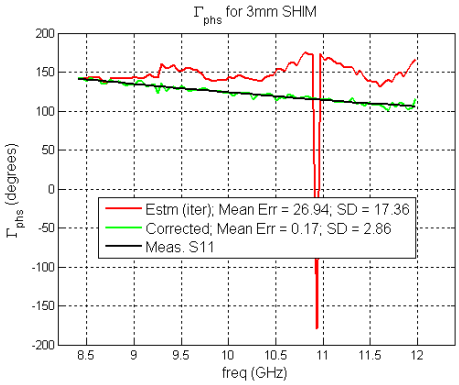

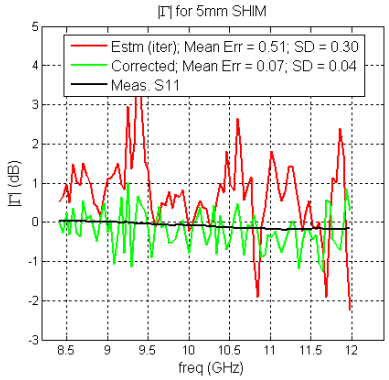
|Γ| for 5mm SHIM
Estm (iter); Mean Err = 0.51; SD = 0.30
Corrected; Mean Err = 0.07; SD = 0.04
Meas. S11
|Γ| (dB)
freq (GHz)

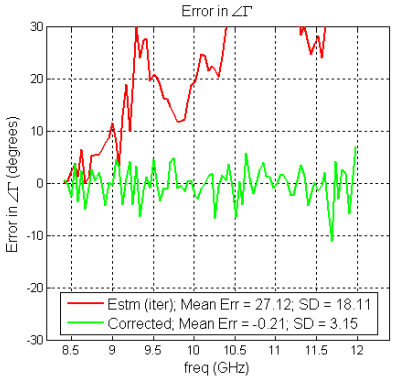
Error in ∠Γ
Estm (iter); Mean Err = 27.12; SD = 18.11
Corrected; Mean Err = -0.21; SD = 3.15
Error in ∠Γ (degrees)
freq (GHz)

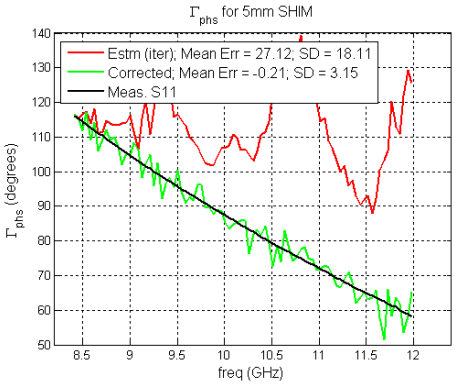
Γphs for 5mm SHIM
Estm (iter); Mean Err = 27.12; SD = 18.11
Corrected; Mean Err = -0.21; SD = 3.15
Meas. S11
Γphs (degrees)
freq (GHz)

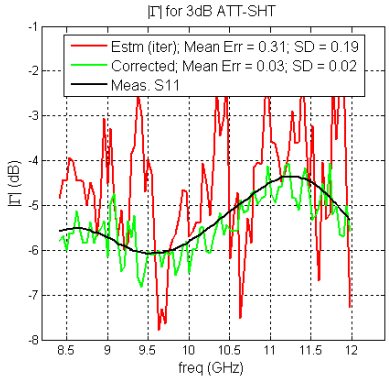
|Γ| for 3dB ATT-SHT
Estm (iter); Mean Err = 0.31; SD = 0.19
Corrected; Mean Err = 0.03; SD = 0.02
Meas. S11
|Γ| (dB)
freq (GHz)

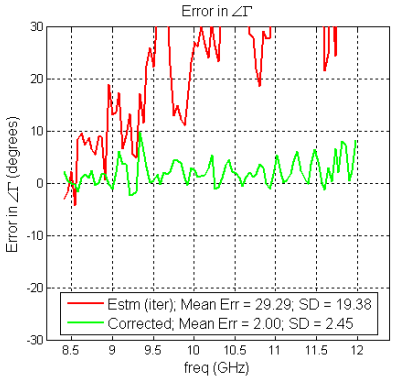
Error in ∠Γ
Estm (iter); Mean Err = 29.29; SD = 19.38
Corrected; Mean Err = 2.00; SD = 2.45
Error in ∠Γ (degrees)
freq (GHz)

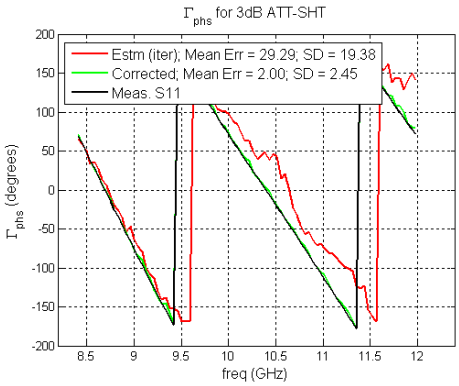
Γphs for 3dB ATT-SHT
Estm (iter); Mean Err = 29.29; SD = 19.38
Corrected; Mean Err = 2.00; SD = 2.45
Meas. S11
Γphs (degrees)
freq (GHz)

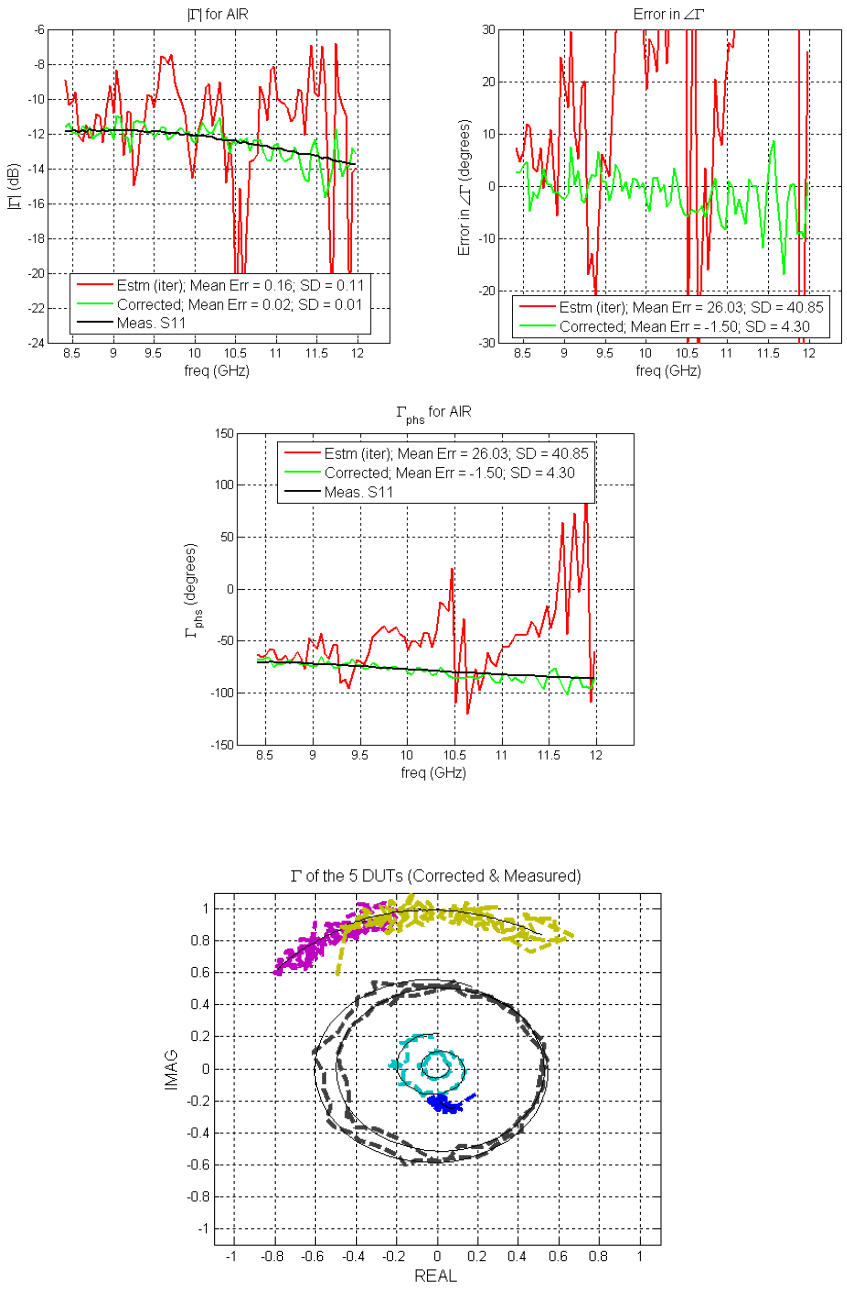

Corrected Γ of the five "non-calibration" DUTs shown on a complex plane.

Measurements and results using the spectrum analyzer (Agilent's 8563E) for measurement standing wave voltage at a source power level of 10dBm:

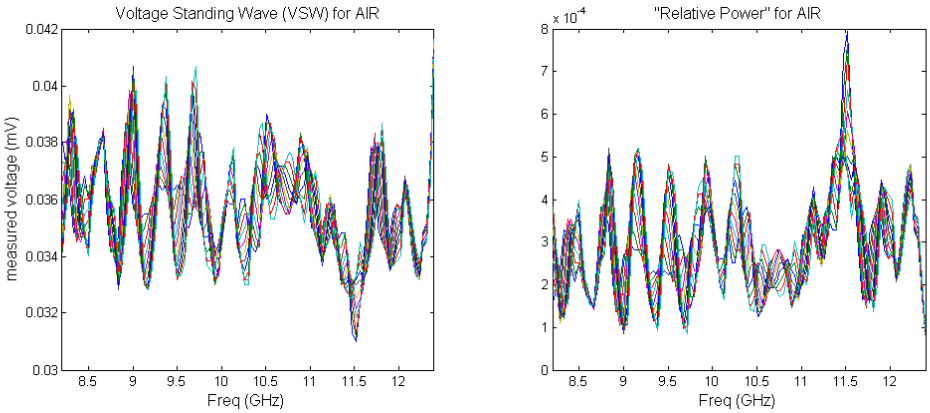

Measured and corrected voltages measured from the standing wave as a function of frequency.

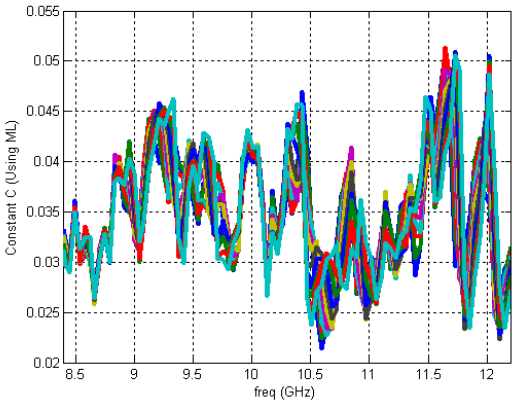

Calculation of the constant C using the 11 phase shifts. C is the average of these measured values.

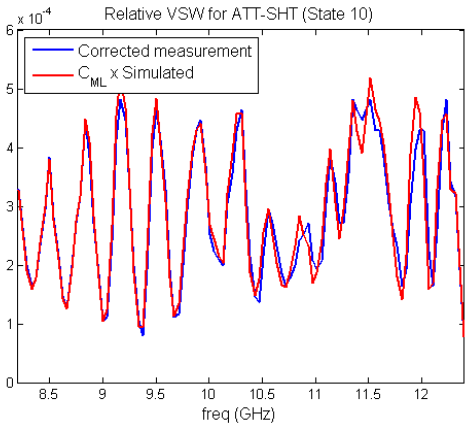

Matching the corrected standing wave measurement and the modeled voltages using the constant C.

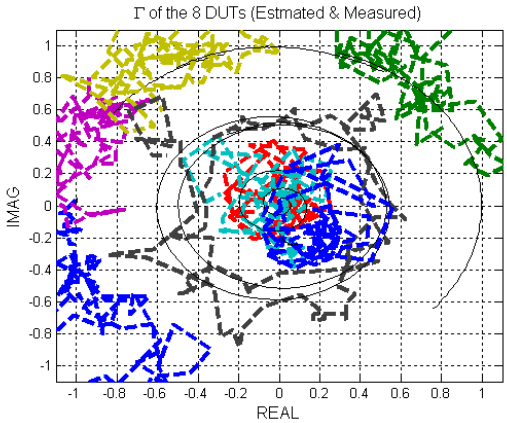

Figure 37. Estimated Γ for the eight DUTs.

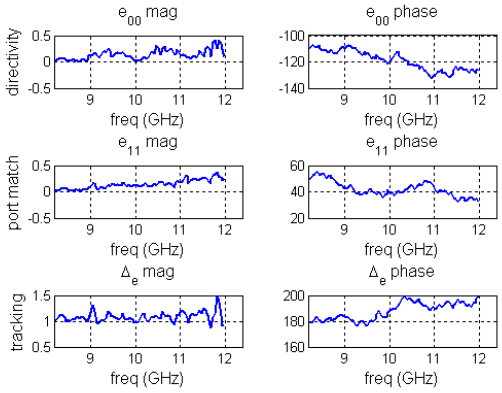

The three error terms calculated form measured and estimated reflection coefficients.

Comparing the measured, estimated and corrected Γ values and the corresponding errors for each of the five "non-calibration" loads:

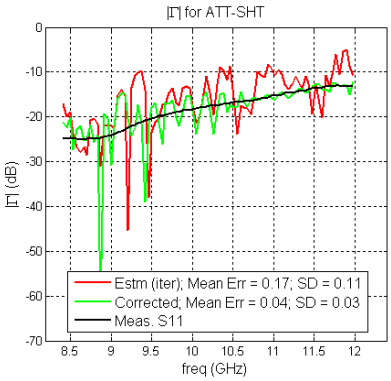

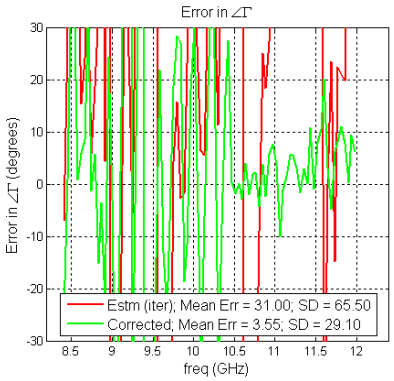

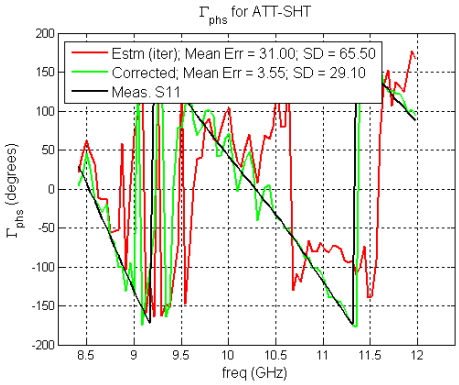

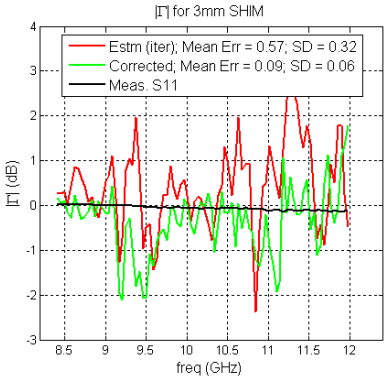

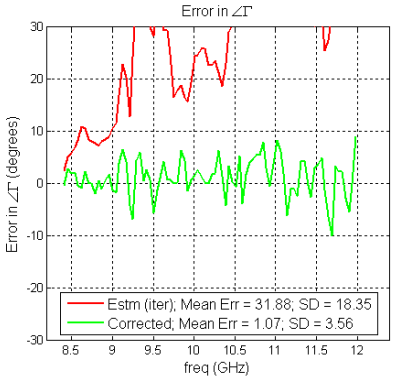

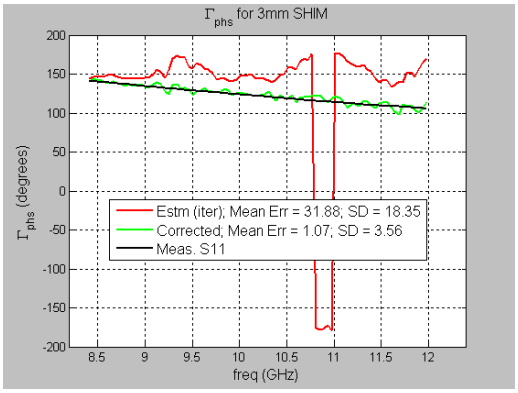

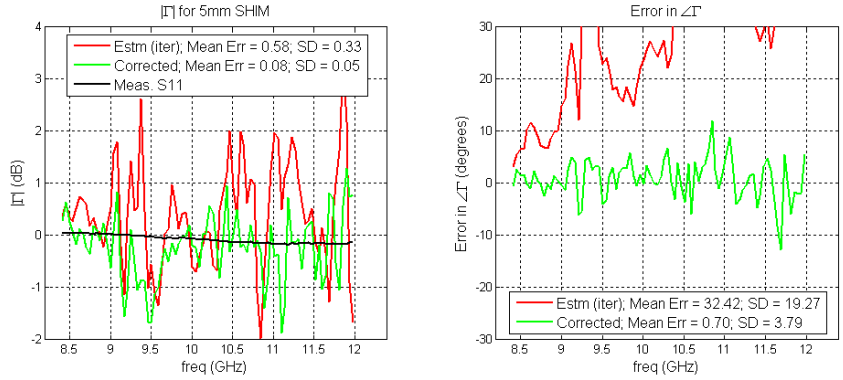
|Γ| for 5mm SHIM
Estm (iter); Mean Err = 0.58; SD = 0.33
Corrected; Mean Err = 0.08; SD = 0.05
Meas. S11
|Γ| (dB)
freq (GHz)
Error in ∠Γ
Estm (iter); Mean Err = 32.42; SD = 19.27
Corrected; Mean Err = 0.70; SD = 3.79
Error in ∠Γ (degrees)
freq (GHz)

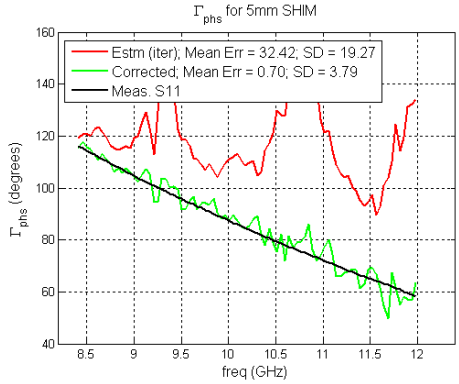
Γphs for 5mm SHIM
Estm (iter); Mean Err = 32.42; SD = 19.27
Corrected; Mean Err = 0.70; SD = 3.79
Meas. S11
Γphs (degrees)
freq (GHz)

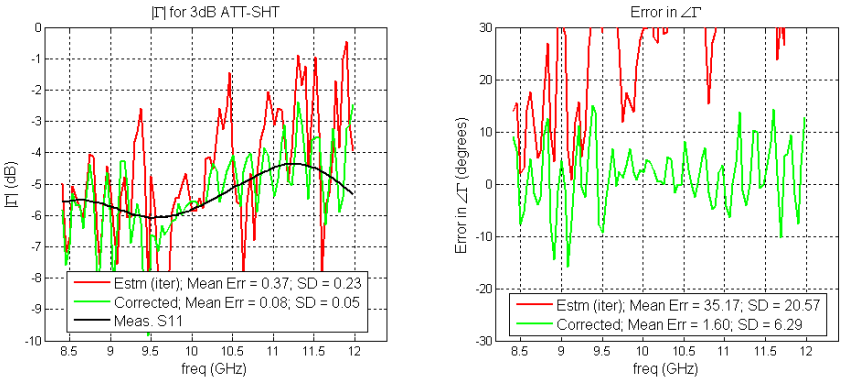
|Γ| for 3dB ATT-SHT
Estm (iter); Mean Err = 0.37; SD = 0.23
Corrected; Mean Err = 0.08; SD = 0.05
Meas. S11
|Γ| (dB)
freq (GHz)
Error in ∠Γ
Estm (iter); Mean Err = 35.17; SD = 20.57
Corrected; Mean Err = 1.60; SD = 6.29
Error in ∠Γ (degrees)
freq (GHz)

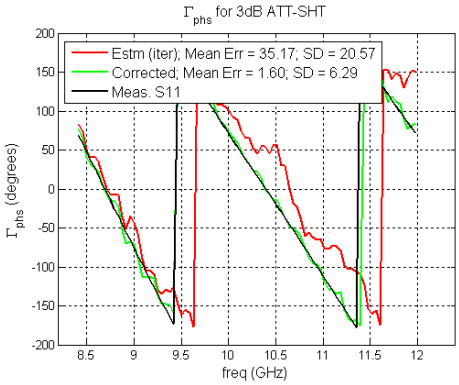
Γphs for 3dB ATT-SHT
Estm (iter); Mean Err = 35.17; SD = 20.57
Corrected; Mean Err = 1.60; SD = 6.29
Meas. S11
Γphs (degrees)
freq (GHz)

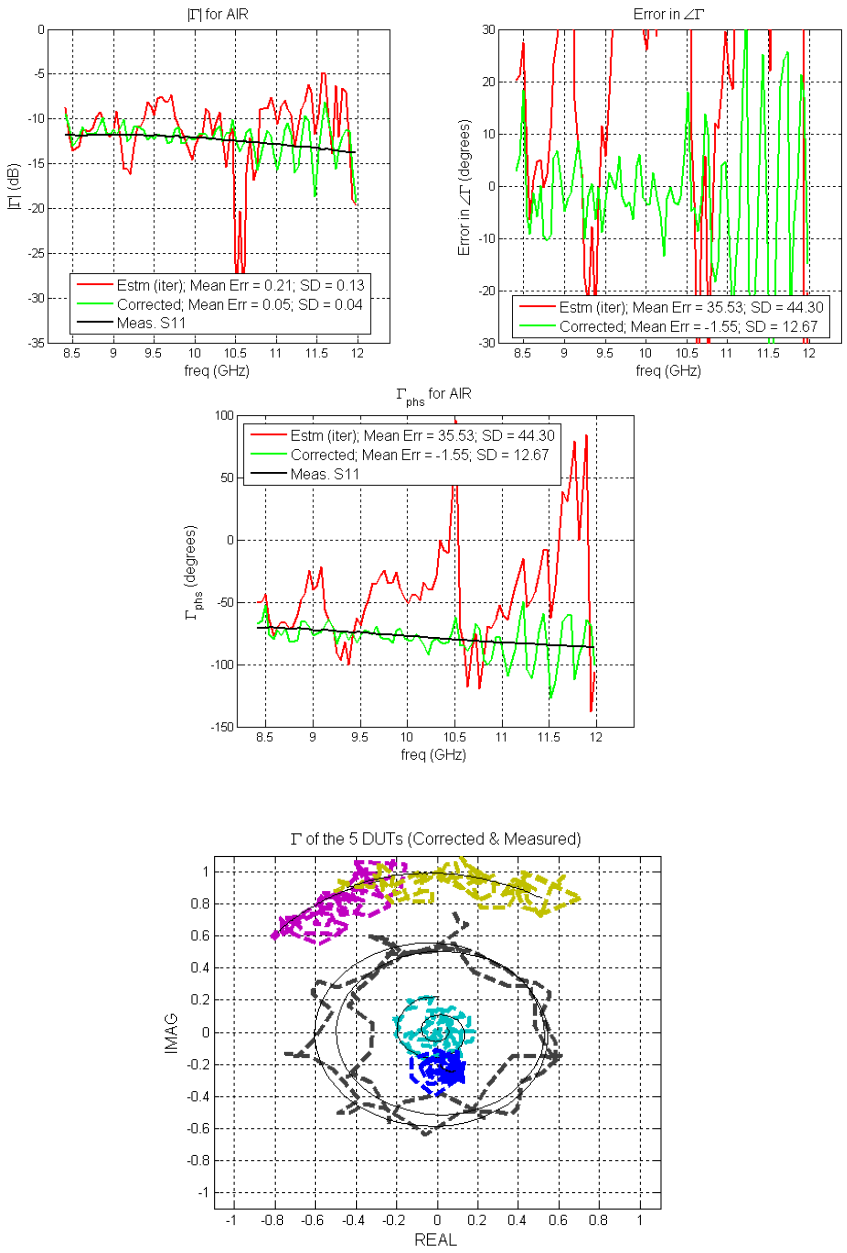

Corrected Γ of the five "non-calibration" DUTs shown on a complex plane.

Measurements and results using the spectrum analyzer (SA, Agilent's 8563E) for measurement of standing wave voltage at a higher source power level of 15dBm to account for the extra losses in the SA system:

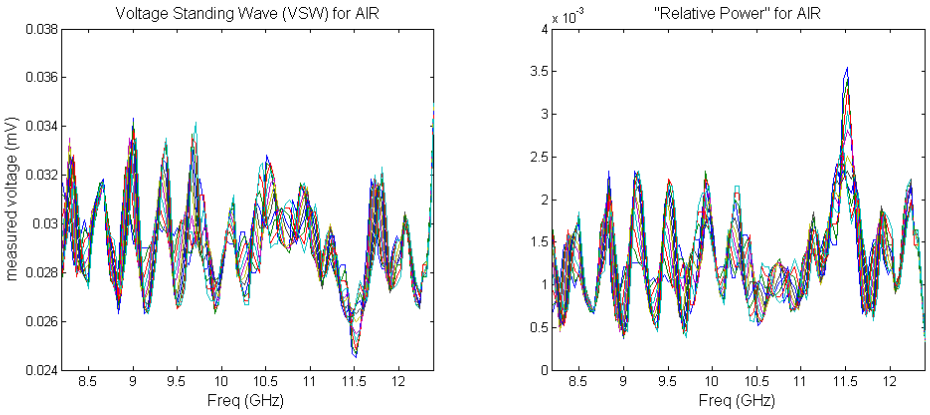

Measured and corrected voltages measured from the standing wave as a function of frequency.

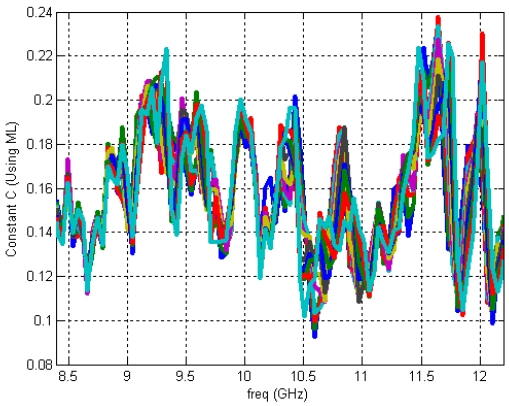

Calculation of the constant C using the 11 phase shifts. C is the average of these measured values.

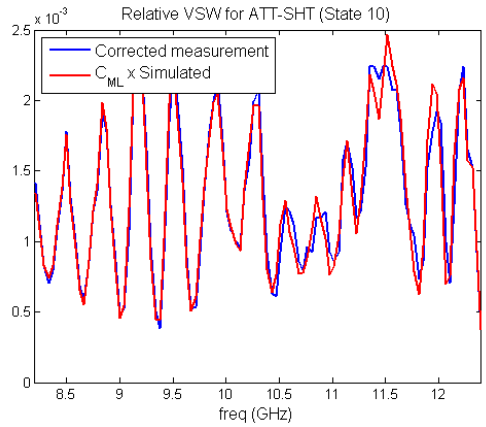

Matching the corrected standing wave measurement and the modeled voltages using the constant C.

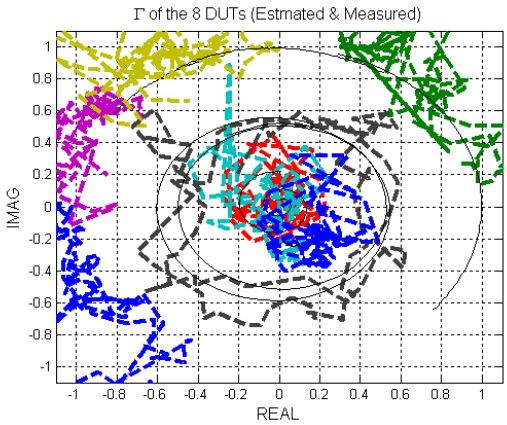

Figure 38. Estimated Γ for the eight DUTs.

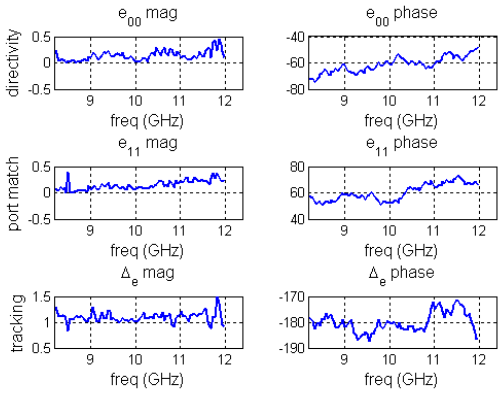

The three error terms calculated form measured and estimated reflection coefficients.

Comparing the measured, estimated and corrected Γ and the corresponding errors for each of the five "non-calibration" loads:

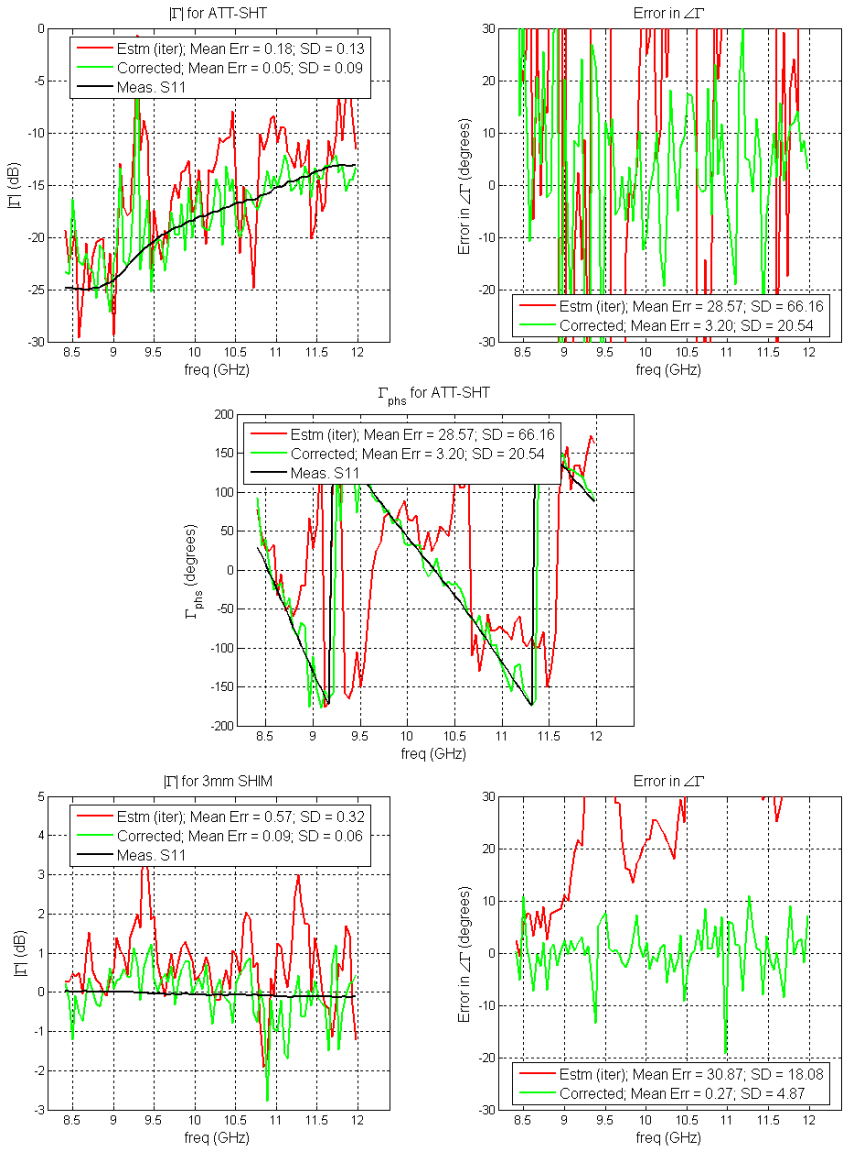

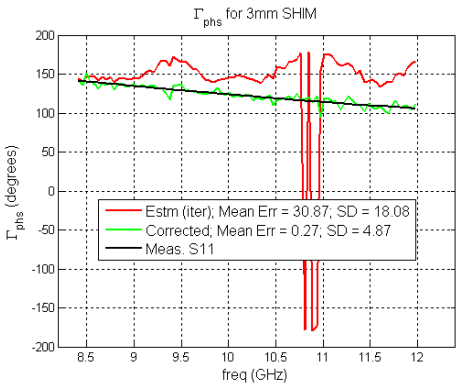
Γphs for 3mm SHIM
Γphs (degrees)
freq (GHz)
Estm (iter); Mean Err = 30.87; SD = 18.08
Corrected; Mean Err = 0.27; SD = 4.87
Meas. S11

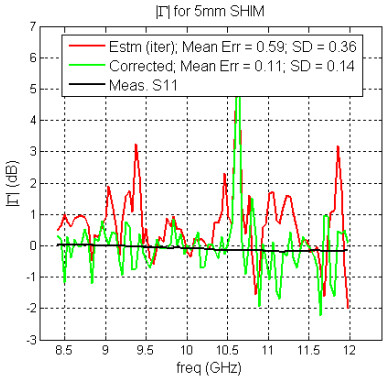
|Γ| for 5mm SHIM
|Γ| (dB)
freq (GHz)
Estm (iter); Mean Err = 0.59; SD = 0.36
Corrected; Mean Err = 0.11; SD = 0.14
Meas. S11

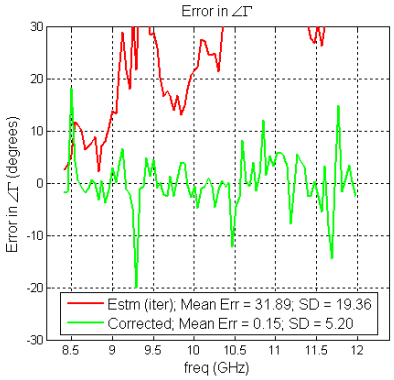
Error in ∠Γ
Error in ∠Γ (degrees)
freq (GHz)
Estm (iter); Mean Err = 31.89; SD = 19.36
Corrected; Mean Err = 0.15; SD = 5.20

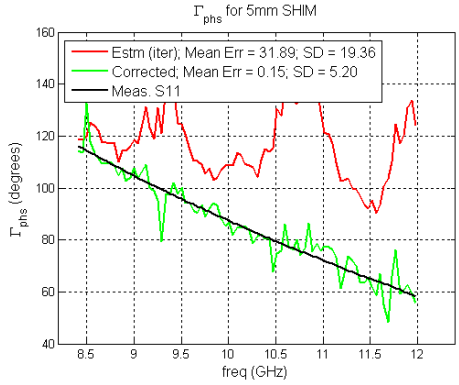
Γphs for 5mm SHIM
Γphs (degrees)
freq (GHz)
Estm (iter); Mean Err = 31.89; SD = 19.36
Corrected; Mean Err = 0.15; SD = 5.20
Meas. S11

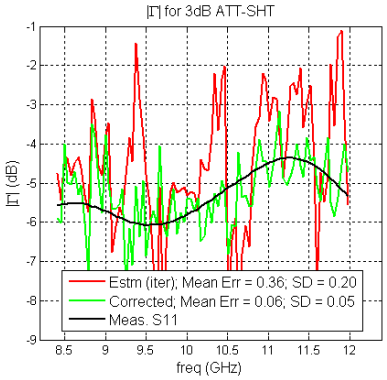
|Γ| for 3dB ATT-SHT
|Γ| (dB)
freq (GHz)
Estm (iter); Mean Err = 0.36; SD = 0.20
Corrected; Mean Err = 0.06; SD = 0.05
Meas. S11

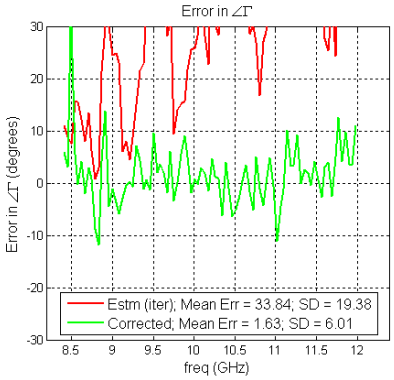
Error in ∠Γ
Error in ∠Γ (degrees)
freq (GHz)
Estm (iter); Mean Err = 33.84; SD = 19.38
Corrected; Mean Err = 1.63; SD = 6.01

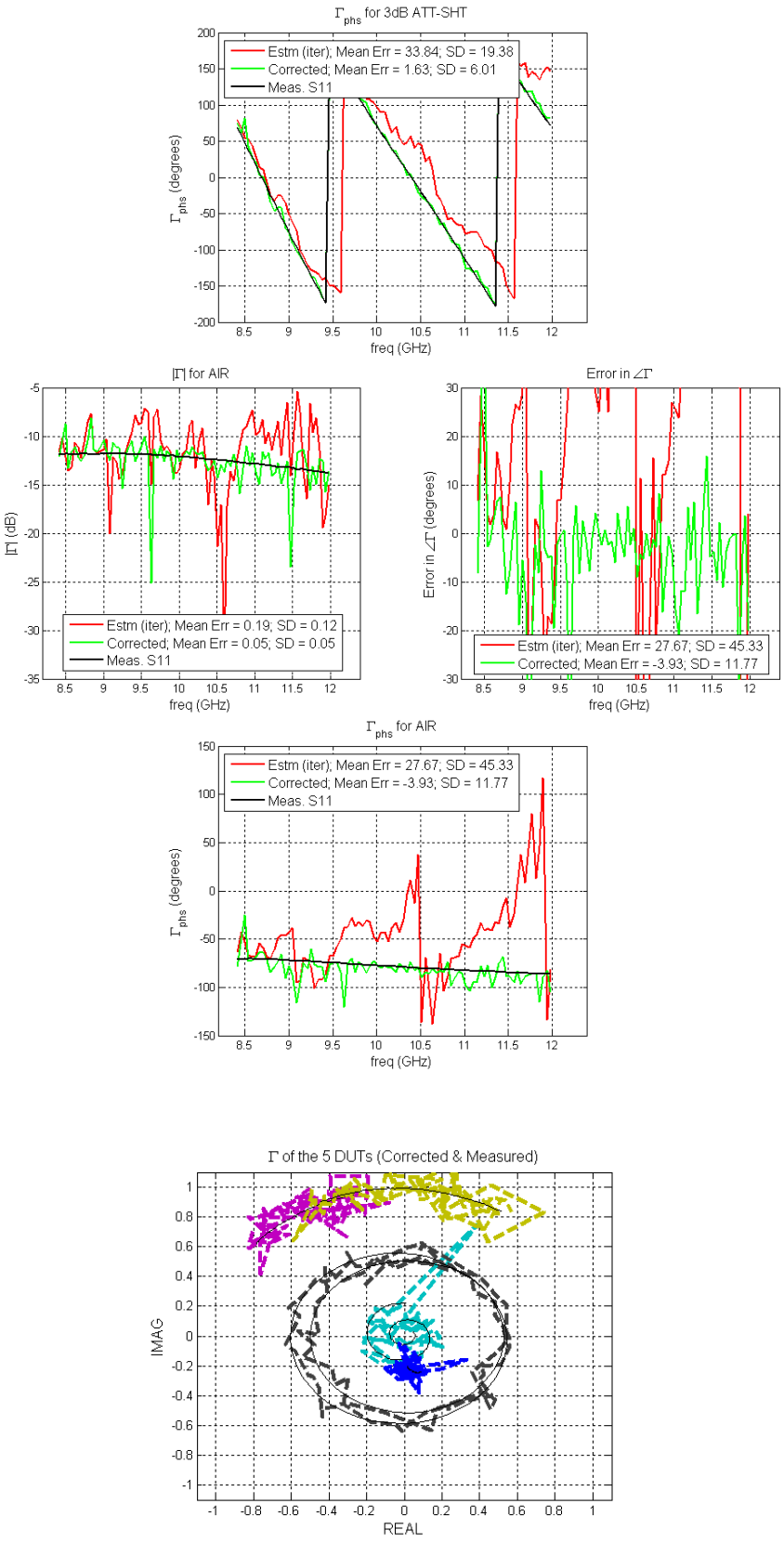

Corrected Γ of the five "non-calibration" DUTs shown on a complex plane.

APPENDIX F

FREQUENCY STABILITY OF THE 8510C VECTOR NETWORK ANALYZER SYSTEM

To test the frequency accuracy of the HP 8510 C vector network analyzer, after setting the VNA to a specific X-band frequency, peak of the spectrum was centered on the connected spectrum analyzer (Agilent's 8563E). This center frequency was measured for multiple resolution bandwidth values (RBW) for each of the eight X-band microwave loads: calibration short, shims (3 mm, 5 mm and 9 mm), matched load, an attenuated short with frequency dependent attenuation, a wideband 3 dB attenuated short and an open-ended waveguide radiating into air (AIR) as described in Section 4. Error was calculated between the frequency set on 8510 VNA and the value measured by the spectrum analyzer. This error, its mean and standard deviation (SD) plotted as a function of frequency for the variable attenuated short is shown in Figures 1 to 5.

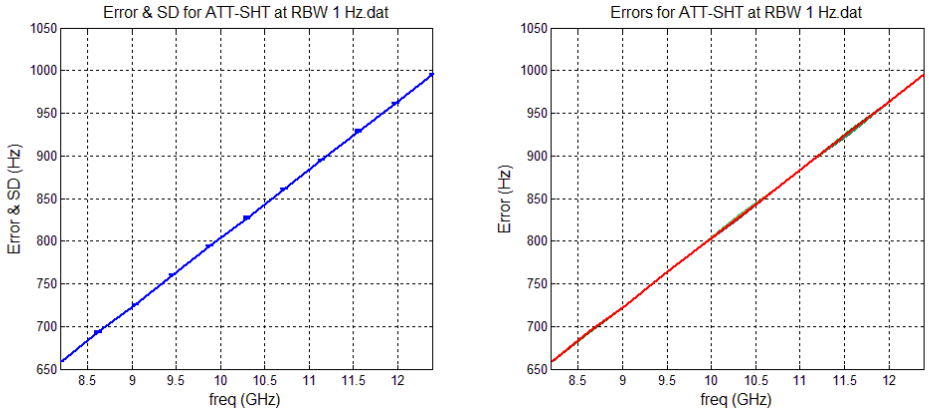

Errors for RBW of 1 Hz.

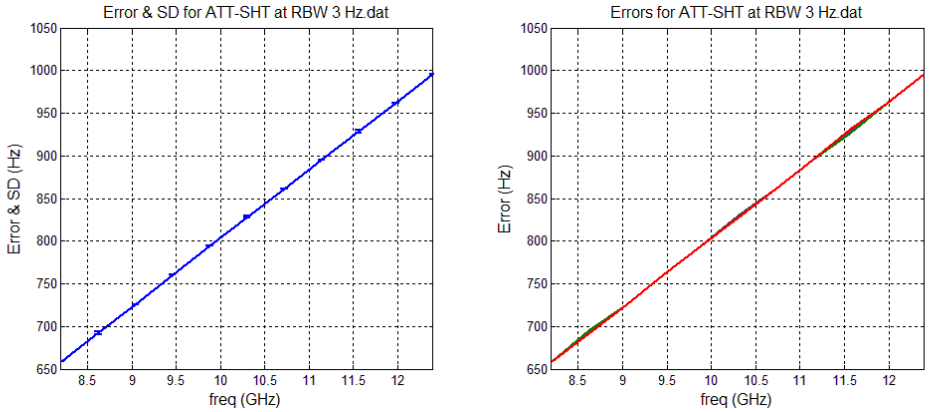

Errors for RBW of 3 Hz.

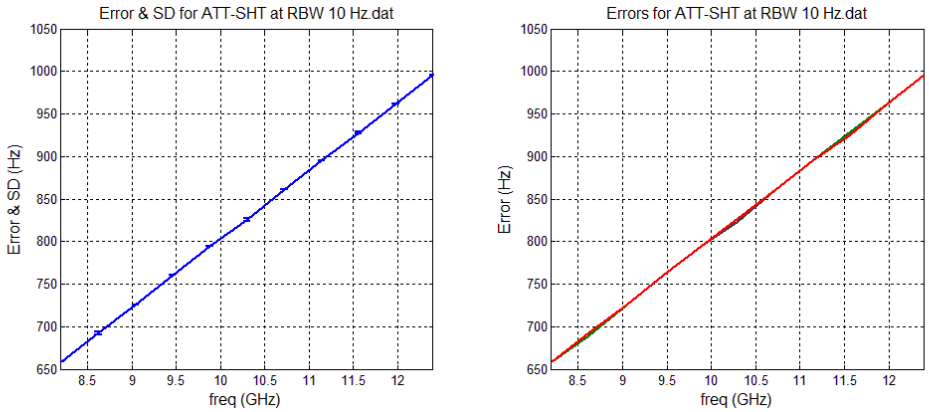

Errors for RBW of 10 Hz.

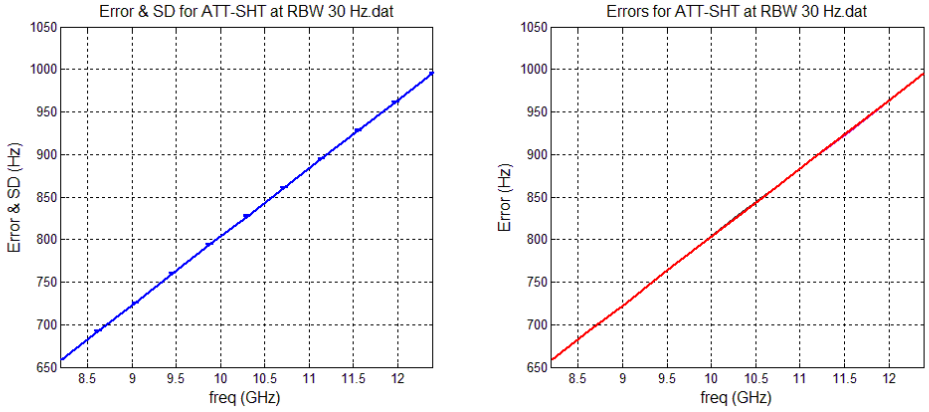

Errors for RBW of 30 Hz.

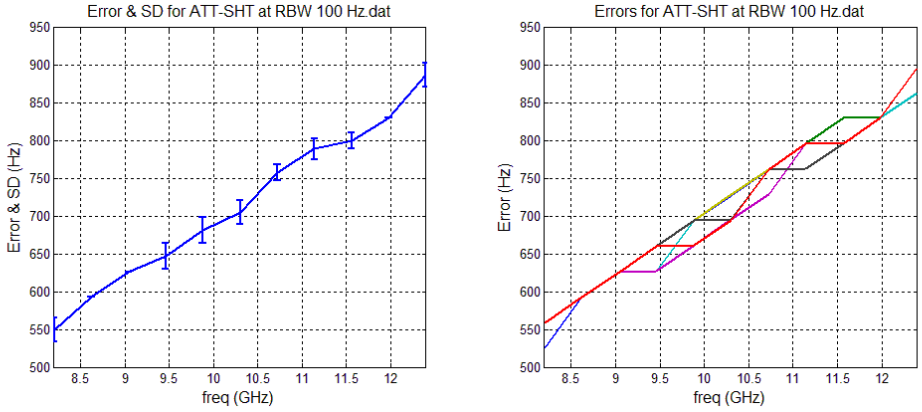

Errors for RBW of 100 Hz.

The error in the above is a low value compared to the set frequency (8.2 to 12.4 GHz) and increases linearly with frequency with an extremely low standard deviation.

This shows that the frequency of the source is very stable and the observed error is only due to a slight offset in their 10 MHz reference which adds up during frequency up-conversion. Similar results were obtained with other DUTs as shown in Figures 6 and 7.

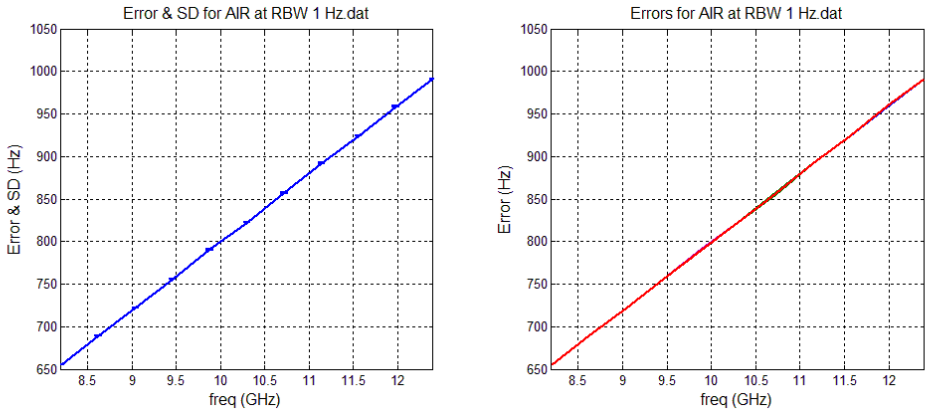

Errors for AIR.

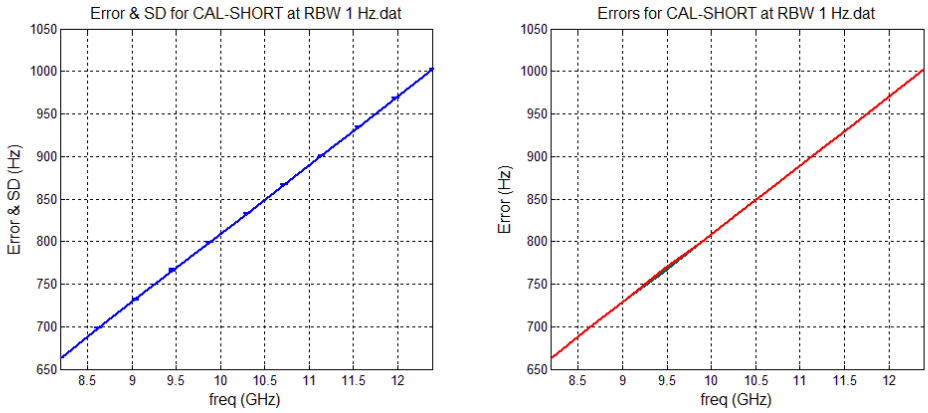

Errors for the calibration short.

APPENDIX G

RESULTS OF MEASUREMENTS USING THE MAGIC-T

Magic-T measurements and results: (1) Using the HP 8510 VNA as a detector (measuring S21) at one end of the Magic T:

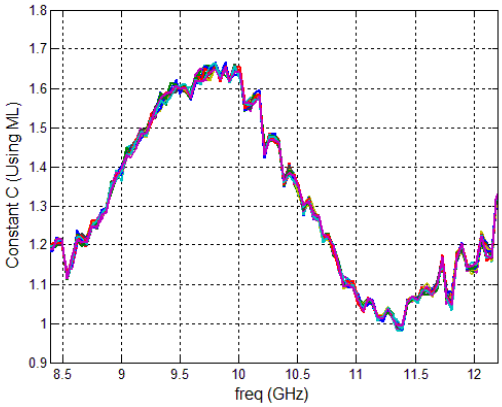

Calculation of the constant C using the 11 phase shifts. C is the average of these measured values.

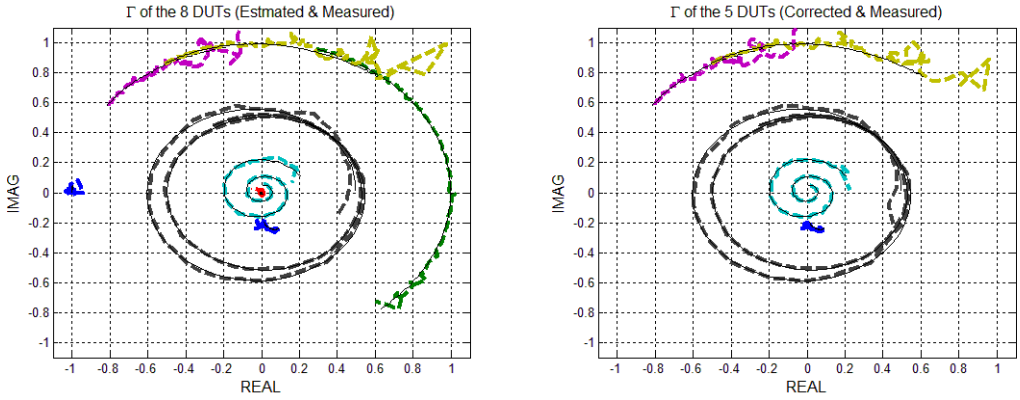

Estimated and corrected Γ for the DUTs.

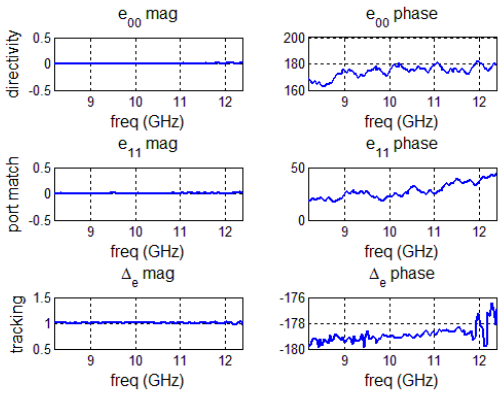

The three error terms calculated form measured and estimated reflection coefficients.

Comparing the measured, estimated and corrected Γ values and the corresponding errors for each of the five "non-calibration" loads:

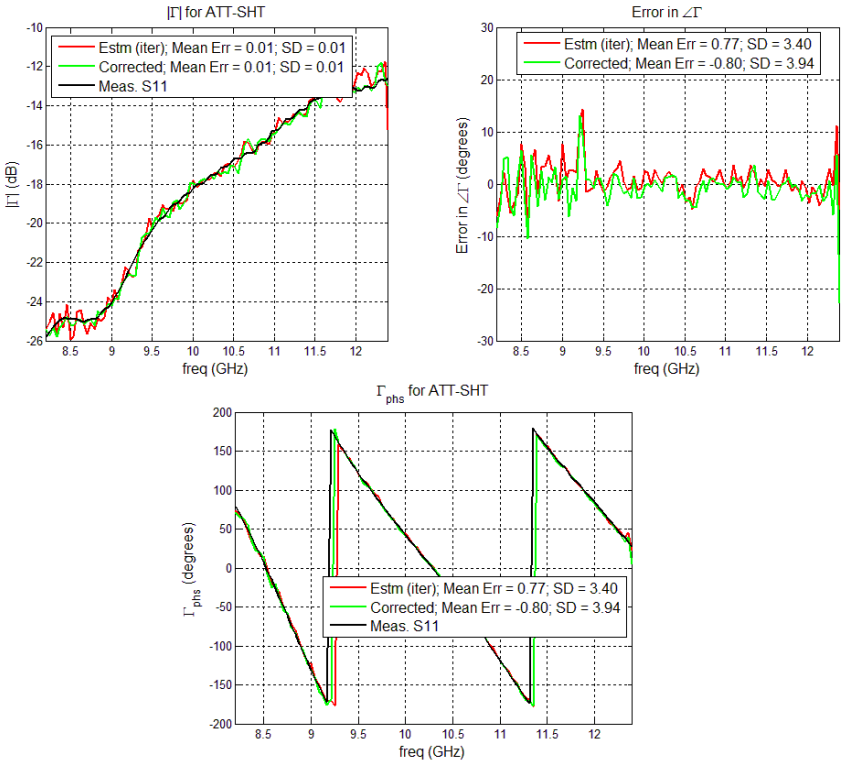

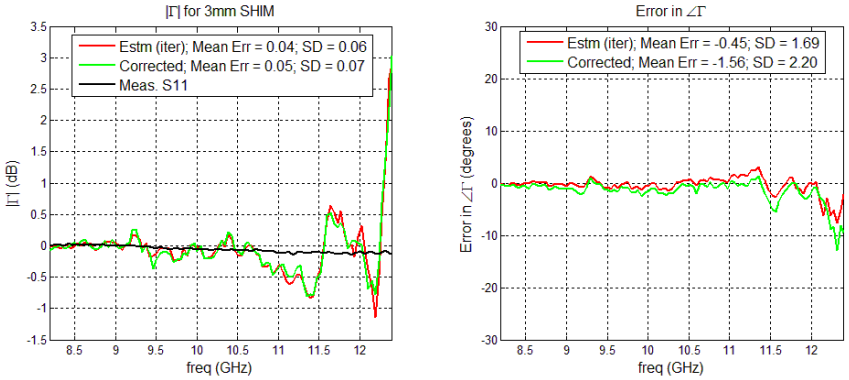
|Γ| for 3mm SHIM
Estm (iter); Mean Err = 0.04; SD = 0.06
Corrected; Mean Err = 0.05; SD = 0.07
Meas. S11
|Γ| (dB)
freq (GHz)

Error in ∠Γ
Estm (iter); Mean Err = -0.45; SD = 1.69
Corrected; Mean Err = -1.56; SD = 2.20
Error in ∠Γ (degrees)
freq (GHz)

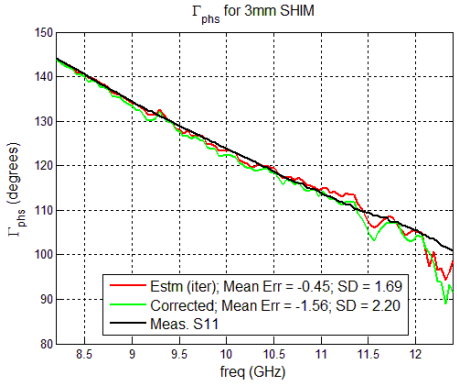
Γphs for 3mm SHIM
Estm (iter); Mean Err = -0.45; SD = 1.69
Corrected; Mean Err = -1.56; SD = 2.20
Meas. S11
Γphs (degrees)
freq (GHz)

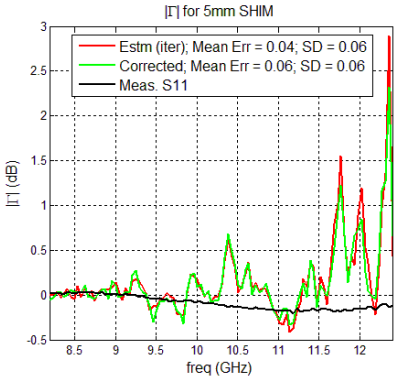
|Γ| for 5mm SHIM
Estm (iter); Mean Err = 0.04; SD = 0.06
Corrected; Mean Err = 0.06; SD = 0.06
Meas. S11
|Γ| (dB)
freq (GHz)

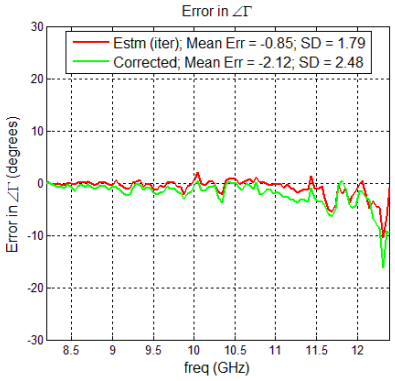
Error in ∠Γ
Estm (iter); Mean Err = -0.85; SD = 1.79
Corrected; Mean Err = -2.12; SD = 2.48
Error in ∠Γ (degrees)
freq (GHz)

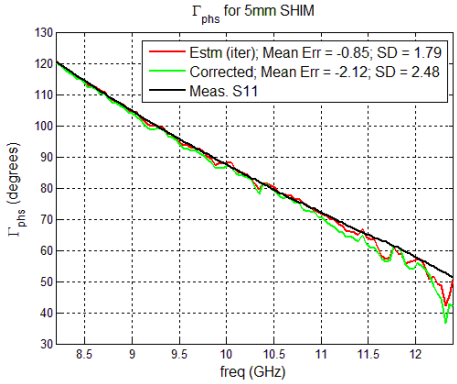
Γphs for 5mm SHIM
Estm (iter); Mean Err = -0.85; SD = 1.79
Corrected; Mean Err = -2.12; SD = 2.48
Meas. S11
Γphs (degrees)
freq (GHz)

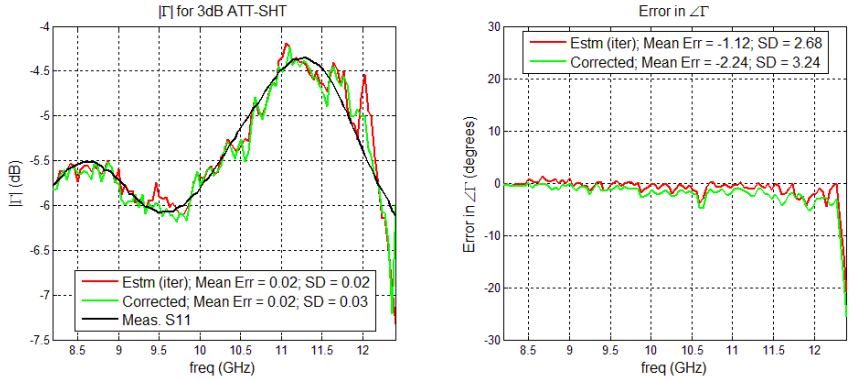
|Γ| for 3dB ATT-SHT
|Γ| (dB)
freq (GHz)
Estm (iter); Mean Err = 0.02; SD = 0.02
Corrected; Mean Err = 0.02; SD = 0.03
Meas. S11
Error in ∠Γ
Error in ∠Γ (degrees)
freq (GHz)
Estm (iter); Mean Err = -1.12; SD = 2.68
Corrected; Mean Err = -2.24; SD = 3.24

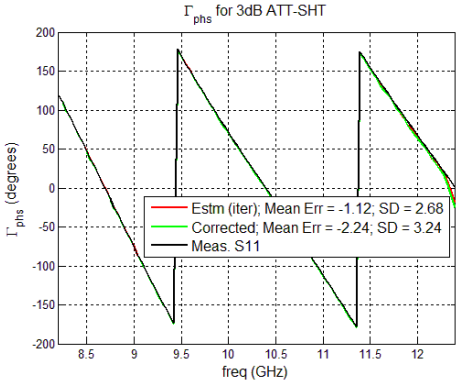
Γphs for 3dB ATT-SHT
Γphs (degrees)
freq (GHz)
Estm (iter); Mean Err = -1.12; SD = 2.68
Corrected; Mean Err = -2.24; SD = 3.24
Meas. S11

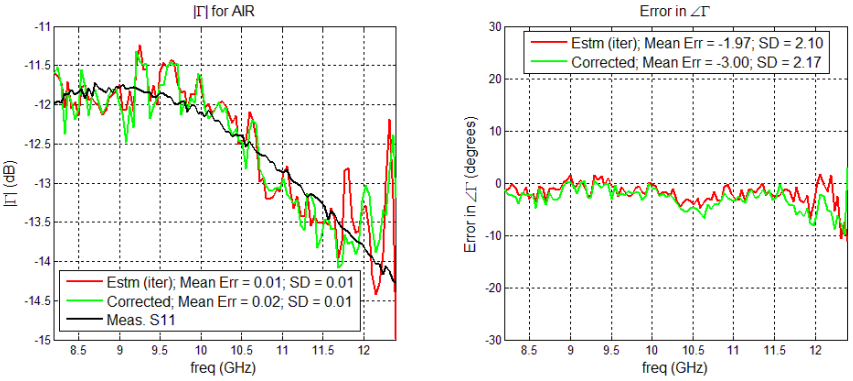
|Γ| for AIR
|Γ| (dB)
freq (GHz)
Estm (iter); Mean Err = 0.01; SD = 0.01
Corrected; Mean Err = 0.02; SD = 0.01
Meas. S11
Error in ∠Γ
Error in ∠Γ (degrees)
freq (GHz)
Estm (iter); Mean Err = -1.97; SD = 2.10
Corrected; Mean Err = -3.00; SD = 2.17

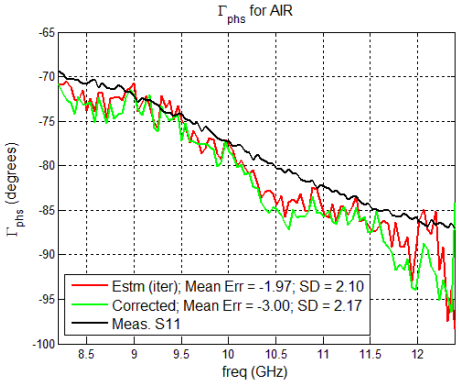
Γphs for AIR
Γphs (degrees)
freq (GHz)
Estm (iter); Mean Err = -1.97; SD = 2.10
Corrected; Mean Err = -3.00; SD = 2.17
Meas. S11

Magic-T measurements and results for (2) Using the Krytar Schottky detector at the second end of the Magic T:

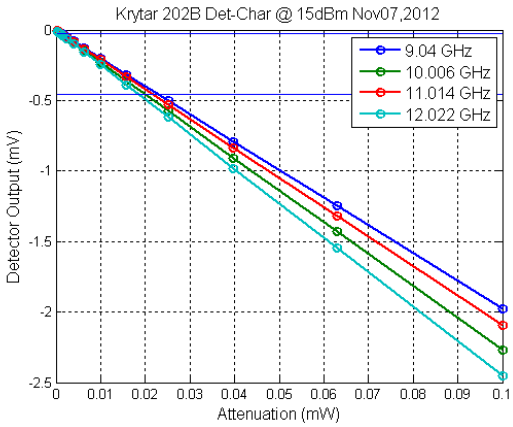

Krytar detector characterization showing the maximum and minimum values of the measured voltage.

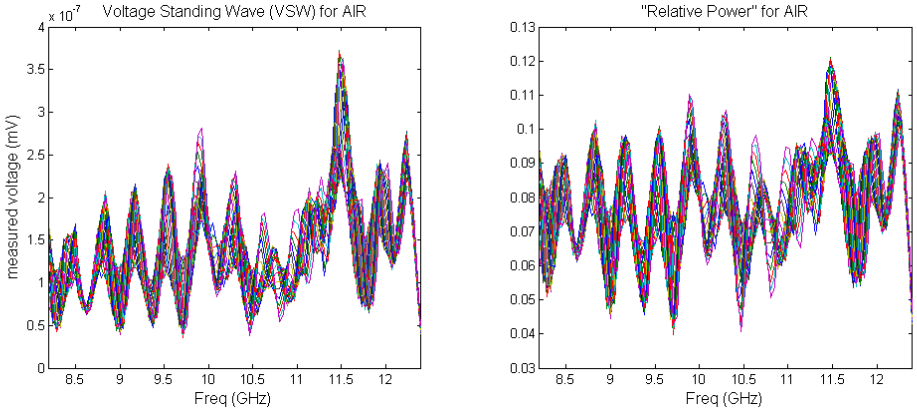

Measured and corrected voltages measured from the standing wave as a function of frequency.

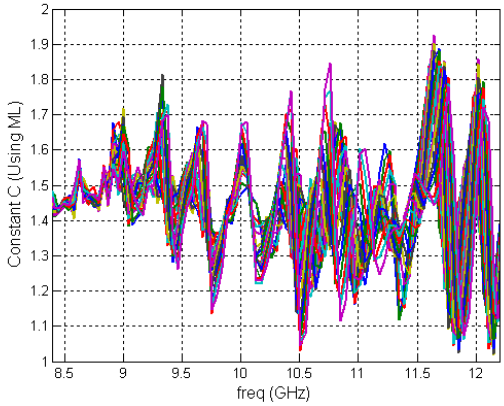

Calculation of the constant C using the 11 phase shifts. C is the average of these measured values.

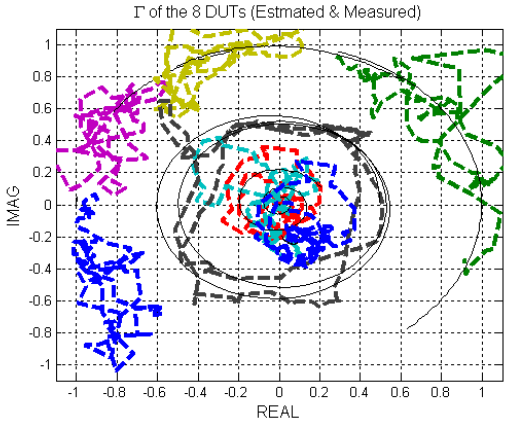

Estimated Γ for the eight DUTs.

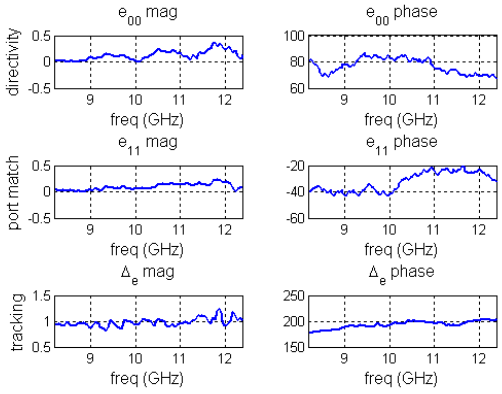

The three error terms calculated form measured and estimated reflection coefficients.

Comparing the measured, estimated and corrected Γ values and the corresponding errors for each of the five "non-calibration" loads:

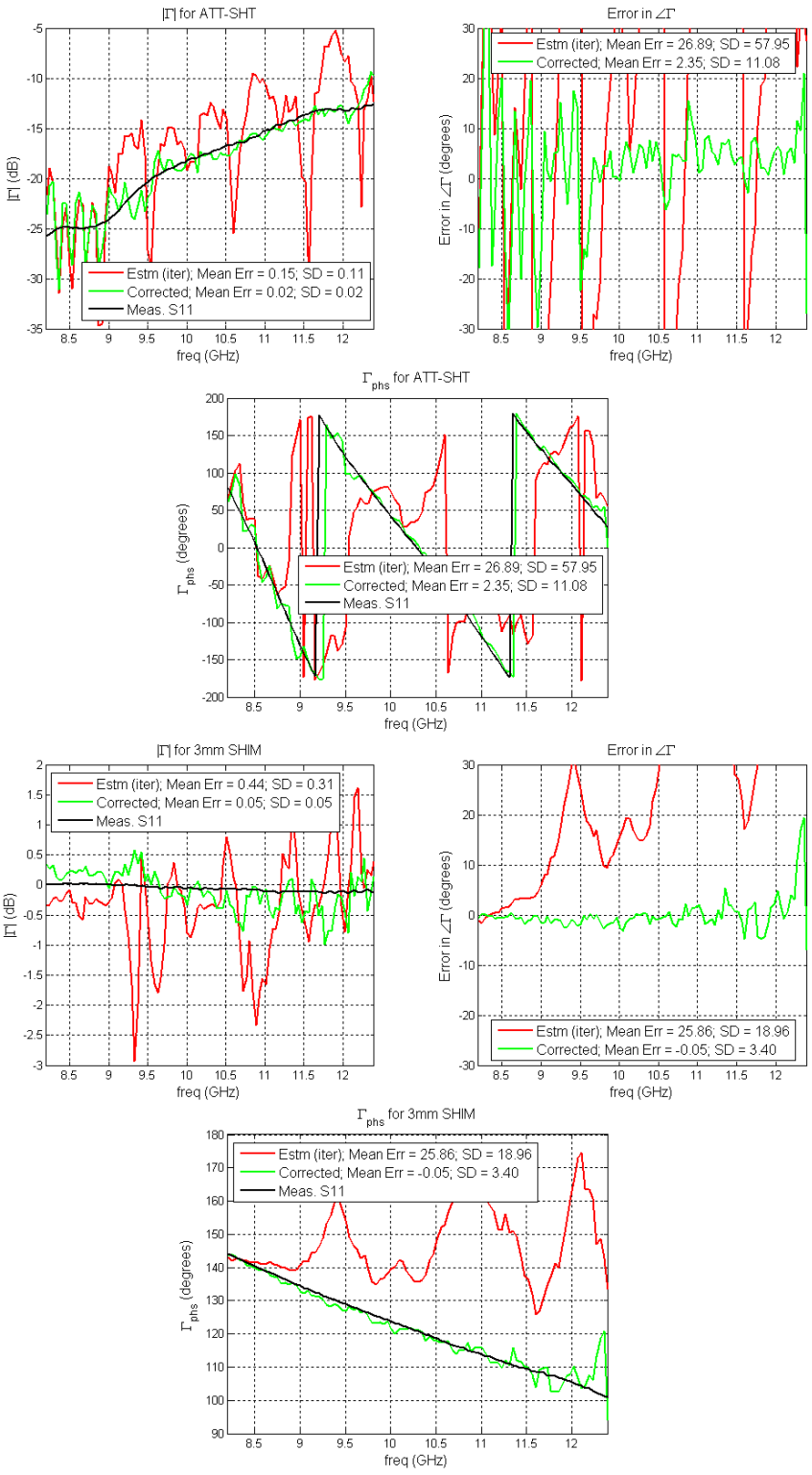

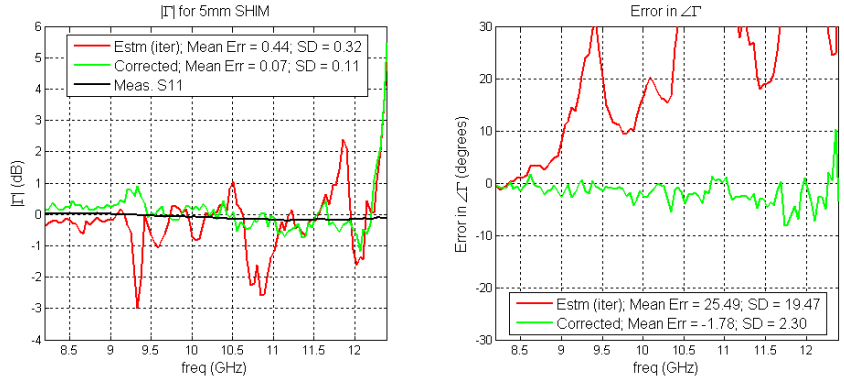
|Γ| for 5mm SHIM
Estm (iter); Mean Err = 0.44; SD = 0.32
Corrected; Mean Err = 0.07; SD = 0.11
Meas. S11
|Γ| (dB)
freq (GHz)

Error in ∠Γ
Estm (iter); Mean Err = 25.49; SD = 19.47
Corrected; Mean Err = -1.78; SD = 2.30
Error in ∠Γ (degrees)
freq (GHz)

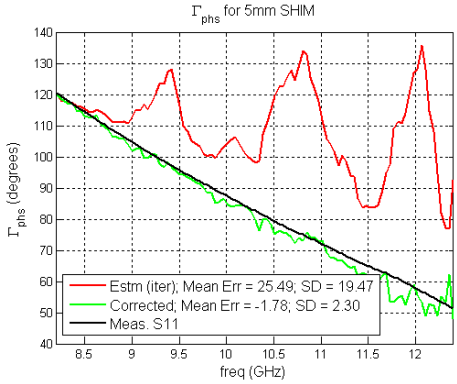
Γphs for 5mm SHIM
Estm (iter); Mean Err = 25.49; SD = 19.47
Corrected; Mean Err = -1.78; SD = 2.30
Meas. S11
Γphs (degrees)
freq (GHz)

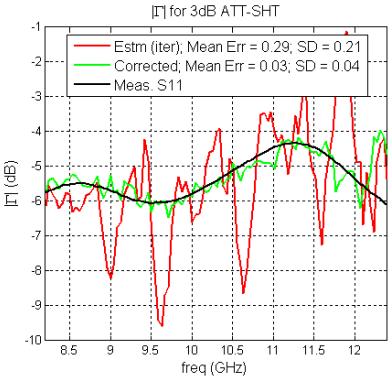
|Γ| for 3dB ATT-SHT
Estm (iter); Mean Err = 0.29; SD = 0.21
Corrected; Mean Err = 0.03; SD = 0.04
Meas. S11
|Γ| (dB)
freq (GHz)

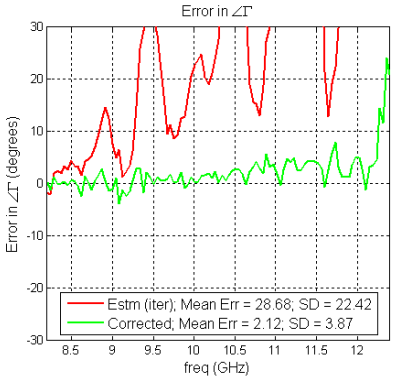
Error in ∠Γ
Estm (iter); Mean Err = 28.68; SD = 22.42
Corrected; Mean Err = 2.12; SD = 3.87
Error in ∠Γ (degrees)
freq (GHz)

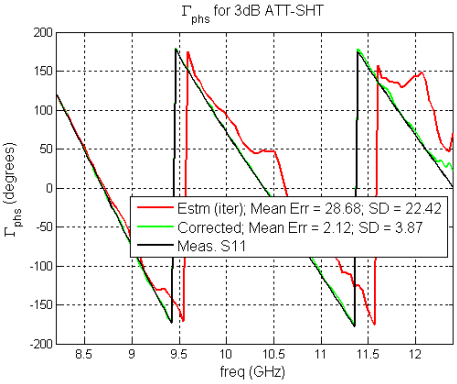
Γphs for 3dB ATT-SHT
Estm (iter); Mean Err = 28.68; SD = 22.42
Corrected; Mean Err = 2.12; SD = 3.87
Meas. S11
Γphs (degrees)
freq (GHz)

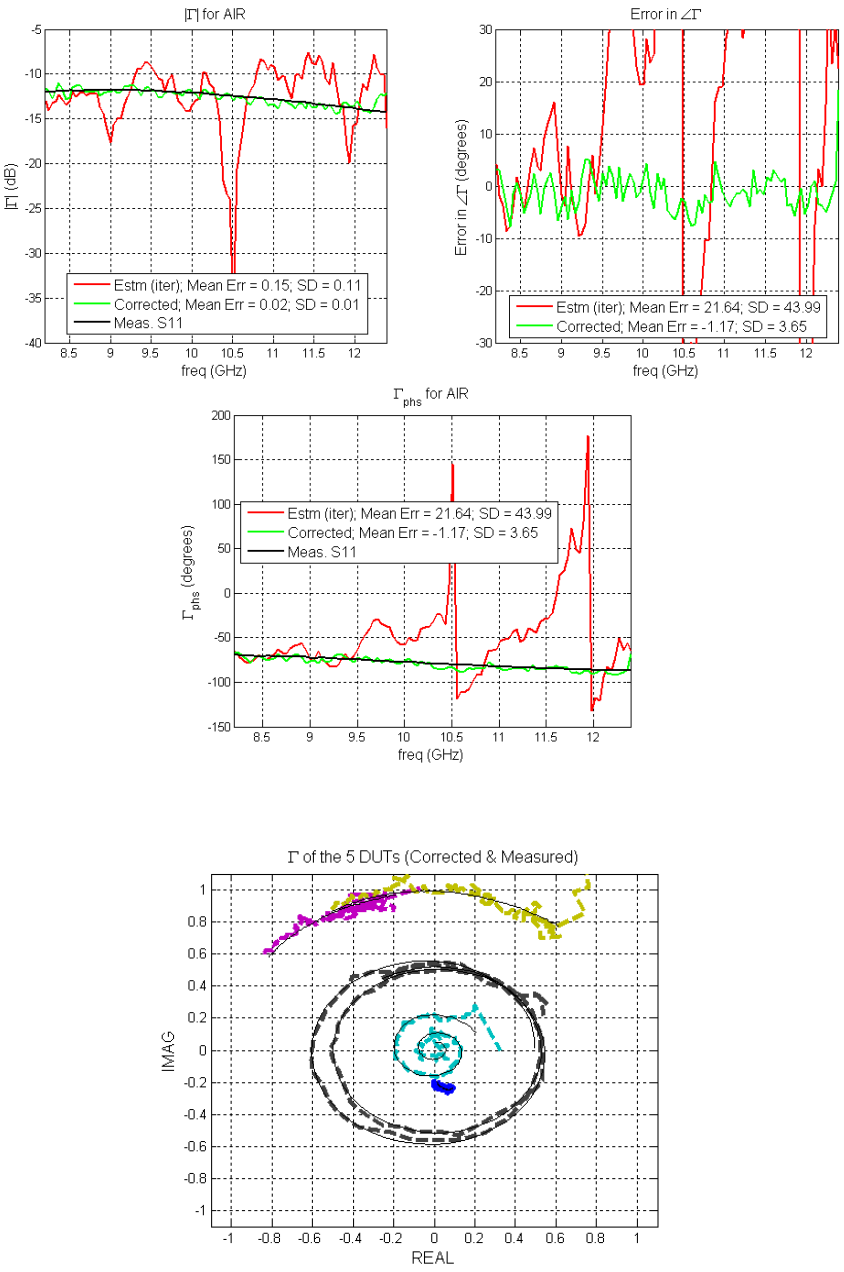

Γ of the five "non-calibration" DUTs shown on a complex plane.

BIBLIOGRAPHY

[1] Exploring the Architectures of Network Analyzers. [Agilent Technologies Application Note]. *Agilent AN 1287-2*. Available: http://cp.literature.agilent.com/litweb/pdf/5965-7708E.pdf, Dec 2012.

[2] D. Rytting, "ARFTG 50 year network analyzer history," in *Microwave Symposium Digest, 2008 IEEE MTT-S International*, 2008, pp. 11-18.

[3] K. Jayong, H. Lijun, S. Herrin, R. Moseley, R. Carlton, D. G. Beetner, and D. Pommerenke, "A Nonlinear Microcontroller Power Distribution Network Model for the Characterization of Immunity to Electrical Fast Transients," *Electromagnetic Compatibility, IEEE Transactions on,* vol. 51, pp. 611-619, 2009.

[4] R. Zoughi, *Microwave Non-Destructive Testing and Evaluation Principles* vol. 4: Springer, 2000.

[5] M. T. Ghasr, D. Pommerenke, J. T. Case, A. McClanahan, A. Aflaki-Beni, M. Abou-Khousa, S. Kharkovsky, K. Guinn, F. De Paulis, and R. Zoughi, "Rapid Rotary Scanner and Portable Coherent Wideband Q-Band Transceiver for High-Resolution Millimeter-Wave Imaging Applications," *Instrumentation and Measurement, IEEE Transactions on,* vol. 60, pp. 186-197, 2011.

[6] R. Caldecott, "The generalized multiprobe reflectometer and its application to automated transmission line measurements," *Antennas and Propagation, IEEE Transactions on,* vol. 21, pp. 550-554, 1973.

[7] W. J. Duffin, "Three-Probe Method of Impedance Measurement," *Wireless Engineer,* vol. 29 pp. 317-320, 1952.

[8] M. A. Abou-Khousa, M. A. Baumgartner, S. Kharkovsky, and R. Zoughi, "Novel and Simple High-Frequency Single-Port Vector Network Analyzer," *Instrumentation and Measurement, IEEE Transactions on,* vol. 59, pp. 534-542, 2010.

[9] M. A. Abou-Khousa, M. A. Baumgartner, S. Kharkovsky, and R. Zoughi, "Ka-Band Vector Reflectometer Based on Simple Phase-Shifter Design," *Instrumentation and Measurement, IEEE Transactions on,* vol. 60, pp. 618-624, 2011.

[10] M. Fallahpour, M. A. Baumgartner, A. Kothari, M. T. Ghasr, D. Pommerenke, and R. Zoughi, "Compact Ka-Band One-Port Vector Reflectometer Using a Wideband Electronically Controlled Phase Shifter," *Instrumentation and Measurement, IEEE Transactions on,* vol. 61, pp. 2807-2816, 2012.

[11] G. F. Engen, "The Six-Port Reflectometer: An Alternative Network Analyzer," *Microwave Theory and Techniques, IEEE Transactions on,* vol. 25, pp. 1075-1080, 1977.

[12] G. F. Engen, "Calibrating the Six-Port Reflectometer by Means of Sliding Terminations," *Microwave Theory and Techniques, IEEE Transactions on,* vol. 26, pp. 951-957, 1978.

[13] K. Haddadi and T. Lasri, "Formulation for Complete and Accurate Calibration of Six-Port Reflectometer," *Microwave Theory and Techniques, IEEE Transactions on,* vol. 60, pp. 574-581, 2012.

[14] E. Martin, J. Margineda, and J. M. Zamarro, "An Automatic Network Analyzer Using a Slotted Line Reflectometer," *Microwave Theory and Techniques, IEEE Transactions on,* vol. 30, pp. 667-670, 1982.

[15] K. Hoffmann and Z. Skvor, "A novel vector network analyzer," *Microwave Theory and Techniques, IEEE Transactions on,* vol. 46, pp. 2520-2523, 1998.

[16] E. W. Herold, "The Impact of Receiving Tubes on Broadcast and TV Receivers," *Consumer Electronics, IEEE Transactions on,* vol. CE-30, pp. 206-211, 1984.

[17] J. H. Hammond and E. S. Purington, "A History of Some Foundations of Modern Radio-Electronic Technology," *Proceedings of the IRE,* vol. 45, pp. 1191-1208, 1957.

[18] K. Hoffmann and Z. Skvor, "Authors' reply," *Microwave Theory and Techniques, IEEE Transactions on,* vol. 58, pp. 2518-2518, 2010.

[19] D. K. Rytting. Network analyzer error models and calibration methods [Online]. Available: http://www-ee.uta.edu/online/adavis/ee5349/NA_Error_Models_and_Cal_Methods.pdf, Dec 2012.

[20] D. M. Pozar, *Microwave Engineering*: Wiley, 1998.

[21] *Krytar shottkey detector datasheet (2012).* Available: http://www.krytar.com/pdf/200zbs.pdf, Dec 2012.

[22] *Hittite analog phase-shifter IC datasheet (2012).* Available: http://www.hittite.com/content/documents/data_sheet/hmc935lp5e.pdf, Dec 2012.

[23] Schottky detector datasheet. Available: http://www.krytar.com/pdf/300zbs.pdf, Dec 2012.

[24] Fundamentals of RF and Microwave Power Measurements. Available: cp.literature.agilent.com/litweb/pdf/5989-6255EN.pdf, Dec 2012.

VITA

Arpit Kothari, born on Dec 2, 1983, received his Bachelor of Engineering degree in 2007 in ‘Instrumentation Technology’ from Vishveshwarya Technological University, India. After his graduation, from July 2007 to April 2010, he worked on Distributed Control System (DCS) at Yokogawa India Limited, a firm specializing in Measurement, Control and Industrial Automation. His area of focus was Power Plant Instrumentation and Control. He received his Master of Science degree in Electrical Engineering at Missouri University of Science & Technology in August 2013. At Missouri S&T he did graduate research on millimeter wave vector network analyzer (VNA) calibration at the Applied Microwave Nondestructive Testing Laboratory (*amntl*). Presently, he's working as a hardware engineering intern at Cisco Systems in San Jose, California. His research interests are radio frequency (RF) design, measurement and instrumentation and signal integrity.